SNC·LAVALIN

TECHNICAL JOURNAL

Engineering excellence around the globe

Volume 3 | Issue 1 | 2021

SNC·LAVALIN

Foreword

CHRIS HENDY

Editor-in-Chief SNC-Lavalin Technical Journal

Professional Head of Bridge Engineering and Transportation Technical Director, EDPM

Welcome to the fifth edition of our SNC-Lavalin Technical Journal, established to showcase the fantastic depth and breadth of our engineering expertise across a wide range of disciplines and domains and to demonstrate that technical excellence is at the heart of everything we do. This fifth edition highlights the impressive work we have been doing from the development of innovative designs and design methods which protect the environment and improve the efficiency and constructability of new highway projects, to optimising the operations and asset management of existing highways, railways and nuclear facilities.

In design, we have significantly improved the efficiency of pile design in the UK through application of the overarching principles of the Eurocode design standards in a new way on the A14 Cambridge to Huntingdon project. And we have advanced industry understanding of the true distribution of soil forces behind bridge abutments in integral bridges through studies we have undertaken on rail bridges. On the A465 Heads of the Valleys scheme, also in the UK, we have developed numerous innovations to increase the sustainability of our designs. This has included: the design of a new precast bridge deck solution that is both simple and easy to construct, whilst simultaneously allowing the main bridge steelwork to be optimised; development of a lightweight distribution structure to allow highway traffic to be carried over an existing underlying cave system, accommodating a protected natural bat habitat; and design of a signature skewed arch bridge that acts as a gateway structure. In asset operation, we have demonstrated for highways that we can improve incident detection and automated signalling using floating vehicle data from mobile devices, as compared to the use of fixed roadside detectors which themselves need maintenance. For rail projects, we have proposed new improved methods for assessing track buckling risk and have also proposed means of mitigating this risk.

In the field of asset management, we have efficiently extended the life of over 1000 km of Victorian earthworks for Network Rail's Anglia region in the UK through detailed investigation and monitoring to minimise the number of interventions needed. We have also developed techniques to not only automatically identify road markings from vehicle mounted camera surveys but also to classify their condition and advise on maintenance requirements. And in nuclear, we have worked with Boston Dynamics to develop robots capable of carrying out surveys and inspections in hazardous environments not suitable for human access.

The above examples provide only a small insight into the wealth of innovation that SNC-Lavalin creates day to day.

I hope you enjoy the selection of technical papers included in this edition as much as we have enjoyed compiling them.

Editor-in-chief

Chris Hendy
Editor-in-Chief

FREng, MA (Cantab) CEng FICE Eur Ing
Technical Director, Atkins Fellow, Professional Head of Bridge Engineering
Engineering, Design and Project Management
Epsom, UK

2021 Editorial Board Members

Ramy Azar
Ph.D, Ing.

Vice-President of Engineering and CTO - Grid Solutions & Renewables
Power, Grid and Industrial Solutions
Infrastructure
Montreal, Canada

Vinod Batta
Ph.D., P.Eng.

Vice President & General Manager, Power Solutions - Western Canada
Power, Grid & Industrial Solutions
Infrastructure
Chief Technology Officer - Hydro Vancouver, Canada

Donna Huey
GISP

Atkins Fellow and Sr. Vice President, Client Technology Director
Engineering, Design and Project Management
Orlando, FL, USA

Richard Moura
P.Eng.

Vice-President, Major Projects Global Business Development
Infrastructure
Toronto, Canada

Tim Milner
CSci CChem MRSC

Atkins Fellow and Chief Technology Officer
Nuclear
Columbia, SC, USA

Samuel Fradd

Technology Manager
Engineering, Design and Project Management
Epsom, UK

Matt Keys
PhD BEng CEng

Fellow, Technical Director, Global Technical Authority – Offshore Structures
Oil & Gas
Perth, Australia

Navil Shetty
PhD, DIC, FIAM

Atkins Fellow and Technical Chair for Asset Management
Centre of Excellence for Digital Asset Management & Operations
Bangalore, India

Patrick Sikka
P. Eng

Vice-President
Mining & Metallurgy – North America
Toronto, Canada

2021 Editorial Board Members

Jill Hayden
PhD FIET

Technical Director, Atkins Fellow (Intelligent Mobility & Smart Technologies)
Engineering, Design and Project Management
Manchester, UK

Sarah-Jane Stewart
BEng MArch MCIBSE

Global Head of Sustainability
Corporate Sustainability
Glasgow, Scotland

Tracey Radford
BSc MSc CGeol FGS

Practice Manager, Geotech Network Chair
Engineering, Design and Project Management
Epsom, UK

Roger Cruickshank
BEng

Senior Director, Strategic Transport Planning, Atkins Fellow, Atkins Acuity
Engineering, Design and Project Management
Dubai, UAE

Dr. Santhosh Kumar M
PhD CEng MIET

Technical Director, GTC and Atkins Fellow of Digital Engineering, Design and Project Management
Bangalore, India

Kan Pang
BEng CEng

Senior Technical Director
Engineering, Design and Project Management
Hong Kong, China

Akshaye Sikand
MS, P.Eng.

Manager, Knowledge Management
Project Oversight
Toronto, Canada

Production Team

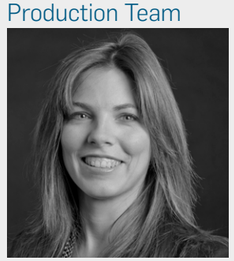

Dorothy Gartner
MLIS

Librarian
Project Oversight
Montreal, Canada

Samantha Morley
CAPM

Operations Coordinator
Technical Professional Organization, Atkins North America
Denver, CO, USA

Cheryl Law
MEng CEng MICE

Associate Engineer, Infrastructure Engineering, Design and Project Management
Epsom, UK

About the Cover

SNC-Lavalin's Atkins Nuclear Secured (ANS) business has entered the autonomous robotic market through the procurement and development of the Boston Dynamics SPOT® robot.

Contents

Floating Vehicle Data (FVD) for Queue Protection on Motorways

Marianna Imprialou

Principal Data Scientist
Engineering, Design and Project Management,
London, UK

Peter Kirby

Principal Consultant
Engineering, Design and Project Management,
Manchester, UK

Jill Hayden

Technical Director
Engineering, Design and Project Management,
Manchester, UK

Andy Fisher

Highways England
Peterborough, UK

Abstract

Highways England's motorway incident detection and automatic signalling (MIDAS) system uses traffic detectors at fixed locations to monitor traffic conditions. Roadside traffic detectors, typically inductive loops or side fire radar monitor the carriageway and continually provide traffic data to MIDAS outstations located approximately every 500m on equipped sections of the network (smart motorways and legacy MIDAS). This paper investigates the potential to use floating vehicle data (FVD) as an alternative data source as an input to the Queue Protection (QP) algorithm which is used to protect the queue on motorway networks. The results provide positive indications that FVD could be used as a data source, providing the potential to remove some or most roadside traffic detectors in future.

KEYWORDS

Floating Vehicle Data; Queue Protection; Traffic management algorithms

1. Introduction

Highways England has been investigating the potential to improve their existing algorithms. Hayden et al [1] describes the result of the initial research into the feasibility. Following the successful feasibility work, this paper presents the results of the microsimulation modelling which has been performed to investigate speed-based Queue Protection (QP) algorithms and compare their performance with that of Highways England's existing HiOcc2 algorithm. Harrison et al [2] describes the algorithms and provides some extra detail about the methodology used for this research.

2. Methodology

2.1 THE SIMULATION ENVIRONMENT

As testing and comparing the new QP algorithms directly on a real-world network section is impractical, microsimulation models were used to initially test speed-based (QP) algorithms. The new algorithms will be capable of operating with data sources based on fixed detectors and / or FVD technology. Within the microsimulation environment the existing HiOcc2 algorithm can be replicated and used as a benchmark against other QP algorithms, new algorithms can be implemented and multiple penetration rate scenarios can be tested and compared and overall network performance can be measured.

A simulation environment has been created which allows testing of control algorithms in a range of different scenarios. For this work, the microsimulation software PTV VISSIM 10 (hereafter known as VISSIM) has been used.

VISSIM is a microscopic traffic simulation software package that considers the movement of individual vehicles. The physical movement and decision-making process of each vehicle within the model is determined in response to infrastructure, traffic control systems and other vehicles.

VISSIM also contains an API (application programming interface), an implementation of Microsoft's component object model (COM) which enables access to the VISSIM model through external programming languages. In this instance, traffic control algorithms can be developed in Python and then implemented in VISSIM. This simplified architecture is shown in Figure 1.

FIGURE 1

Simplified model architecture

Traffic microsimulation environments by default represent a "perfect" system that is free of traffic incidents. Therefore, implementation of flow breakdown scenarios is not one of the standard capabilities of VISSIM. In order to allow the triggering of QP algorithms in the models that have been developed for this project, the behaviour of a subset of vehicles/traffic signals has been altered within the COM interface so as to "generate" flow breakdown conditions. These conditions are expected to be representative of the actual conditions observed in real queues however they are by no means identical.

2.2 SITE SELECTION

The modelling activities focussed on sub-sections of two network sections (M25 J20-19 and M42 J10-9). The models used data from representative high-density conditions following morning peak hour periods. The chosen sites are representative of typical motorway and a typical expressway which permits generalisation of outcomes for the wider road network.

Within the microsimulation environment the existing HiOcc2 algorithm has been replicated and used as a benchmark against other QP algorithms. Different scenarios have been tested and compared to objectively understand their relative performance.

2.3 MODELLING FLOW BREAKDOWN

One of the most critical tasks of this work is the representation of queues within the models. Queue creation is not a built-in capability in simulation software. Therefore, queues had to be created by altering vehicle behaviour within the models in a way that low speed and high-occupancy conditions would "naturally" occur in the models.

- On the M25 J20-19 the queue was created by artificially slowing down simultaneously a subset of the vehicle fleet (approximately 10 vehicles per simulation run) for a short period of time within a limited network area (up to 500 metres long). The speeds of the slowing vehicles were changed from free flow speed to 7mph for 15 to 20 seconds. This activity occurred once per seed and created a shockwave condition which propagated upstream, akin to that created from vehicle interactions in high-density traffic environments.

› On the M42 J10-9 the queue was generated by extending the duration of the red phase of traffic signals at the end of the off-slip. In this way, the slip road became saturated leading to the development of upstream queues on the mainline.

2.4 QP ALGORITHMS

The simulation models were built in order to examine and compare network performance under different QP-algorithm scenarios and data collection methods in the two study areas. The existing QP algorithm (HiOcc2) was set to be the baseline scenario of these comparisons. Table 1 summarises the main characteristics of the QP algorithms.

TABLE 1:

Examined QP algorithms

Algorithm name	Data source	Variables used	Data temporal aggregation	Data spatial aggregation	Penetration rate
QP-FVD 3%	Floating vehicles	Speed	60 or 30 sec*	100 metres	3%
QP-FVD 15%	Floating vehicles	Speed	60 or 30 sec*	100 metres	15%
QP-FVD 25%	Floating vehicles	Speed	60 or 30 sec*	100 metres	25%
HiOcc2	Fixed infra-structure (MIDAS)	Speed & occupancy	1 sec	MIDAS site (location specific)	N/A
QP-Watchdog	Fixed infra-structure (MIDAS)	Speed	1 sec	MIDAS site (location specific)	N/A

** Both 60sec and 30sec temporal aggregation have been modelled*

The microsimulation models have been developed to demonstrate the relative differences between the QP algorithms. Each model was run using 15no. independent seeds. To demonstrate suitability of the traffic models, the modelled and observed speed distributions have been assessed. In both models, the modelled distribution is not identical to the observed, but they are not significantly different in terms of range central tendency measures.

Each algorithm will be referred to using the above names in the results section. At this point it is important to note that all QP-FVD algorithms have been tested separately under two temporal aggregation scenarios of 60 and 30 seconds respectively. Typically, FVD are provided with every 60 seconds by most providers, which might not be sufficient for timely queue detection. Therefore a 30-second aggregation has been also tested.

2.5 PERFORMANCE MEASURES AND EVALUATION

In order to compare the various data collection methods and the different QP algorithm scenarios it is essential to develop a performance measure for QP algorithms. As QP aims to reduce the risk of accidents due to sudden braking, an appropriate QP algorithm should foremost identify queues as soon possible so as for the reduced speed limits to be set in time. The measure that has been established to evaluate the ability of a QP algorithm to identify queues is “time to detect” (TTD). TTD is the difference between the time point that a queue is generated with the time point that the QP raises the alert.

Additionally, a QP algorithm should stop the alert when traffic in the affected area has recovered to increase traffic throughput. The measure that has been selected for that purpose is “duration of alert” (DOA). DOA can be estimated as the difference of the time point that the initial alert was raised with the time point when the alert was stopped. As QP is primarily a safety-related application the project evaluated QP algorithms by comparing mainly TTD. DOA has also been estimated and is presented in the results section for completeness.

3. Results

3.1 M25 JUNCTION 20-19

Figures 3 and 4 show the results as ‘boxplots’ relating to TTD for the various scenarios, using 60 and 30 second periods, respectively. The charts show the minimum, maximum, 25th, 50th, 75th percentile values and the mean time to detect (see Figure 2).

FIGURE 2

Key to boxplot data

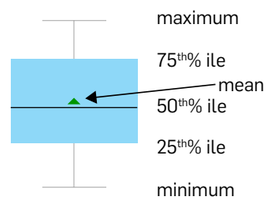

The mean TTD is significantly higher for all QP-FVD algorithms compared to both QP algorithms (HiOcc2 and QP-Watchdog) which employ fixed infrastructure data. The differences in TTD between FVD-based and MIDAS-based algorithms spans between 17 to 40 seconds which is considerable for safety-related applications. This finding does not immediately suggest that FVD inputs are unsuitable for QP algorithms and should be attributed primarily to the high temporal aggregation of FVD. In other words, QP-FVD algorithms can update their alert state on a minute-by-minute basis which often leads to delays in the detection of queues.

FIGURE 3

Boxplots of TTD on M25 J20-19 (QP-FVD @ 60-second speed data)

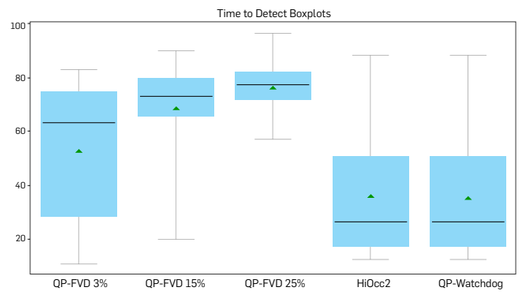

FIGURE 4

Boxplots of TTD on M25 J20-19 (QP-FVD @ 30-second speed data)

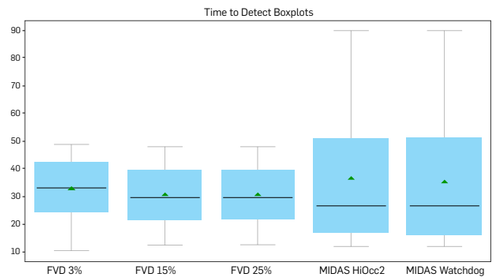

It can be observed that the average TTD is lower for the QP-FVD algorithms which employ a smaller proportion of floating vehicles. Although this result is counterintuitive, as higher penetration rates are expected to enhance data quality and results' robustness, it can be explained. At very low penetration rates, (i.e. 3% in this case) the sample of vehicles is more likely not to be representative of the entire vehicle fleet. The average speed produced by a non-representative vehicle sample could be different from the dominant traffic conditions on the network. This is supported by the fact that the coefficient of variation of TTD rises as the penetration rate was observed to decrease. This means that between independent simulation runs the speeds that were reported by FVD at low penetration rates were more inconsistent and hence sometimes significantly lower than other times, mainly by chance. As measures of central tendency like the mean are often affected by extremely high or low observations, this results to lower the mean values.

3.2 M42 JUNCTION 10-9

Figures 5 and 6 show the results relating to TTD for the various scenarios, using 60 and 30 second periods, respectively. On the M42, the FVD-QP algorithms outperform both HiOcc2 and QP-Watchdog even at the minute-level aggregation. The relatively low performance of the MIDAS-based algorithms in this case is mainly related with the relative positioning of MIDAS stations and the congestion seedpoint. As the queue always starts at the diverge area and the closest upstream MIDAS detector is ~400m upstream from it, the queue is not detected until it propagates to that point. This highlights the flexibility of FVD for similar applications that in some road geometries and queueing scenarios could prove very beneficial.

Lower temporal aggregation of FVD seems to reduce TTD by approximately 20-40 seconds. Therefore, both models suggest that FVD would perform significantly better at lower temporal aggregations for a queue protection application.

FIGURE 5

Boxplots of TTD on M42 J10-9 (QP-FVD @ 60-second speed data)

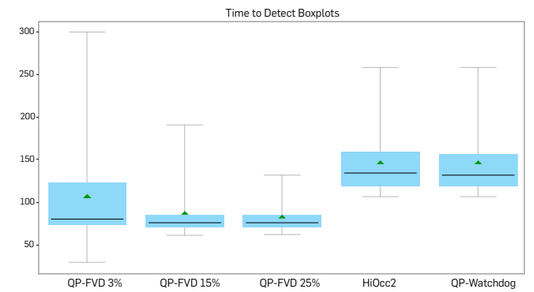

FIGURE 6

Boxplots of TTD on M42 J10-9 (QP-FVD @ 30-second speed data)

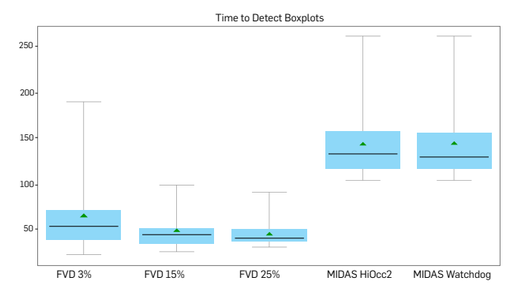

In terms of the FVD penetration rates, in this case results are comparable between all FV penetrations with lower penetrations having slightly lower performance. Additionally, as expected, low penetration (3%) includes higher variability between simulation runs which implies potential performance inconsistencies in a real-world application.

In the M25 model with closely spaced MIDAS detectors, the MIDAS TTD is shorter than it would be in more typical locations with 500m spacing. This means that with a 60 second aggregation period the QP-FVD is slower to detect, and the results show that a 30 second aggregation would be required to match the existing MIDAS performance at this location.

In the M42 model the MIDAS detector is 400m upstream of the off-slip where the queue forms, so the QP-FVD TTD performance is consistently better than the MIDAS. This demonstrates that FVD has the potential to match MIDAS TTD performance; in some cases, a 60 second aggregation period would be sufficient, but in others not.

The project also investigated the DOA metrics across all modelled scenarios. Whilst not presented in this short paper, the results show that DOA performance is generally worse with FVD than with existing MIDAS; however, this situation could be improved with further calibration and modifications to the algorithm. The impact of the high DOA on the actual signal settings would need to be investigated further, as the response of the overall system is dependent on other factors as well as individual alerts being cleared.

4. Summary and Conclusions

The two models used different techniques to generate queuing traffic profiles representing the formation of queues due to both capacity exceedances and off-slip queuing; both common characteristics on the motorway network. The models used observed speed and flow data and were validated using the speed distributions.

The modelling results demonstrate that FVD should be suitable for QP applications on the strategic road network. However, the performance relies heavily on temporal aggregation. Minute-by-minute speed measurement updates in FVD may not be sufficient to match existing MIDAS in all scenarios, as found in the M25 model. However, the performance of 30 second FVD is comparable and often outperforms MIDAS data in terms of the TTD a queue. More sophisticated speed only FVD algorithms could possibly improve this performance further.

Low FVD penetration rates are prone to variable and inconsistent speed measurements, a fact that may have direct impact on the performance of the QP algorithm. Higher penetration rates provide more reliable speed measurements However, the results also show that very high penetration rates do not necessarily improve data quality and hence performance of the algorithms. It is likely that the minimum penetration is between 3% and 15%.

Speed-based QP algorithms perform very well in queue detection but seem to achieve a longer duration of alert. This limitation could be fixed with further exploration and refinement of the algorithm thresholds. It might also be the case that this would not have a significant impact on signal settings when the system is considered overall.

Acknowledgements

This paper draws on the work undertaken for Highways England and is published with the permission of Highways England. The views contained in this paper are those of the authors and not necessarily those of Highways England. © Crown

This paper was originally accepted for publication at the 14th ITS European Congress, Lisbon, Portugal, 18 - 20 May 2020.

References

› [1] J Hayden, P Kirby, A Fisher, O Haas; Investigating the feasibility of improving strategic road network management algorithms in England; 25th ITS World Congress, Copenhagen, Denmark, 17-21 September 2018

› [2] A Harrison, D Williams, J Hayden, P Kirby, A Fisher; Simulation of queue protection algorithms for inter-urban highways; 13th ITS European Congress, Brainport, the Netherlands, 3-6 June 2019

A Road Marking Recognition and Condition Assessment System

Swarup Patra

Data Scientist, Global Design Centre
Engineering, Design and Project Management
Bangalore, India

Anshika Rawal

Data Scientist, Global Design Centre
Engineering, Design and Project Management
Bangalore, India

Vaishak Shanbhag

Technical Manager- Data Analytics, Global Design Centre
Engineering, Design and Project Management
Bangalore, India

Abstract

The advent of deep learning in computer vision has made Autonomous driving assistant systems (ADAS) and pavement asset management more efficient. With more open datasets, we predominantly see objects like traffic signs, signals, pedestrians, and potential road damage. Road Markings are an important aspect in these pavement assets because they provide traffic guidance information for vehicles and pedestrians. In this paper, we have proposed a Road Marking recognition and condition assessment system. We have used a state-of-the-art segmentation model (Mask R-CNN) as the baseline and carried out different experiments to detect and classify the Road Markings; thereby giving us a mean average precision (mAP) of 0.84. Furthermore, we have used ResNet-50 to classify the condition of these road markings into six categories (No Wear, Very Little Wear, Marginal Wear, Visible, Barely Visible, Non-Existent Wear) with 85% accuracy. Additionally, we have produced a dataset that gives a holistic view of Road Marking asset condition, which covers the commonly found 5 types of markings on the road.

KEYWORDS

Road Marking detection; Instance Segmentation; Classification; Mask RCNN, ResNet 50

1. Introduction

Road surface markings are the signs drawn on the surface of the road to convey official information. These markings are used on paved roadways to provide direction and information to drivers and pedestrians. An autonomous system or driver assist system has a wide range of sensors to recognize several factors of the environment and the road. Road markings indicate many of these characteristics and play a major role in the environment by providing uniform and unique information like arrows for turn lanes, overtaking regulations, and other information. Road markings are just as important to detect as traffic lights and road signs when it comes to driver assistance and navigation systems. It's a constant challenge to keep track of wear and tear of road markings. Regular estimates and action plans are necessary for conditioning the road markings. Throughout the world, the process of monitoring the state of road markings and conditioning them is completely manual or forgone altogether because it is time consuming and highly inefficient. With recent advancements in hardware, deep learning has been extensively used in computer vision tasks such as object detection and classification with real-time performance and good accuracy.

There has been a large amount of work done on traffic signals and road signs but the computer vision work on road markings is limited. Traditionally, road marking detection methods [1][2] mainly depend on highly specialized hand-crafted features such as FAST [3] and HOG [4], etc. These traditional approaches are not robust enough to handle variations in road scenes, weather, and lighting. This which results in a drop in performance.

Most recent methods include deep neural networks to replace traditional handcrafted feature-based detectors. A paper by Bailo, et al. [5] proposes a method to extract the MSERs (multiple regions of interest) [6] and classifies region proposals by PCANet [7] and a neural network after merging the MSER, which likely belong to the same class.

Recent work on road markings does not include information about the conditions of the markings themselves. The condition of the road markings in data can be used for quality assurance and road maintenance, which leads to improved autonomous driving and traffic safety.

The lack of public dataset for road markings and their respective condition remains another challenge. Large datasets for training and evaluation of road markings are scarce and some of the popular datasets do not contain labels. Available datasets are often insufficient and limited. A paper by Veit, et al. [8] provides a comparison of different methods for road marking detection along with the dataset. In another paper, Lee et al. [9] published benchmarks for road marking detection along with a custom algorithm, VPGNet.

However, these datasets do not contain the type of road markings in ground truth or the condition of the markings.

In this paper, we have produced a dataset that covers the most commonly found road markings. To the best of our knowledge, this dataset gives the most holistic view of the conditions of Road Markings. Currently, the dataset is used for detection of five categories of Road Markings: No Obvious Wear, Very Little Wear, Marginal Wear, Visible, Barely Visible, Non-existent. The dataset consists of 7,376 images that are manually annotated with respective road markings and their conditions. In addition to that, we have used a Mask R-CNN baseline and carried out different experiments to detect and classify the Road Markings. Furthermore, we have used ResNet-50 to classify the condition of these road markings in six categories to assess the condition of these road markings.

Our contributions cover the following:

- We designed an end-to-end unified, trainable multitasking pipeline that jointly handles the detection and recognition of road markings and the assessment of their condition to classify the severity of the wear.
- We have provided the evaluation of both neural networks used for detection and recognition of the road marking using Mask RCNN along with classification using ResNet-50 to classify the condition of these road markings in six categories on the produced dataset. The results show robustness with real-time performance.

The rest of the paper is organized as follows:

- Section 2 describes the dataset produced for road markings and explains the pipeline for road marking detection and the assessment of their conditions along with the network architectures and training scheme used in our methodology.
- Results are reported and explained in Section 3.
- Section 4 provides the discussion.
- Section 5 concludes what we achieved.

2. Methodology

2.1. DATASET DESCRIPTION

We had access to frontal images, collected using a camera mounted on vehicle provided by CPS. The types of road surfaces in our dataset varied from concrete to asphalt. Images are captured sequentially at one image per second. The density of traffic varied from a few vehicles to no vehicles on the road. The entire dataset was comprised of 7,376 images of roads in the UK. The images were primarily captured during sunny and dry conditions. Shapes and symbols of the road markings followed UK regulations. We collected images in two runs: the first run produced 5,664 images at 2160*3840 resolution and the second run produced 1,712 images at 1080*1920 resolution.

The dataset was divided into five Road Markings categories: arrows, boundary, chevron, line - demarcation, and slips along with their respective condition. We used "UEA COMPUTER VISION" annotation tool [10] to annotate the images with the five types of road markings. The markings were also classified based on their conditions: no obvious wear, very little wear, marginal wear, visible, barely visible, and non-existent only. The annotation tool generates a JSON file containing the following information: i) bounding box around road marking(s); ii) annotated road marking class(es);

TABLE 1:

Number of instance for each road marking in dataset

Road Marking	Number of Instances
Line - demarcation	54122
Boundary	20983
Chevron	9778
Arrows	984
Slips	7488

and iii) condition class(es) of that road marking(s). Considering the input size of our network, all the images are resized to a fixed 512*512 resolution. In total, 7,376 images are split in training and testing set with 6,270, 1,106 number of images respectively. The number of instances for each road marking classification in the dataset is shown (Table 1) as well as the number of instances for corresponding conditions of road marking (Table 2).

TABLE 2:

Number of instances for each severity type in dataset

Condition of Road Markings	Number of Instances
No-wear	76797
Very little wear	9451
Marginal	3309
Visible	1858
Barely visible	1289
Non-existent	651

2.2. Algorithms

The purpose of this system is to detect and recognize the road markings and classify them based on their condition. For this purpose, we have used instance segmentation using Mask RCNN. Additionally, we have classified detected road markings under different conditions (no wear, very little wear, marginal, visible, barely visible and non-existent) using a classification network.

FIGURE 1

Training pipeline

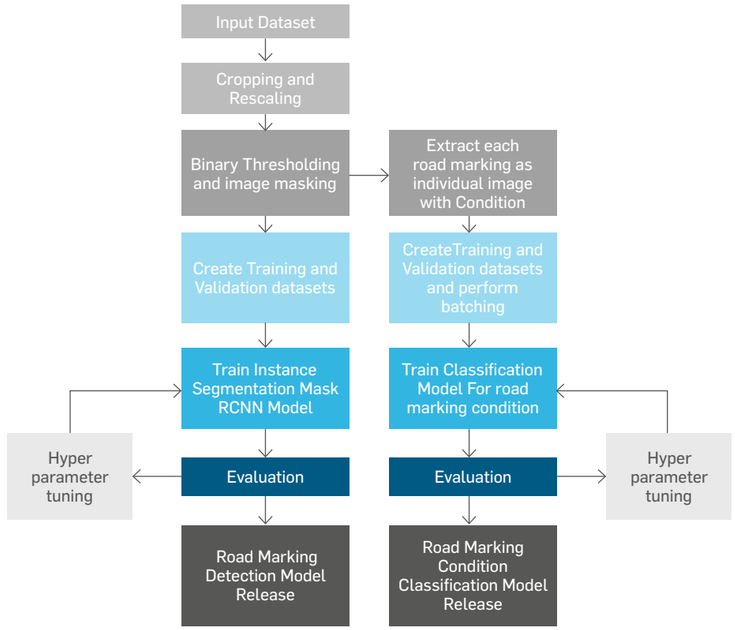

The training pipeline is shown in Figure 1. The description of each step is given below. In order to execute the whole pipeline, we need to train two networks. The first network is trained for detection and recognition of road markings and the second network is trained for classification of detected road marking condition. The two networks are:

- Mask R-CNN instance segmentation network
- Classification network for condition

2.2.1. MASK R-CNN INSTANCE SEGMENTATION NETWORK

This process is typically distributed into two parts, where the first part deals with the data preparation for training and the second part involves the training of actual network. Each process is explained in more detail below.

2.2.1.1. TRAINING DATA PREPARATION

Due to the neural network input size, all of the images have to be resized into a fixed dimension of 512*512. In annotation files, the same transformation has to be applied to corresponding bounding box. As the road markings were in white pixel, the binary threshold (>0.55) was applied to enhance the visibility of the road markings. Binary thresholding converts the colored image (see Figure 2(a)) into a greyscale image that contains the road marking information in white pixels while the rest of the image contains black pixels (see Figure 2(b)). After applying the binary threshold, the resized greyscale images are sent through training process along with an array that contains the bounding box(es) and class(es) for each road marking.

FIGURE 2

(a) Original input image [left] and (b) Processed image [right]

2.2.1.2. TRAINING THE ACTUAL NETWORK

We have only considered the road marking classifications while leaving the condition classes out of the training process of Mask RCNN.

The Mask-RCNN [11] model was developed in 2017. The model an extension of the Faster-RCNN model for semantic segmentation and object instance segmentation of images. Mask-RCNN outperformed all existing single-model programs for object detection in the 2016 COCO Challenge. Mask-RCNN relies on a region proposals which are generated via a region proposal network.
A few of the important steps that we have used for training are:

- The model was trained on network heads using pretrained model weights with a learning rate of 0.001. After a few epochs it was changed to 0.0001. For the last 5 epochs, 15 to 20, the model was trained with a learning rate of 0.00001.
- We have used different types of image augmentation such as flipping and rotating of images, scaling of images, etc. The purpose of augmentation is to provide the model with a wider variety of data distribution that may be available in the unseen data.
- Number of training steps per epoch was around 3,000.
- Figure 3 indicates that the model has learned well as the training loss function has subsequently decreased.

FIGURE 3

Training Loss

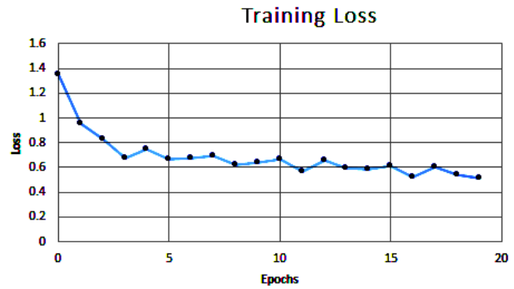

2.2.2. CLASSIFICATION NETWORK FOR CONDITION

For classifying the condition of the road markings into 6 classes mentioned above, we took individual detected road markings, cropped and resized them into a fixed size (32,32). Similar to the segmentation network training, the classification network training consists of two parts.

2.2.2.1. TRAINING DATA PREPARATION

For data preparation of classification network, we created a table (DataFrame) which extracts the bounding box information and corresponding condition classes from annotation files while leaving out the road marking classes for each image in training dataset. We cropped the images using bounding box information into a fixed size (32*32). We exported the table (DataFrame) for further training process.

2.2.2.2. TRAINING ACTUAL NETWORK

We imported the file generated in previous training data preparation and split the entire table (DataFrame) into training and validation sets. We considered a batch size of 32. So, before passing the image into the network, we grouped the entire table (DataFrame) rows into a batch of 32 so that new dimension of each data would be 32*32*32. Each batch data is fed to the network after normalizing to scale [0:1],

We used a simple ResNet50 backbone network followed by few convolutional layers and a fully connected layer. The Residual Network (ResNet) is a model that makes use of the residual module involving shortcut connections. It was developed by researchers at Microsoft and described in the 2015 paper "Deep Residual Learning for Image Recognition." [12].

FIGURE 4A

Learning rates during each epoch

Figure 4(a) depicts the learning rate used at each epoch and Figure 4(b) shows the training loss curve that indicates that the model has learned well due to the loss decreasing at subsequent epochs. The best model weights were saved to be used for the inference.

FIGURE 4B

Training loss curve after each epoch

2.2.3. INFERENCE PIPELINE

As shown in the block diagram below, the data preparation process remains the same for the inference process. The pre-processed data is consecutively passed into both of the models to predict the road marking class(es) and the condition class(es). The evaluation of performance of both the models was conducted by comparing the prediction output to the ground truth value and measured using different metrices such as mAP, confusion metrics, and accuracy.

FIGURE 5

Inference Pipeline

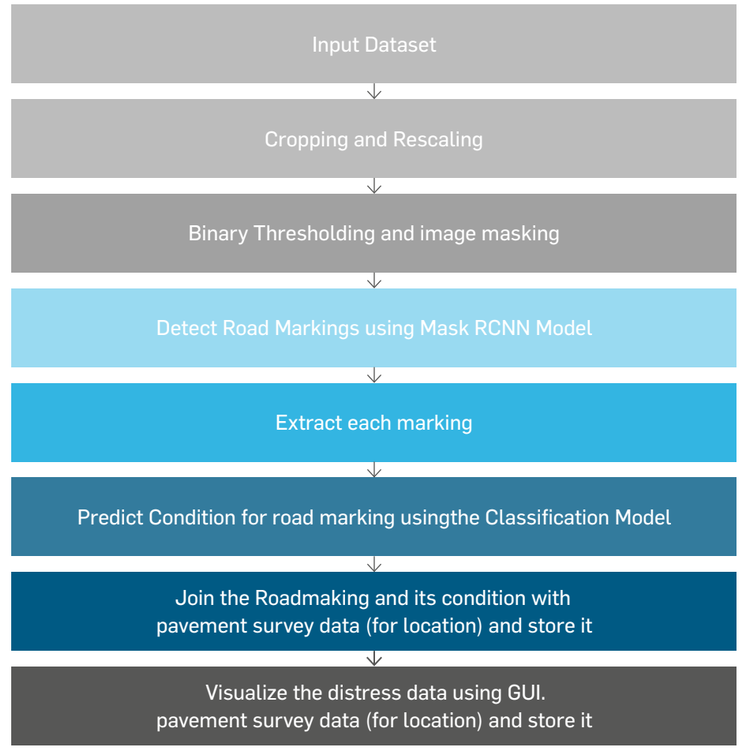

3. Results

We used a total of 1,100 images for testing. The image below represents the confusion metrics which depicts number of classes in the ground truth data and how many were accurately classified. In Figure 6, the i^{th} row shows the predicted values and the j^{th} column shows the actual ground truth values. For example, Line-Demarcation has been classified correctly for 6,737 samples, majorly misclassified 48 of them as boundary and misclassified 11 as chevron.

FIGURE 6

Confusion matrix

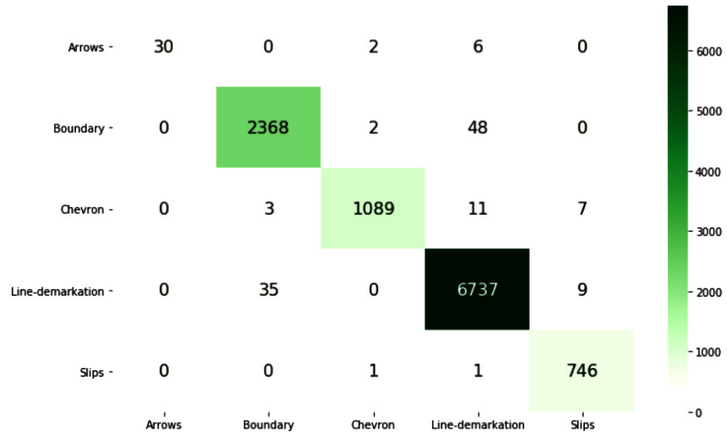

The mean average precision (mAP) is the metric used to quantify the accuracy of the model. Table 3 shows the mAP values along with true positive (TP), false positive (FP), and false negative (FN) for each of the class.

TABLE 3

Performance metric for Mask RCNN

No.	Asset Name	Number of Assets	mAP	TP	FP	FN
0	Arrows	62	0.717029	30	8	32
1	Boundary	2997	0.803494	2368	691	629
2	Chevron	1448	0. 810548	1089	289	359
3	Line Demarcation	7798	0. 883560	6737	552	1061
4	Slips	911	0. 851882	746	291	165

Figure 7 shows the accuracy on the validation dataset for the ResNet50 classification model. We reached an accuracy 85%.

FIGURE 7

Accuracy plot for ResNet50

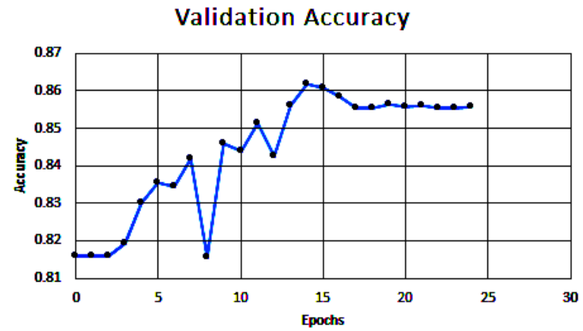

FIGURE 8

Sample input

FIGURE 9

Sample output

Figure 8 is the original image captured by a camera mounted on a vehicle. It shows several road markings such as chevron, line-demarcation, and boundary. As we can see in Figure 9, the system successfully recognized the chevrons and determined its condition assessment as very little wear with 0.99 probability. Similarly, other markings, such as line-demarcation and boundary, are recognized with adequate probabilities and the conditions of detected road markings are classified with considerably good accuracy.

4. Discussion

We explained a system for detecting road markings and classifying their conditions along with the dataset that we've produced. Our experiments for road markings detection are carried out using Mask RCNN baseline and the classification of detected road markings condition was done by using ResNet50. This system can be easily adapted for an increased number of road markings. This system has ability to work well in proper light condition and with a few variations in road scenes.

There is a wide area of application for computer vision using deep learning in the ACE industry. Just sticking to roadways, the technique can be used to create inventory of right-of-way assets along the road. Conditions of roads and right-of-way assets can be evaluated using this technique. Additional benefit is that all of this data can be collected as part of single survey. Condition of footpath and cycle paths can be done much more efficiently using this technique, thus helping local transport agencies offer better services to pedestrians and cyclists.

Remote sensing or aerial survey using fixed wing aircrafts or drones can also be used to study geological features for analysis. This could include applications in ecological study or for horizontal assets like roads, rails, pipelines, etc. Unmanned vehicles can undertake inspections of large structures like bridges, tanks or underwater structures. The video data collected can be inspected using smart algorithms to detect defects, like corrosion, for early intervention.

Some areas, like underground sewers or subway tunnels, are difficult to inspect and can potentially be unsafe. Video survey for such assists can be analyzed by algorithms to spot vulnerabilities in structure which might lead to unsafe situations or disruptions, thus avoiding costly unplanned repairs and losses in terms of claims/penalties. Use of automated analysis will allow improved coverage of the network considering only sample surveys are carried out for assets when done manually.

We apply the binary thresholding to make the road markings more visible, which enables neural net to perform better. However, when lighting conditions are poor or there are too many shadows, it might be difficult to separate out the road marking after binary thresholding due to the impacts on contrast. As of now, we have not included these scenarios in our experiments. Also, our dataset does not include data under challenging weather conditions or different lighting conditions (night, shadows, etc.).

We believe that the training on providing more diverse data will enhance the ability to perform better under different weather and lighting. Some shadow removal techniques can be used in the future to eliminate the difference in contrast while applying the binary threshold. Aside from that, in future work, we can add more instances of existing road marking types under varying lighting as well as we can increase the number of road markings by adding the images of new road markings and labelling them.

Additionally, we have developed a user-friendly interface to interact with the output of the model, where images are presented with geospatial context. As we can see in Figure 10, a section can be selected from selection control on the left side of UI to visualize an overview of the condition of road markings. The right side of Figure 10 shows how each image can be inspected for the detected road markings and their conditions. Additionally, you can filter the type of wear for granular analysis. This detailed condition data can be aggregated further and joined up with other data sets to create a decision support tool for effective upkeep of the assets. We believe that AI assisted road marking detection and the condition assessment system is more cost and time effective than any existing process.

FIGURE 10

User Interface for Road Marking Detection and Condition Assessment

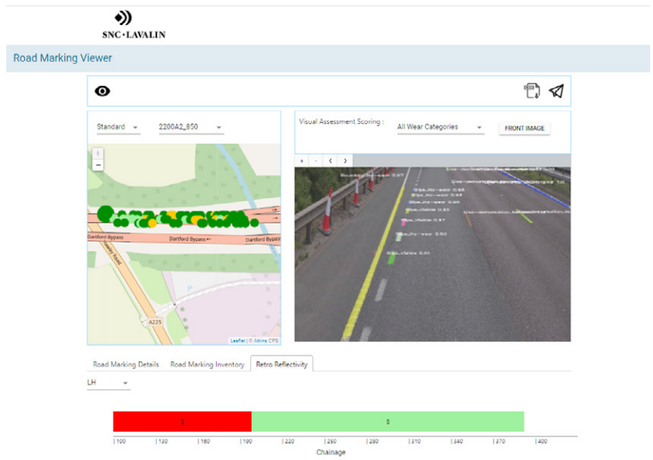

5. Conclusion

In this paper, we have proposed systems for detecting and recognizing road markings as well as for evaluating the conditions of detected road markings. We used a state-of-the-art segmentation technique and carried out experiments to detect road markings with considerably good accuracy. Furthermore, we used ResNet-50 to classify the condition of these road markings into six categories. Additionally, we produced a dataset containing ground truth labels for road marking detection and assessments of their conditions. To avail the dataset please reach out to the authors or the organization.

We have concluded that the produced dataset presents a holistic view of road marking asset condition which can be efficiently used by various underlying tasks. The performance evaluation of the proposed system proved that it is robust and a potential solution for assisting local transport agencies to offer better service to their users. Moreover, enhanced analysis can be undertaken if the image/video dataset can be fused with other dataset like LIDAR point cloud data. Additionally, we have developed a user-friendly interface which enables the users to visualize the results as well as assisting in rapid decision making about the conditions of road markings.

Acknowledgements

We would like to extend our appreciation to Janpreet Singh and Martyn Clarke for their valuable input and fruitful technical discussions to enrich our work. We would also like to thank Ewan Hobbs, Kiran k., Michael Wright, Santhosh M Kumar for providing their valuable suggestions, enthusiastic encouragement and constructive critiques during the planning and development of this project. We would also like to thank Maheshwar Behera for developing a user interface for the visualisations. This work was part of the deliverable to our esteemed client Connect Plus UK.

References

- Wu, Tao, and Ananth Ranganathan. “A practical system for road marking detection and recognition.” In 2012 IEEE Intelligent Vehicles Symposium, pp. 25-30. IEEE, 2012.
- Greenhalgh, Jack, and Majid Mirmehdi. “Automatic detection and recognition of symbols and text on the road surface.” In International Conference on Pattern Recognition Applications and Methods, pp. 124-140. Springer, Cham, 2015.
- Viswanathan, Deepak Geetha. “Features from accelerated segment test (fast).” In Proceedings of the 10th workshop on Image Analysis for Multimedia Interactive Services, London, UK, pp. 6-8. 2009.
- Dalal, Navneet, and Bill Triggs. “Histograms of oriented gradients for human detection.” In 2005 IEEE computer society conference on computer vision and pattern recognition (CVPR’05), vol. 1, pp. 886-893. Ieee, 2005.
- Bailo, Oleksandr, Seokju Lee, Francois Rameau, Jae Shin Yoon, and In So Kweon. “Robust road marking detection and recognition using density-based grouping and machine learning techniques.” In 2017 IEEE Winter Conference on Applications of Computer Vision (WACV), pp. 760-768. IEEE, 2017.
- Matas, Jiri, Ondrej Chum, Martin Urban, and Tomás Pajdla. “Robust wide-baseline stereo from maximally stable extremal regions.” Image and vision computing 22, no. 10 (2004): 761-767.
- Chan, Tsung-Han, Kui Jia, Shenghua Gao, Jiwen Lu, Zinan Zeng, and Yi Ma. “PCANet: A simple deep learning baseline for image classification.” IEEE transactions on image processing 24, no. 12 (2015): 5017-5032.
- Veit, Thomas, Jean-Philippe Tarel, Philippe Nicolle, and Pierre Charbonnier. “Evaluation of road marking feature extraction.” In 2008 11th International IEEE Conference on Intelligent Transportation Systems, pp. 174-181. IEEE, 2008.
- Lee, Seokju, Junsik Kim, Jae Shin Yoon, Seunghak Shin, Oleksandr Bailo, Namil Kim, Tae-Hee Lee, Hyun Seok Hong, Seung-Hoon Han, and In So Kweon. “Vpgnet: Vanishing point guided network for lane and road marking detection and recognition.” In Proceedings of the IEEE international conference on computer vision, pp. 1947-1955. 2017.

- University of East Anglia, Norwich, UK (2020) Image labelling tool [Source Code]. https://bitbucket.org/ueacomputervision/image-labelling-tool/.
- He, Kaiming, Georgia Gkioxari, and Piotr Doll. “ar, and Ross, Girshick.” Mask r-cnn. In, ICCV 1, no. 6 (2017).
- He, Kaiming, Xiangyu Zhang, Shaoqing Ren, and Jian Sun. “Deep residual learning for image recognition (2015).” arXiv preprint arXiv:1512.03385 (2016).

Thermal Buckling of Ballasted Tangent Track

Nazmul Hasan

Principal Track Expert
Engineering
Engineering Design and Project Management
Vancouver, Canada

Abstract

Euler-type analysis usually used for compression members in structural engineering does not work for railroad track. Euler-type analytical formulas for horizontal and vertical buckling endorsed in a recent literature is reviewed to demonstrate its weakness. Using definition of moment and curvature as well as principle of equilibrium, the author suggests formula for horizontal buckling load of railroad track and demonstrates validation in context with currently accepted values, published results, and past field tests. The buckling load from suggested formula agrees with the recent buckling load formula based on total energy theorem. A vertical buckling load formula is derived from horizontal buckling load formula. A buckling process is narrated through step by step computation. Formulas are suggested to compute the effect of track misalignment on critical buckling load and threshold radius of a vertical curve.

KEYWORDS

Ballast resistance; Critical temperature differential; Euler buckling load; Stress neutral temperature; Thermal buckling

1. Introduction

In terms of analysis, buckling in a railroad track is a quite complex phenomenon due to the following:

- The “end” conditions of the rails are neither perfectly fixed nor perfectly pinned nor free, but provide varying rotational and lateral resistance depending on numerous factors;
- Resistance to lateral displacement is provided by the lateral stiffness of rails, track frame, and ballast resistance;
- Railroad track invariably contains initial curvature and imperfections; and,
- Axial loading through the centroid of the track would seldom occur, etc.

Literature review of track buckling field tests is done to present the track buckling load, amplitude of deflection, etc. The information from these field tests are subsequently used to validate assumption used, findings made, and formula derived by the author.

In 1975, Kerr detailed the short comings of field tests and analytical formula (Kerr, 1978). Kerr stated that the field test spans were short. The author established that field tests spans are not short to determine buckling load only, rather they are short to capture the whole buckling process. The author suggests two field test spans: one to determine only buckling load, and the other to capture both buckling load and modal shape of buckling.

Since the early 1930s till 1978, many track stability analyses were published but no reliable analyses are available to compute the buckling load or buckling temperature differential of a railroad track (Kerr, 1978). The linear differential equation used to describe lateral response of a buckled track is based on the plane section hypothesis whereas in an actual track this assumption is not satisfied, because the ties and fasteners are not rigid (Kerr, 1978). Euler-type analysis is applied on compression members; if the length between two supports increases buckling load decreases. In case of track, lateral displacement is resisted by ballast resistance and the buckling load remains same whatever be the track length. The length of a test track should be sum of length of buckled track and breathing length at both ends of buckled track (Kerr, 1978). The actual buckling load is supposed to be more than the buckling load in the field if the test track is too short. Thus, a minimum length is required for a test track; buckling load would be same for all test spans beyond the minimum length as buckling in railroad track is essentially a local phenomenon. A sufficiently long test track as suggested by Kerr would exhibit real life modal shapes in addition to buckling load. In 1932, A. Bloch showed that the analysis needed for thermal track buckling is different than the Euler-type analysis usually utilized in structural mechanics (Kerr, 1978).

A formula based on total energy theorem from recent literature is found to offer acceptable value of critical buckling load (Esveld, 2001). Two analytical formulas for horizontal buckling from recent literature are reviewed – Euler type one is found to be unacceptable and the other based on energy theorem is found to be acceptable. In the course of review, the equivalent lateral moment of inertia of a track frame is suggested to be ten (10%) more than the lateral moment of inertia of two rails of track. One Euler-type analytical formula for vertical buckling is reviewed and found to be unacceptable too.

Using definition of moment and curvature as well as principle of equilibrium, the author suggests formulas for horizontal and vertical buckling load and corresponding critical temperature differential. The formulas are applied and the results are validated against current acceptable formula from Esveld, field test data, currently accepted value, and published values of critical buckling load and temperature differential. A vertical buckling load formula is derived from the horizontal buckling load formula.

The buckling process from critical to fully buckled state is described step-by-step with related calculations. Finally, threshold radius of a vertical railroad curve is suggested to avoid vertical buckling.

2. Literature Review of Track Buckling Tests

The possibility of buckling of a pointless track due to constrained thermal expansion was discussed, as early as, 1902 by A. Harmann. This problem did not get attention of railroad research engineers until about 30 years later. From 1932, field tests were conducted to investigate track buckling on a test track segment. Some test cases are summarized from literature (Kerr, 1978).

A. Researchers, year	: O. Ammann and C.v. Gruenewaltt; 1932
Test track length	: 30m
Rail, tie, and track type	: Steel tie, K-type track
Load introduced by	: Hydraulic jack
Buckling mode	: Buckled in vertical plane
Track condition	: No information
Number of half waves	: One, 30m
Buckled length	: 30m
Amplitude of deflection	: 800mm
Critical/Buckling load, Pc	: 200 tons (approximately)
Critical temperature differential,	: 490C assuming E = 2.1x10^6 kg/cm^2, $\alpha = 1.18x10^{-5}/^0C$,
ΔT_C	A = 2x82.5 = 165 cm^2

B. Researchers, year	: O. Ammann and C.v. Gruenewaltt; 1932
Test track length	: 60m
Tie and track type	: Wood tie, K-type track
Load introduced by	: Hydraulic jack
Buckling mode	: Buckled in horizontal plane
Track condition	: No information
Number of half waves	: Two, each 19m
Buckled length	: 38m (= 2x19m)
Amplitude of deflection	: 400mm
Pc	: 200 tons (approximately)
ΔT_C	: 49^0C as calculated under A

C. Researchers, year, reference	: J. Nemcsek; 1933
Test track length	: 60m
Tie and track type	: Wood tie
Load introduced by	: Hydraulic jack
Buckling mode	: Except for one test, all seven test tracks buckled in horizontal plane. However, in a number of tests, a small lift off was observed before the test track buckled sideways.
Track condition	: Made up of worn rails with sizeable geometric imperfections
Number of half waves	: Two
Buckled length	: No information
Amplitude of deflection	: No information
Pc	: 180 tons
ΔT_C	: 44^0C (= 49x180/200; cf. case A)

D. Researchers, year	: F. Rabb; Technical University of Karlsruhe, Germany, 1934
Test track length	: 46.17m
Tie and track type	: Wood tie, K-type track
Load introduced by	: Heating rails by electric current
Buckling mode	: Buckled in horizontal plane
Track condition	: no information
Number of half waves	: Three
Buckled length	: No information
Amplitude of deflection	: No information
Pc	: 173 tons
ΔT_C	: 42.5^0C (= 49x173/200, cf. case A)

E. Researchers, year	: F. Birmann and F. Rabb; Technical University of Karlsruhe, Germany, 1960
Test track length	: 46.17m
Tie and track type	: Wood tie, K-type track
Load introduced by	: Electric current
Buckling mode	: The rail-tie structure did not lift off prior to horizontal buckling, but rather it lifted off simultaneously and gradually with increasing lateral displacements.

Track condition	: track has geometric imperfections.
Number of half waves	: Two, three or four, each 5m
Buckled length	: 10, 15, and 20m (computed)
Amplitude of deflection	: 250mm (max)
Pc	: 173 tons
ΔT_c	: 42.5^{0}C (= 49x173/200, cf. case A)
F. Researchers, year	**: British Transport Commission, 1961**
Test track length	: 36.6m
Rail, tie and track type	: Wood and reinforced concrete tie
Load introduced by	: parabolic reflector fitted with electric elements
Buckling mode	: The observed buckling mode consists of 1, 2, 3, or 4 half-waves. No information was given regarding vertical lift-off prior to and during buckling.
Track condition	: No information
Number of half waves	: One, two, three or four
Buckled length	: No information
Amplitude of deflection	: 250mm (max)
Pc	: 173 tons
ΔT_c	: 42.5^{0}C (= 49x173/200, cf. case A)
G. Researchers, year	**: E. M. Bromberg, Central Railroad Research Institute, USSR, 1966**
Test track length	: 100m
Rail, tie and track type	: P 65, Wood and reinforced concrete tie
Load introduced by	: Heating by electric current
Buckling mode	: The observed buckling mode consists of 3, 4 or 5 half-waves. No information was given regarding vertical lift-off prior to and during buckling.
Track condition	: Weakly compacted ballast
Number of half waves	: Three, four or five
Buckled length	: No information
Amplitude of deflection	: No information
Pc	: No information
ΔT_c	: No information
Observation	: When the temperature is raised from 60^{0}C to 103^{0}C, the track did not buckle. It means the track did not buckle at a temperature differential of 43^{0}C which corresponds to a load of 176 tons.

The aforementioned seven field tests yield a critical temperature differential of 42.5 -50^{0}C corresponding to a track buckling load of 173–200 tons; the lower buckling load was observed on test tracks with geometric imperfection. It appears that tie type does not influence buckling load. Geometric imperfections reduce the buckling load by 14%. The test track length varies between 30–100m with no significant drop of buckling load with increased length. This implies the buckling is essentially a local phenomenon and a test track of 30m length is adequate to capture buckling load only.

3. Literature Review of Formula to Compute the Critical Buckling Load: Tangent Track

Lichtberger endorses an analytical formula for tangent track from 1969 with a calculation example (Litchtberger, 2005 & Nemesdy, 1969). The following formulas and data are given for critical increase in temperature, critical load, and buckling length for a tangent track as under:

$$\Delta T_c = \sqrt{\frac{8.7 F_{QVW} I^*}{\alpha^2 A^2 E.f^*}} \quad (1)$$

$$F_0 = \alpha \Delta T_c . E . A \quad (2)$$

$$L = 3\pi \sqrt{\frac{2EI}{F_0}} \quad (3)$$

Data:
Rail: UIC 60
Tie: Concrete B70w tie, tensioned

I*	2200cm^4
A	2x76.9=153.8cm^2
F_{QVW}	100 N/cm
E	21000000 N/cm^2
α	0.000012/0C
f*	2-2.5cm

The critical temperature differential, ΔT_C and critical buckling load, F_0 are 115.7^{0}C and 4484 kN (450 tons) as per Eqs. (1 & 2). The ΔT_C of 115.7^{0}C is more than double of the field tests values (cf. 42.5–50^{0}C) and currently accepted value (cf. 50^{0}C). The critical buckling load of 4484 kN (450 tons) is more than double of the field tests values (cf. 173-200 tons) and currently accepted value (200 tons). Interestingly, Lichtberger labelled 50^{0}C temperature differential as a critical value for buckling (Litchtberger, 2005). A uniform temperature rise of 50^{0}C induces in the track an axial compression force of 204 tons which may be sufficient to buckle the track (Kerr, 1978). The following Table 1 gives some published values of critical temperature differential.

TABLE 1

ΔT_C compared to vertical and horizontal buckling with a tie spacing of 60 cm (American) [Esveld, 2001 & AREMA, 2019]

Rail weight (kg/m)	Comparable to rail profile	Mode of buckling vertical / horizontal	Critical increase in temperature [^{0}C]		
			wood	concrete	steel
47	115 RE	vertical / horizontal	46 / 49	-	46 / 56
59	UIC 60	vertical / horizontal	48 / 43	70 / 48	52 / 48
68	136 RE	vertical / horizontal	50 / 42	69/46	52 / 47

AREMA allows a thermal stress of 124 N/mm^2 (18000 psi) which corresponds to a temperature differential of 50°C (AREMA, 2019). AREMA needs to review its allowable thermal stress. The actual rise in temperature, ΔT amounts to 45–50°C considering the deviations occurring in practice when rails are tensioned (Lichtberger, 2005); from this it is evident that the critical temperature differential might be above 50°C but considering 50°C would be conservative. The Eq. (1) would suggest ΔT_C = 80°C if the lateral resistance, F_{QVW} is reduced by 50%; this implies that a track would not buckle at above 100°C (assuming a stress neutral temperature of 20°C) even if all ballast above tie-ballast interface is removed. Thus, if the value by the Eq. (1) is correct then there would have been no requirement of hot weather patrolling, no speed restriction on a tamped track without dynamic track stabilizer, no speed restriction on a newly laid track built without dynamic stabilizer, and no further research to enhancement tie resistance since 1969, etc.

The author intends to modify two aforementioned input data to check if the formula can still be used:

The equivalent moment of inertia of the track grid, I* with UIC 90 rail and concrete B70w tie is taken to be 2200cm^4 (Lichtberger, 2005). The moment of inertia of two UIC 90 rails, 2I is 1026cm^4 (Lichtberger, 2005). This implies track frame increases the lateral stiffness by 54%. The stiffness of rail-tie structure does not play a very important role in the lateral rigidity of the entire track. For example, it has been estimated that a ballast resistance increased by 10% is sufficient to compensate for the difference in stiffness of the tested track panels (Dogneton, 1978). The longitudinal load developed by the combination of thermal stress in a continuously welded rail and by traffic is restrained by mass internal friction of ballast (AREMA, 2019). The track frame contributes 5-10% towards the lateral resistance of the track (Esveld, 2001). The longitudinal resistance of a track equals to the lateral resistance of the track (Lichtberger, 2005); this implies that almost entire resistance comes from the ballast. Thus, the equivalent inertia of a track frame with UIC 60 rail can be at best 1130cm4 (= 1.1x1026cm^4). Using this value in the Eq. (1), the ΔT_C would be 83^{0}C; still the value is unacceptable.

The critical misalignment value, *f** given is in a range of 2-2.5cm. If 2.5cm is used, the ΔT_C would be 74^{0}C ((= 83x (2/2.5)$^{0.5}$); still the value is high and unacceptable.

The buckling length formula (ref: Eq. (3)) offers a buckling length of 13.53m which seems to be acceptable. The value of buckling length cannot be correct if the buckling load is faulty. The equivalent moment of inertia of the track grid is multiplied by two in the Eq. (3) which is not understood. With modified input data, the buckling length would be 6.85m (= 13.53(1130/(2x2200)$^{0.5}$)) which is too short to accept.

Thus, even with the modified input data, the above analytical equation (1) does not work.

On the basis of total energy theorem, the critical load is given by (Esveld, 2001):

$$P_c = 2\sqrt{\frac{\tau_0 EI}{\pi f_0}} \qquad (4)$$

The critical length is given by

$$L_c^2 = 2\sqrt{\frac{\pi^5 f_0 EI}{\tau_0}} \tag{5}$$

in which

EI bending stiffness,

f_0 critical misalignment,

τ_0 displacement resistance.

Based on following parameters:

$\tau_0 = 10\ \ kN/m,\ EI = 8000\ kNm^2, and\ f_0 = 0.025m$

the critical load is calculated to be 2018 kN which agrees with the past field test values. The wavelength is calculated to be 12.51m.

4. Derivation of a New Formula

A centerline of an initially tangent track which has been bent by the thermal load, P is shown in Fig 1.

FIGURE 1

Center line of a track under compressive load.

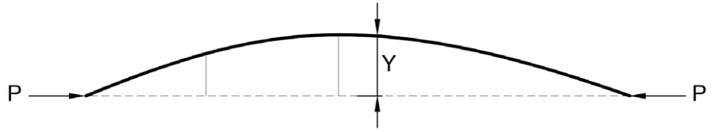

The bending moment at any point of the deflected centerline is given by

$$M = Py \tag{6}$$

$$2EI\frac{d^2y}{dx^2} = Py \tag{7}$$

$$\frac{d^2y}{dx^2} = \frac{Py}{2EI} \tag{8}$$

The curvature k(x) for an arc of the form y = f(x) is given by (Protter & Morrey, 1977):

$$k(x) = \frac{\frac{d^2y}{dx^2}}{\left(1+\left(\frac{dy}{dx}\right)^2\right)^{\frac{3}{2}}} \tag{9}$$

Neglecting being small compared to unity,

$$k(x) = \frac{d^2y}{dx^2} \tag{10}$$

The radius of curvature of an arc at a point is defined as the reciprocal of the absolute value of curvature at that point (Protter & Morrey, 1977); that is

$$R = \frac{1}{k(x)} \tag{11}$$

From Eqs. (10 & 11),

$$\frac{1}{R} = \frac{d^2y}{dx^2} \tag{12}$$

The curvature is approximated by the above relation in the Klingel theory on lateral movement of a wheelset on tangent track (Esveld, 2001). The same relation is used to derive the formula of vertical curve in railway engineering. From Eqs. (8 & 12),

$$\frac{1}{R} = \frac{Py}{2EI} \tag{13}$$

Equating thermal load per unit length of track with the lateral resistance of track, it may be written,

$$\frac{P}{R} = F_{QVW} \tag{14}$$

$$\frac{1}{R} = \frac{F_{QVW}}{P} \tag{15}$$

From Eqs. (13 & 15),

$$\frac{Py}{2EI} = \frac{F_{QVW}}{P} \tag{16}$$

$$y = \frac{2F_{QVW}EI}{P^2} \tag{17}$$

$$y_c = \frac{2F_{QVW}EI}{P_c^2} \tag{18}$$

Changing the unit of critical load, Pc from N to kN, unit of lateral resistance, FQVW from N/mm to N/cm, the Eq. (18) is written as

$$y_c = \frac{2F_{QVW}EI}{10^7 P_C^2} \tag{19}$$

Considering 10% contribution towards lateral rigidity by track frame as explained earlier, the Eq. (19) is modified as

$$y_c = \frac{2.2 F_{QVW} EI}{10^7 P_c^2} \tag{20}$$

$$P_c = \sqrt{\frac{2.2 F_{QVW} EI}{10^7 y_c}} \tag{21}$$

The equation (21) shows a correlation between four parameters and critical load which is exactly same as the correlation shown in the equation (4) based on energy theorem from Esveld. The derivation of equation (21) is much simpler than that of equation (4).

$$P_c = 2\alpha \Delta T_c . E . A \tag{22}$$

The force value arising when ties are displaced by 2mm is usually taken as lateral displacement resistance. Where there is greater displacement the tie begins to slide as static friction changes to sliding friction as shown in Figure 2 (Lichtberger, 2005).

FIGURE 2:

Lateral displacement resistance diagram.

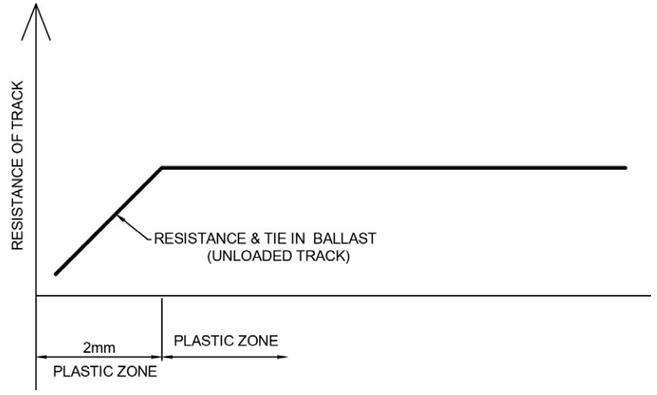

Thus, the tie would starts sliding in a plastic zone at a displacement beyond 2mm. In the aforementioned calculation example, a critical misalignment of 2cm is assumed to compute the ΔT_C. There is no suitable theoretical model to compute the critical misalignment (Kish, 2011). The assumption of critical misalignment of 2-2.5cm is questionable for at least three reasons: (1) A tie resistance is determined at a displacement of 2mm, the track displacement enters into plastic zone after 2mm displacement.

Thus, the critical misalignment is expected to be close to, not far off 2mm. (2) As per European (EN) specification, the admissible limit of misalignment is 2mm on a 10m chord; this limit would have been more than 2mm if the critical value is 25mm. (3) As per Eqs. (1, 4, 21),

$$\Delta T_C \quad \alpha \quad \frac{1}{\sqrt{y_c}} \tag{23}$$

With a track misalignment of the reduced temperature differential is given by

$$\Delta T_C^* \quad \alpha \quad \frac{1}{\sqrt{y_c + y_{mis}}} \tag{24}$$

$$\Delta T_C^* = \frac{\Delta T_C}{\left(\sqrt{1 + \frac{y_{mis}}{y_c}}\right)} \tag{25}$$

The Eq. (25) is used to study the effect of track misalignment on critical temperature differential and critical buckling load. The ΔT_C and P_C is reduced by 13.4% for y_{mis} = 2mm and y_c = 6mm. This is supported by the field tests where the critical load is reduced to 173 -180 tons from 200 tons i.e. 10 - 13.5% due to geometric imperfections (ref: cases under B, C, E). On the other hand, the ΔT_C and F_0 is reduced by 3.8% for y_{mis} = 2mm and y_c = 25mm which is not sensible. Moreover, for y_{mis} = 3.36mm and y_c = 6mm, $\Delta T^*_C = 40^0C$, the track is supposed to buckle at 60^0C assuming SNT=20^0C and $\Delta T_C = 50^0C$. Thus, a misalignment of 3.36mm is risky as the rail temperature in North America might hit 60^0C. On the other hand, for y_{mis} = 14mm and y_c = 25mm, $\Delta T^*_C = 40^0C$, the track is supposed to buckle at 60^0C. Thus, a misalignment of 14mm is risky which implies a misalignment below 14mm may be admissible which is unacceptable.

The Buckling analysis normally gives only the upper bound of load that can be applied to the system before encountering loss of stability. The Eq. (20) is a single equation with two unknown values; thus one value is to be assumed to solve it. Lichtberger suggests lateral displacement resistance of 90 N/cm and 150 N/cm for well ballasted and fully stabilized wood and concrete tie track respectively. As ballast resistance plays significant role in buckling issue, hence it is chosen as basis to select the critical misalignment value. A critical misalignment of 6mm is assumed for a ballast resistance of 90 N/cm (wood tie track) and 9mm for 150 N/cm (concrete tie track).

Incorporating F_{QVW} =100 N/cm, E=210000 N/mm^2 and I=5130000 mm^4 (UIC 90 rail), y_c = 6mm in the Eq. (20) the critical load or upper bound of buckling load comes out to be 1987 kN (cf. Eq. (4) from Esveld gives 2018 kN). The critical load and critical temperature differential are computed in Table 2.

TABLE 2:

Computation of critical bulking load and critical temperature differential by the Eqs. (19 & 20)

Rail profile	y_c (mm)	F_{QVW} (N/cm)	I_{y-y} (mm^4)	A (mm2)	P_c (kN)	ΔT_C (^{0}C)	Tie type
115 RE	6	90	4453676	7232	1757	49	wood
115 RE	9	150	4453676	7232	1852	52	concrete
136 RE	6	90	6010382	8597	2041	48	wood
136 RE	9	150	6010382	8597	2151	50	concrete

A published value from Table 1 shows 49^{0}C (cf. 49^{0}C on 1st row in Table 2) as critical temperature differential for horizontal buckling with wood tie and 47kg/m rail (Lichtberger 2005, Brown 1979). No value is given for concrete tie. The Table 1 shows 42^{0}C (cf. 48^{0}C on 3rd row in Table 2) as critical temperature differential with wood tie and 68 kg/m rail. The Table 1 shows 46^{0}C (cf. 50^{0}C on last row in Table 2) as critical temperature differential with concrete tie and 68 kg/m rail. Thus, the values computed in Table 2 are comparable with the published values in Table 1. The assumption of critical misalignment of 6mm for displacement resistance of 90 N/cm and 9mm for 150 N/cm render acceptable value of critical load and critical temperature differential. The modal shape of buckling of a tangent track is usually assumed as a sine wave shown in Figure 3.

FIGURE 3:

Buckled track.

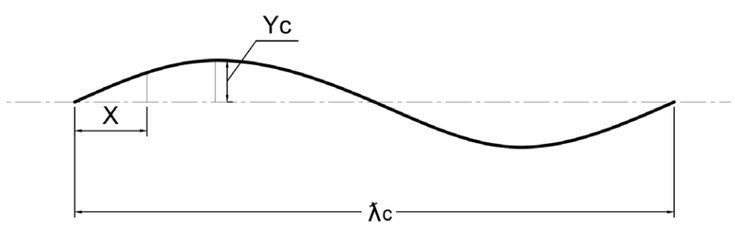

$$y = y_c . Sin\left(2\pi \frac{x}{\lambda_c}\right) \tag{26}$$

$$\lambda_c = \frac{2\pi x}{Sin^{-1}\left(\frac{y}{y_c}\right)} \tag{27}$$

Assuming first tie at the point of deflection, the second tie would be at a distance of S. The second tie should be displaced by at least 2mm or a little more. Incorporating x = S = 0.75m and y/y_c = 2/6 in the Eq. (25), the wavelength, λ_C = 13.8m for 115 RE rail track. The wavelength of the traditional buckling is up to 15m with amplitudes of up to 1m (Lichtberger 2005). The Eq. (20) gives a buckling load of 1987 kN and the Eq. (4) from Esveld gives a buckling load of 2018 kN.

A buckling process for the above buckled track of 13.8 m wavelength is depicted below:

A stress neutral temperature, SNT of 20^{0}C is assumed. The track is expected to buckle at 70^{0}C (= 50+20^{0}C). The arc length of the rail is calculated to be 13800.04mm by integration; the extra 0.04mm is breathed from two ends of the buckled track. Assuming F_{QVW}=90N/cm for wood tie track, a breathing length, L_{B1} of 2.6m is required to breath 0.02mm from each end of buckled track and the corresponding ΔT_1 = 1.3^{0}C. The rail temperature will drop to 68.7^{0}C (= 70-1.3); the affected track length in critical state, L_C = 19m (= 2.6+13.8+2.6m). If the temperature increases to a value below 68.7^{0}C, the track is not supposed to distort. The track starts to move at 68.7^{0}C. The minimum length of test track shall be 19m to determine the buckling load only. A solution based on true expression for curvature enables the deflection to be determined and shows that small increases in load above the Euler value produces significantly large deflection (Gaylord, 1957). With a slight increase in buckling load, the track is exploded to full buckling state releasing more energy. This is why buckling load is assumed to be constant throughout the buckling process (Esveld, 2001). Assume the rail temperature drops to SNT i.e. 20^{0}C; the temperature differential, ΔT_2 = 48.7^{0}C (= 68.7-20^{0}C) and the corresponding breathing length, L_{B2} = 97m. The breathing lengths contribute 55.72mm (= 2x27.86mm) of rail into the buckled track; all parameters - amplitude, wavelength, and affected track length would grow further. The Eq. (23) may be applied to compute the amplitude of the full buckled track. In practice ΔT^*_C would not be zero as the amplitude of a buckled track has a finite value. Assuming, ΔT^*_C=4.5-5^{0}C, the amplitude comes out to be 594-735mm. The affected track length after buckling, L_F would be 213m (= 97+19+97m). Thus, a test track length of 213m would capture both buckling load and modal shape of buckling. Kerr mentioned that the test track lengths (ref: case A-E) are inadequate (Kerr, 1978). In aforementioned field test cases the maximum amplitude observed

is 400mm due to inadequate test lengths. Some author assumes critical wave length to remain same through entire process of buckling (Esveld, 2001). As the breathing lengths breathe at the ends only, the final wave length is not expected to change significantly. The critical wavelength would be disturbed by the sudden buckling movement of the track. Thus, the final wavelength, λ_F may be estimated by $(\lambda_C+L_C)/2$ i.e.16.4 (= 13.8+ 19)/2). Similar calculations are done for three other cases and results are shown in Table 3.

TABLE 3:

Computation of critical bulking load and critical temperature differential by the Eqs. (19 & 20)

Rail	Tie	y_c	λ_c	ΔT_1	L_{b1}	L_C	ΔT_2	L_{b2}	L_F	λ_F
115 RE	concrete	6	13.8	1.7	2.0	17.8	48.3	57.7	133	15.8
136 RE	concrete	9	21	1.5	2.2	25.4	48.5	68.8	163	23.2
115 RE	wood	6	13.8	1.2	2.76	19.3	48.8	109.3	238	16.5
136 RE	wood	9	21	1.1	3.00	27.0	48.5	130.0	287	24.0

Note: ΔT_C = 50^{0}C, SNT=20^{0}C (assumed)

From Table 3, the wavelength of a concrete tie track is about 23–24m and that of wood tie track, 16–17m. The chord length to measure longitudinal alignment may be half of wavelength i.e. 8-12m, currently 10m chord is used. A test track length of 30m (ref: L_c in Table 3) is quite adequate to capture buckling load only. The track lengths in aforementioned field tests are 30, 36.6, 46.17, 60 and 100m; hence the buckling load from field tests are acceptable. The minimum test track length shall be 250m (ref: L_F in Table 3) for wood tie track and 220m (ref: L_F in Table 3) for concrete tie track to capture modal shapes of a buckled track. The test track lengths in aforementioned field test are not adequate to capture modal shapes, hence the descriptions of modal shape e.g. amplitude, wavelength from aforementioned field tests are unacceptable.

If a track is buckled then at least a track length equal to full affected length, L_F should be distressed to put it at original design SNT.

5. Vertical Buckling

A relation between critical vertical misalignment and critical vertical buckling load may be expressed from the Eq. (16) simply replacing lateral resistance term, F_{QVW} by the weight of track, w (N/cm) and moment of inertia, I (I_{y-y}) term by I_{x-x} as under:

$$y_c = \frac{2wEI_{x-x}}{10^7 P_c^2} \tag{28}$$

The product of two terms i.e. $y_c P^2_c$ is an indicator of track buckling strength. Thus, the ratio of vertical buckling to lateral buckling strength, r is given by

$$r = \frac{w}{F_{QVW}} \cdot \frac{I_{x-x}}{I_{y-y}} = 6.25 \frac{w}{F_{QVW}} \tag{29}$$

The critical temperature differential for vertical buckling is given by

$$\Delta T_C^V = 6.25 . \frac{w}{F_{QVW}} . \Delta T_C \tag{30}$$

The vertical buckling of a track can occur simultaneously with the horizontal buckling if the following condition is met:

$$F_{QVW} = 6.25w \tag{31}$$

The vertical buckling of a track can occur prior to horizontal buckling if the following condition is met:

$$F_{QVW} >> 6.25w \tag{32}$$

A well ballasted and fully stabilized concrete tie track exhibits a lateral displacement resistance of 150 N/cm (Lichtberger, 2005). The weight of track with UIC 60 rail and B70 concrete tie@ 60cm, w is 62.6 N/cm (Lichtberger, 2005). The ΔT_C for horizontal buckling is calculated to be 51^{0}C for horizontal buckling of a track with UIC 60 rail and B70 concrete tie. Thus ΔT^V_C for vertical buckling will be 2.6 (= 6.25x62.6/150) times the ΔT_C i.e. 133^{0}C (= 2.6x51^{0}C). The critical misalignment for vertical buckling would be 0.15 times (= 1/2.6^2) the critical misalignment of horizontal buckling i.e. 0.9-1.35 mm (= 0.15x6 – 0.15x9) if the track resistance exceeds 391 N/cm (= 6.25x62.6). But the lateral resistance of the track is only 150 N/cm. Hence, lateral buckling will take place (cf. 51^{0}C, 133^{0}C); vertical buckling is an absurd event with concrete tie track.

A well ballasted and fully stabilized wood tie track exhibits a lateral displacement resistance of 80 N/cm (Lichtberger 2005). The weight of track with UIC 90 rail and wood tie@ 60cm, w is 28.1 N/cm[4]. The ΔT_C for horizontal buckling of a track with UIC 60 rail and wood tie is assumed to be 45^{0}C. Thus ΔT^V_C for vertical buckling will be 2.2 times the critical temperature for horizontal buckling i.e. 99^{0}C. The critical misalignment for vertical buckling would be 0.2 times (= 1/2.2^2) the critical misalignment of horizontal buckling i.e. 1.2-1.8mm (= 0.2x6 – 0.2x9) if the track resistance exceeds 175 N/cm (= 6.25x28.1). But the lateral displacement resistance is only 80 N/cm. Hence, lateral buckling will take place (cf. 45^{0}C, 99^{0}C), vertical buckling is an absurd event with wood tie track.

Under the influence of the lift-off wave, the bottom friction is reduced by 20–40%. Typical track buckling below train in summertime at high rail temperature is caused in the area of the lift-off wave ((Lichtberger, 2005). There is always a segment of unloaded track in front of wheel or in between two trucks due to negative deflection or rail lifting. The distance between first and second point of zero deflection from a wheel load is πL (= 7πL/4 -3πL/4), approximately 3m, which is the maximum length of unloaded lifted track. The negative deflection is $e^{-\pi}$ i.e. 4.3% of the deflection under the wheel; the negative deflection computation does not consider weight of the track. If the deflection under the wheel is 6mm, the negative deflection would be 0.26mm. The dead weight of modern concrete tie track compensates the negative deflection (Esveld, 2001). The dead weight of wood tie track would reduce the negative deflection. Thus, the misalignment of lift-off wave is zero for concrete tie and less than critical misalignment of wood tie track. Moreover, the length of the lifted track is very small. Thus, lift-off wave under wheel load is not a concern for buckling of the track.

6. Literature Review on Vertical Buckling

There is an analytical formula with a calculation example for computing critical temperature differential for vertical buckling in literature as follows (Lichtberger, 2005 & Eisenmann, 1995):

$$\Delta T_C = \frac{4}{\alpha A}\sqrt{\frac{I.G_{crit}}{E.f^*}} \tag{33}$$

$$F_0 = \alpha \Delta T_C EA \tag{34}$$

$$L = 2\pi\sqrt{\frac{2EI}{F_0}} \tag{35}$$

$$G_{crit} = \frac{EA}{16I}\left(\alpha A \Delta T_{crit}\right)^2 \tag{36}$$

Data:
Rail: UIC 60
Tie: Concrete B70w tie, tensioned

I	6110cm^4
A	2x76.9=153.8cm^2
E	21000000 N/cm^2
α	0.000012/^{0}C
f*	1.5cm
G	62.6 N/cm

The formula offers a critical temperature differential of 238.8^{0}C for vertical buckling for a track with B70w concrete tie and UIC 60 rail. The published value is 70^{0}C with concrete tie and 59kg/m rail (Lichtberger, 2005 & Brown, 1979). Thus, the computed value is simply unacceptable in context with the published value, test value from field (ref: case A), and aforementioned discussion. Although a formula for critical track weight is given (ref: Eq. (36), but the calculation uses the actual track weight of 62.6 N/cm. Moreover, an assumed value of critical misalignment of 15mm seems to be very high to offset the self- weight of track in light of aforementioned discussion.

The Eq. (1) yields a critical temperature differential of 115.7^{0}C for horizontal buckling for the same track; the ratio of vertical to horizontal buckling load, r is 2.06 (= 238.8/115.7). The ratio of two values seem acceptable although the individual values are unacceptable. The author computes the ratio between vertical and horizontal buckling load to be 2.6. In fact, the ratio can be more than 2.6 as the formulation is based on track weight only which is a simplification; the restraining influence of the ballast around the tie is not considered.

7. Threshold Radius of a Vertical Curve

The threshold radius of a vertical (crest) curve may be expressed by equating track weight and critical buckling load on a curve. Adjusting units, the threshold radius is given by

$$R_T = 10\frac{P_c}{w} \tag{37}$$

For a buckling load of 200 kN, the threshold radius of a vertical (crest) curve on a concrete tie track would be 320m (= 10x2000/62.6). For a buckling load of 200 kN, the threshold radius of a vertical (crest) curve on a wood tie track would be 1779m, (= 10x2000/28.1) say 1800m. If the radius is below the threshold value, thermal load would initiate lifting of the track and tie resistance will be dropped to 50% causing horizontal buckling at a temperature differential lower than the critical temperature differential. A vertical curve radius of 2000m must be considered as the absolute minimum (Esveld 2001). This exercise validates earlier work on vertical buckling indirectly.

8. Conclusion

An analytical formula is suggested to compute the critical load and critical temperature differential for horizontal thermal buckling of a tangent track. The critical temperature differential for horizontal and vertical buckling is related by track weight and lateral ballast resistance; from this relation critical temperature differential for vertical buckling is determined. A track might start to shift at two degree Celsius below the critical temperature for (horizontal) buckling. A track is likely to go under vertical mode of buckling under high compressive load if the lateral displacement resistance of a track exceeds 6.25 times the self-weight of a track. A test track length of 30 m is adequate to capture buckling load only. A calculation process is shown to narrate buckling process and to determine the affected track length, and amplitude of a buckled track. A formula to assess the effect of track misalignment on critical buckling load is given. A formula to determine threshold radius of a vertical curve is suggested; the lighter the track the higher the threshold radius.

Notation

The following symbols are used in this paper:

A	Sectional area of a rail (mm^2),
E	Young's modulus (210,000 N/mm^2),
F_0	Critical rail pressure force (N),
F_{QVW}	Lateral displacement resistance (N/cm),
f*	Critical track defect (2-2.5 cm),
I	Moment of inertia of a single rail (cm^4, mm^4),
I*	Moment of inertia of the track grid (cm^4),
L	Characteristic length (m),
L_C	Affected track length at critical position (m),
L_F	Affected track length after buckling (m),
P_c	Critical (buckling) load (kN),
R	Curve radius (m),
R_T	Threshold radius (m),
r	Ratio between critical temperatures, $\Delta T^{v}_{C} / \Delta T_C$
S	Spacing of tie (m),
SNT	Stress neutral temperature (^0C),
w	Track weight (N/cm),
α	Coefficient of expansion ($0.0000118/^0C$),
ΔT_C	Critical temperature differential for horizontal buckling (^0C),
ΔT^{*}_{C}	Reduced critical temperature differential due to track misalignment (^0C),
ΔT^{v}_{C}	Critical temperature differential for vertical buckling (^0C),
λ_C	Critical wavelength (m) as in Figure 3,
λ	Wavelength after buckling (m).

Data Availability

All data, models or code were generated or used during the study appear in the submitted article.

Acknowledgements

Originally published as: Hasan, N. Thermal Buckling of Ballasted Tangent Track. Advances in Mechanical Engineering, Oct 2020; 12(10) SAGE Publishing, licensed under the Creative Commons Attribution 4.0 License (https://creativecommons.org/licenses/by/4.0/)

References

- Kerr, A.D. Lateral Buckling of railroad tracks due to constrained thermal expansions – A critical survey, a chapter from: Railroad Track Mechanics & Technology, Edited by Arnold D. Kerr, Pergamon Press, UK, London, 1978
- Esveld, C. Modern railway technology, MRT-Productions, the Netherlands, 2001
- Lichtberger, B. Track Compendium – Formation, Permanent Way, Maintenance, Economics, and Eurail press, Germany, 2005.
- Nemesdy, Erwin: Berechnung waagerechter Gleisverwerfugen nach neuen ungarischen Versuchen, ETR Eisenbahntechnische Rundschau 12/1969, S. 514-534 (Calculation of horizontal lateral buckling of rails according to new Hungarian experiments, ETR Eisenbahntechnische Rundschau 12/1969, S. 514-534)
- Association of Railway Engineering and Maintenance-of-Way Association (AREMA). Manual for Railway Engineering, Volume 1B, Track, Lanham, MD, USA, 2019
- Pierre Dogneton. The Experimental determination of the axial and lateral track-ballast resistance, a chapter from: Railroad Track Mechanics & Technology, Edited by Arnold D. Kerr, Pergamon Press, UK, London,1978
- Protter M.H. and Morrey, Jr, C.B. College Calculus with Analytic Geometry, Addison-wesley publishing company, Philippines, World student series edition, 1977
- Kish, A. On the fundamentals of track lateral resistance, 2011
- Brown, J.H. Design refinements make the steel sleeper viable, Railway Gazette International 10/1979, p902-906.
- Gaylord, Jr. E.H. & Gaylord, C.N. Design of steel structures, International student edition, McGraw-Hill Book Company, Inc., NY, 1957
- Eisenmann, Josef: Vertikale Gleisverwerfung eines geraden Gleises, EI Eisenbahningenieur (46) 5/1995, S. 294-296. (Vertical buckling of a straight rail, EI Eisenbahningenieur (46) 5/1995, S. 294-296).

Low Maintenance Multi-Cell Buried Structure Designed for Life

Jan Laco, PhD, CEng. MICE
Associate Principal Engineer
Engineering, Design and Project Management,
Epsom, UK

Robert Wheatley, BEng. (Hons) CEng. FICE
Technical Director,
Engineering, Design and Project Management. Epsom, UK

Paul Nowak, , BSc (HONS), ARSM, CEng, MICE, MIMMM, CGeol, FGS
Technical Director
Engineering, Design and Project Management,
Epsom, UK

Alison Graham, BEng (HONS), MSc, CEng. MICE
Chief Geotechnical Engineer
Engineering, Design and Project Management,
Cardiff, UK

Abstract

Civil engineers often face difficult geological conditions. The challenge may not be only related to the structure itself but also to the surrounding environment, which can be particularly sensitive to human interventions and protected by increasingly tougher environmental laws.

An unusual reinforced concrete structure was designed to permit A465 road widening and prevent damage or collapse of the underlying cave system, accommodating a protected natural bat habitat, by construction operations or the increased traffic from the opening of the widened carriageway. The design concept was to create a cantilever structure that would not increase the net ground pressure over the caves. This was achieved by replacing the original material with the multi-cell buried structure. Special attention was paid to safe construction of the cantilever structure as well as minimising the future maintenance for cost and health & safety aspects.

Most of the surfaces of the structure are buried and, therefore, in permanent contact with ground moisture. The structure, therefore, requires crack width (initiation) control to prevent water ingress into the cells during the design life of the structure. The design focused primarily on the buildability of the structure and the prevention of early thermal cracking by different calculation methods.

KEYWORDS

Environmental sensitive area; Reinforced concrete durability; Early thermal cracking design; Design & Build project.

1. Introduction

The structure is located on the A465 Heads of the Valleys highway in Wales, United Kingdom. The existing single carriageway road is being widened through the Clydach Gorge, part of the Brecon Beacons National Park. Due to the local topographical constrains the road had to be widened over the Carboniferous Limestone caves Ogof Gelynnen and Ogof Capel. The topography of the ground has created a steeply sloping embayment feature known as "The Divot" at the cave entrance and an extensive cave system is close to the road surface. The caves accommodate natural bat habitat that must be protected and not disturbed.

The A465 forms one of the main east/west highway routes in South Wales. The highway also forms a part of Trans-European Road Network (TERN-T). The existing A465 was built in 1964 as a single three-lane carriageway. The need for improvement of the highway alignment arose out of a regional traffic study, which concluded that widening the existing road to provide dual carriageway with grade-separated junctions was desirable. Upgrading to dual carriageway significantly improves transport connectivity and overall capacity of the road and its safety. In addition, the social and economic regeneration of the post-industrial Heads of Valley area was a key objective for construction. The road geometry was designed for vehicles traveling at 50 mph over its full length due to the local topographical conditions and surrounding ecological sites. The carriageways are split level over the 2.2 km section through the Clydach Valley. (CEW 2019)

The A465 project is currently one of the largest ongoing Design & Build projects in the United Kingdom. The whole upgrade consists of 6 sections. Sections 1 ,3 and 4 were completed by the beginning of 2014, Section 2 is currently under construction and sections 5 and 6 are being procured under a single contract.

Costain was awarded the Section 2 contract by the Welsh Government in 2011 supported by Atkins and CH2M Hill (now Jacobs) in a design joint venture. Construction of Section 2 commenced in 2014 and is due for completion in 2020. The overall project cost of the contract is estimated to be £336m. The chosen procurement route was Early Contractor Involvement with the Design and Build Phase carried out under the NEC3 Engineering Construction Contract, Option C. (ICE 2016) A465 Section 2 is shown in Figure 1.

FIGURE 1

South Wales on the left side and zoomed area to A465 section 2 on the right side [Maps retrieved from maps.google.co.uk]

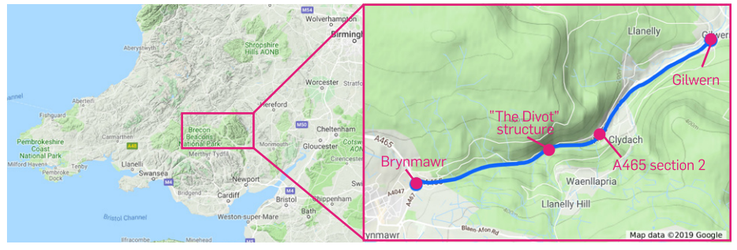

2. Local Constrains

2.1. ENVIRONMENT

The A465 Section 2 is one of the most environmentally challenging schemes in Wales. The section includes a total of 40 statutory designated sites within 10km of the route corridor. Of the sites, 23 are Sites of Special Scientific Interest (SSSI), three are National Nature Reserves (NNR). Nine are Local Nature Reserves (LNR) and five are the European designated Usk Bats Sites Special Conservation Area (SAC). The identified key issues along the route corridor were the effects on the Lesser Horseshoe Bat (Rhinolophus hipposideros) population and a habitat known as Tilio Acerion Woodland.

The Divot construction site is located in one of the Special Areas of Conservation. The Ogen Capel and Ogen Gelynen caves accommodate large habitat of the Lesser Horseshoe bats. Therefore, the design of the structure had to be carried out with respect to the bats' habitat protection. Some photos of the caves and the bats are shown in Figure 2.

FIGURE 2

Capel-Gelynnen caves and lesser horseshoe bat (Rhinol ophus hipposideros) [The cave photos obtained from Smith (2013); the bat photo taken from DCS (2019)]

2.2. GEOMORPHOLOGY

The construction site is located immediately to the south of the existing alignment of the A465 on the northern edge of the river Clydach valley. The current alignment of the A465 at this location is underlain by engineered fill comprising Glacial Till derived material which overlies limestones of the Clydach Valley Group. The project has been assessed as Geotechnical Category 3 as it involves very large, unusual and complex geotechnical activities, earthworks and structures and those involving abnormal geotechnical risks together with unusual and exceptionally difficult ground conditions. The historical and geological maps show that areas of the Clydach Gorge are underlain by strata of the Carboniferous Limestone Super Group, which have been extensively quarried for limestone.

The limestone supports the cave systems, the Ogof Gelynnen and Ogof Capel which run below the existing and new road alignment. A survey indicated that the roof of the systems is at 8.0m and 18.0m below carriageway level respectively. A steeply sloping embayment feature known as “The Divot” is in vicinity of the cave entrances.

The roof of caves at this location is formed in consolidated stone and clay. Vertical fractures in the roof of the caves were identified. It is likely the fractures extend towards the surface, with traffic heard in the caves and water ingresses obvious during wet periods. The cave system in plan is shown in Figure 3.

FIGURE 3

Capel-Gelynnen cave system in plan [Map obtained from Smith (2013)]

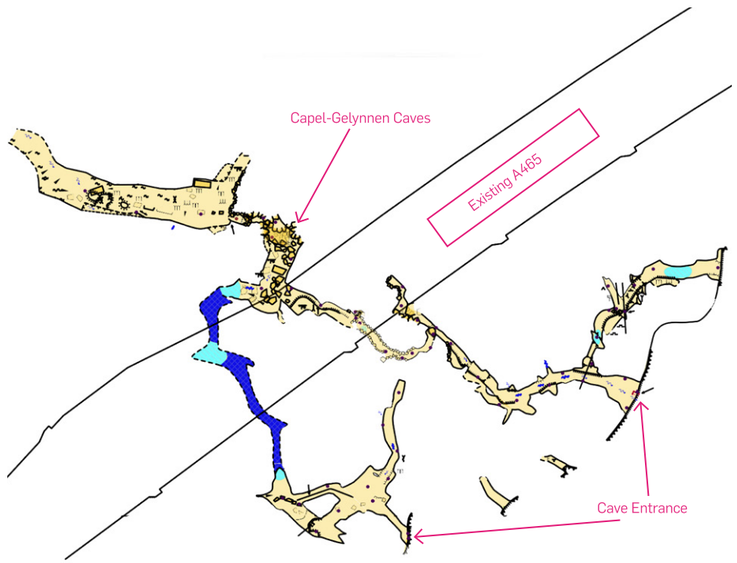

3. “The Divot” Structure

3.1. ASSUMPTIONS AND STRUCTURAL OPTIONS

The overall design of The Divot structure was carried out in consideration of the local environmental and geological constrains. Conventional solutions were likely to compromise this important ecological site. The solution chosen needed to protect the environment, be cost-effective and simple to construct without the need for heavy equipment. Construction operations that compromise the bat habitat are strictly forbidden as even temporary changes in bearing pressure on site could adversely affect the bats. For these reasons it is important to fully understand the local geological and environmental constrains to carry out a design of the structure to meet these requirements.

Several structural and construction options were investigated. Retaining wall solutions represented a low maintenance and easy to construct option. However, the surcharge due to material backfill to achieve desired carriageway width was unacceptable with respect to the cave entrance protection against collapsing. Options of a structure spanning the cave area would be cost-ineffective and difficult to construct due to the requirement of boring piles through the solid rock. The third solution was a voided structure with lesser overall weight than the overlaying material even allowing for the additional carriageway width. The permanent and traffic loads would be distributed by the structure around the caves to the surrounding bedrock. The existing engineering fill material would be replaced by the structure applying less bearing pressure under the structure than the current construction. This assumption provides desired caves stability. The third option was chosen as the most suitable solution from geological, environmental, construction and durability aspects.

Overcoming the geological and environmental constrains the design of the structure left difficulties in terms of durability to overcome, particularly crack control. Non-regulated crack propagation with un-controlled distribution can lead to water ingress to the structure where it is in permanent contact with ground moisture. The water ingress can be prevented by additional waterproofing applied on concrete surfaces in permanent contact with soil. However, the waterproofing layers usually comprise asphalt which can be unacceptable in sensitive ecological sites. Design rules were, therefore, implemented for the structure design to regulate early crack propagation due to cement hydration and prevent excessive cracking, water ingress, reinforcement corrosion and structure deterioration.

3.2. DESIGN OF THE PREFERRED OPTION

The risk to the stability of the cave system has been assessed in the long term and considered no greater than the current situation as the proposed solution does not impart any additional dead load above the caves and additional live load over the new carriageway width is no greater than that on the existing carriageway which has not invoked collapse over the 50 years since the original construction.

The Divot structure was proposed as a voided slab of a rectangular footprint with 3-cells and cantilever edge to accommodate the widened carriageway. The design has sought to keep the overall bearing pressure accounting for overturning less than that from the original material. The overall length of the structure is 24.0m to bridge the cave system and allow ground bearing at a safe distance beyond the caves. The structure is in longitudinal elevation 5%. The overall width of the structure is 11.33 metres. It carries the eastbound carriageway including a part of central reserve. At the edge of the cantilever it is proposed to have a concrete-steel precast parapet. The voids are 2.6m wide and divided by concrete walls of 250mm thick. The top and bottom slabs are both 250mm thick. The voids were proposed to be filled with extruded polystyrene which provides lost formwork for the top slab concrete. The polystyrene fill does not significantly increase the weight of the structure but permanently prevents access to the voids. Therefore, their further inspection cannot be executed.

FIGURE 4

Typical cross section and elevation of the Divot structure

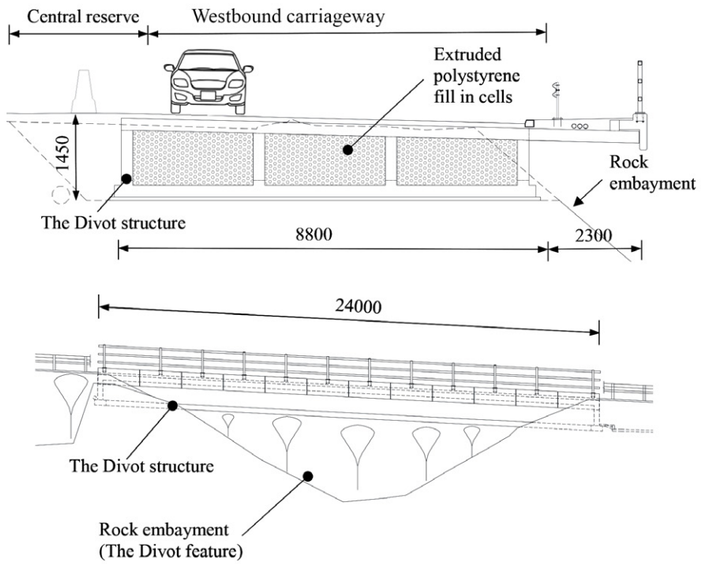

The outer faces of the structure are backfilled with well granulated engineered material. The reinforcement in the structure was designed to withstand traffic loads in accordance with BS EN 1991-2 (2003) and ground pressures in accordance with BS EN 1997-1 (2004). A typical cross section and elevation of the structure is shown in Figure 4.

3.3. EARLY THERMAL CRACKING DESIGN

A majority of the concrete surfaces are in permanent contact with the surrounding soil and ground moisture. The structure was, therefore, designed to prevent concrete cracking due to early thermal actions related to cement hydration as a measure of controlling water ingress and improve durability. The reinforcement spacing was designed with respect to the concrete early age thermal cracking according to CIRIA C660 (2007). The calculation according to C660 provides tensile strains produced by early thermal actions. The strains should be lesser than ultimate tensile strength of the concrete. However, the strains smaller than ultimate tensile strains are difficult to achieve and therefore the cracks, their distribution and widths need to be controlled. The minimum reinforcement area due to early thermal actions was calculated according to BS EN 1992-1-1 (2004).

To refine the early thermal strains calculation a 3D FE model was developed for heat of hydration (HoH) distribution analysis. The analysis considered the assumptions related to specified casting and curing requirements. Specific concrete mix designs and three construction stages, each lasting for five days were considered. Based on these assumptions it was possible to analyse heat of hydration distribution across the structure after pouring and during concrete hardening up to the time when the temperatures were uniform in the whole structure. The maximum temperature difference was applied to the strains calculation and compared to the strains obtained from the analysis. The values obtained from the HoH analysis were lower than calculated values according to C660 guide. This suggests that the C660 guide is conservative in calculating the temperature difference and tensile strains.

The reinforcing design was conservatively carried out with the parameters according to the C660 guide. The reinforcement spacing and diameters were ultimately adjusted to prevent unacceptable cracking. Adopting the conservative design approach, it was found the maximum calculated crack width is 0.072 mm. According to BS EN 1992-3 (2006) the structure was classified as “class 1” where the water ingress to the structure should be limited by the crack width wk1. The limiting crack width value wk1 for this structure is 0.2 mm. Satisfying this criterion should

FIGURE 5

a) 3D FE model, b) heat distribution across the structure before top slab pouring, c) corresponding strain distribution, d) corresponding stress distribution.

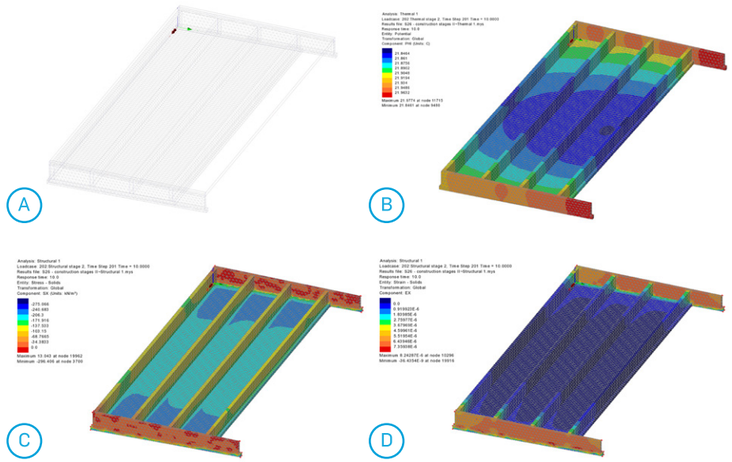

TABLE 1

Maximum temperatures and corresponding strains developed throughout the structure in various construction stages.

	Construction Stage	Time (day)	Temperature (Deg C)				Ex	
			Bot-tom Slab	Bot-tom Slab & Walls	Whole Struc-ture	Bottom Slab	Bottom Slab & Walls	Whole Structure
Stage 1	bottom slab after pouring	0.05	21.47	-	-	0	-	-
	bottom slab max temperature achieved	0.55	45.56	-	-	4.15E-04	-	-
	bottom slab before walls pouring	5	21.53	-	-	1.02E-06	-	-
Stage 2	walls after pouring	5.05	21.55	21.55	-	1.15E-06	1.12E-06	-
	walls'max temperature achieved	5.55	32.14	32.14	-	2.00E-04	1.88E-04	-
	walls before top slab pouring	10	21.98	21.98	-	9.38E-06	8.24E-06	-
Stage 3	top slab after pouring	10.05	21.88	21.88	21.88	7.22E-06	6.21E-06	6.21E-06
	top slab max temperature achieved	10.55	32.52	33.69	35.13	2.85E-04	2.51E-04	2.51E-04
	top slab at final stage	15	22.04	22.07	22.12	1.32E-05	1.13E-05	1.13E-05

result in effective self-sealing of a crack in a relatively short time. The FE model and characteristic heat distribution with corresponding stress and strain distribution is shown in Figure 5. Maximum temperature developed in the structure in various construction stages and corresponding strains are summarised in Table 1.

4. Conclusions

Even though The Divot structure may appear as a simple construction its design is a careful balance between significant environmental and geological constraints and minimising construction costs and risks. The structure was designed to protect the natural bat habitat from collapse due to the potential increased traffic surcharge above the caves compared with a structure constructed close to existing ground level.

The design of the structure was also carried out with respect to minimising maintenance requirements. Close attention to the detail and producing a simple reinforcement arrangement will prevent excessive cracking and enhance durability of the structure for its designed life-time of 120 years.

Heat of hydration analysis has been carried out in addition to the conventional design approaches. The HoH analysis has revealed that the reinforcement design for early age thermal cracking of the concrete according to C660 guide is on the conservative side. The results of HoH analysis need to be verified on the Divot structure. The crack development and its distribution could be usefully monitored on exposed face of the structure during its service to confirm findings of the HoH analysis.

Although, it should be said the CIRIA C660 was superseded by CIRIA C766 (2018) and the calculated results need to be verified against the latest calculation approach.

Acknowledgements

The authors sincerely appreciate Jacobs' input to the design as a part of Design Joint Venture and RPS for environmental design.

Originally published as: Laco, J., Whatley, R., Nowak, P., Graham, A., 2020. "Low Maintenance Multi-Cell Buried Structure Designed for Life, In Concrete Structures for Resilient Society", 22nd-24th November 2020, (pp. 1980-1987, presented online in fib symposium 2020, Shangahi, China)

References

- CEW (Construction Excellence in Wales). (2019). A465 Heads of the Valleys Section 2, Gilwern to Brynmawr. retrieved from URL: http://www.cewales.org.uk/files/2114/9812/2528/A465_Heads_of_the_Valleys_Section_2_Gilwern_to_Brynmawr_Design_Stage.pdf.
- ICE (Institution of Civil Engineers). (2016). New Engineering Contract, option C + Early Contractor Involvment. NEC3 option C ECI, (London, United Kingdom)
- Smith, P. (2013). A465 Section 2: Cave Mapping, Issue 3, Smith Ecology Ltd., Cardiff, Walles
- DCS (Denbighshire Countryside Service). (2019) Lesser horseshoe bat project. retrieved from URL: https://www.denbighshirecountryside.org.uk/lesser-horseshoe-bat-project/
- EN 1991-2-2003. Eurocode 1: Actions on structures – Part 2: Traffic loads on bridges.
- EN 1997-1-2004. Eurocode 7: Geotechnical design – Part 1: General Rules.
- CIRIA C660 (2007). Early-age thermal crack control in concrete. Construction Industry Research and Information Association (CIRIA), London, United Kingdom
- EN 1992-1-1-2004. Eurocode 2: Design of concrete structures, part 1.1: General rules and rules for buildings.
- EN 1992-3-2006. Eurocode 2: Design of concrete structures, part 3: Liquid retaining and containment structures.
- CIRIA C766 (2018). Control of cracking caused by restrained deformation in concrete. Construction Industry Research and Information Association (CIRIA), London, United Kingdom

Eric Smith

Senior Project Manager
Nuclear
Columbia, MD, USA

Gordon Crawford

Chief Engineer
Nuclear
Richland, WA, USA

Brad Bowan

Senior VP and Atkins Fellow
Nuclear
Columbia, MD, USA

Sam Stephens

Chief Engineer, Digital Leader
Nuclear & Power EMEA
Warrington, UK

05: Nuclear Engineering

Mobile Autonomous Robots to Support Risk Reduction in the Nuclear Sector

Abstract

Significant advances in robotics have been seen over the last decade, with a range of technologies reaching commercial maturity. These include Light Detection and Ranging equipment, control systems, artificial intelligence algorithms, camera and vision systems, lithium ion batteries and electric servo motors and actuators. Boston Dynamics has pioneered the development of mobile legged robots, initially for military purposes. In 2020, they released their first commercial robot platform, SPOT®, a quadruped robot 'dog'.

SNC-Lavalin's Atkins Nuclear Secured (ANS) business, based in the USA, has entered the autonomous robotic market through the procurement and development of the Boston Dynamics SPOT® robot. This platform will enable ANS, and SNC-Lavalin, to further the goal of integrating digital technology solutions to reduce risks to people and the environment and drive efficiency on nuclear sites around the world. Initial use cases for SPOT® have been identified to conduct remote surveys and inspections and collect a wide range of data types to integrate in digital twins of assets.

KEYWORDS

Autonomous; Digital technology; Digital twin; Hazardous environment; Inspection; LiDAR; Robot

1. Introduction

Atkins Nuclear Secured (ANS), part of SNC-Lavalin's Nuclear business, has partnered with Boston Dynamics to introduce SPOT®, a four-legged autonomous robot, into the U.S. nuclear market. ANS is an early adopter of the autonomous robot to meet the clear and present interest of customers to lower worker exposure to hazards. ANS sees application of this technology as the preferred method of accomplishing this goal for data collection and simple routine field task with future implementation of more challenging tasks.

2. System Overview

2.2 PRODUCT DESCRIPTION

The small robot is 43in (1092mm) long, 20in (508mm) wide, 33in (838mm) high, weighs just 72lb (33kg) pounds and can support payloads of up to 30.8 pounds (14kg). A schematic of the basic robot anatomy is presented in Figure 1 (Boston Dynamics, 2020).

FIGURE 1

Boston Dynamics
SPOT® robot anatomy

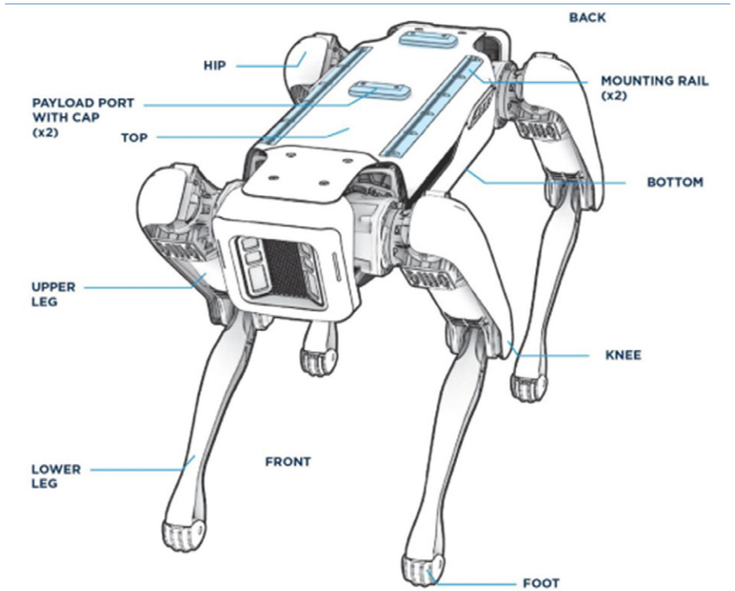

Robot anatomy

It has been designed for search, inspection, and delivery tasks. Unlike other robots, SPOT® can climb stairs and walk over rough terrain (Figure 2). SPOT® is designed to be in resistant to dust and water allowing it to operate in many environments. It can be customized to add many sensors and other payloads. SPOT® is autonomous meaning that it can traverse from one location to another without operator intervention once its path has been set via the handheld control tablet. It is programing also allows it to respond to dynamic situations to avoid obstacles while continuing its mission, can resist forces and can "right" itself if it is unexpectedly knocked over.

FIGURE 2

ANS SPOT®

SPOT® is a quadruped robot has the versatility needed for current applications at the U.S. Department of Energy Hanford site as well as other nuclear, chemical, and petroleum facilities. It autonomously traverses various terrain adapting to and avoiding obstacles. The "dog-like" movement allows for SPOT® to cover diverse types of environment with no fear of getting stuck (in the rare event of a tip over, it can self-right). It can navigate rough terrain including gravel, grass, curbs and slopes up to 30° as well as typical building features, like stairs.

2.3 CUSTOMIZATION

The cost of the SPOT® robot depends on the degree of customization sought by end user. In some cases, highly specialized instrumentation might be selected, which can significantly increase cost. The base unit, without instrumentation, is less than $80,000 USD.

The robot recently obtained by ANS has several systems attached to the SPOT® platform which greatly increase its performance and versatility (Figure 3). The systems are:

- SPOT® Cam – Boston Dynamics's 360° camera as well as a Pan Tilt Zoom (PTZ) camera with 30x optical zoom. This allows for full color images/videos (SPOT's onboard cameras are grayscale) and allows for SPOT® to take survey images from a distance. Soon, Boston Dynamics will be releasing an updated version of this camera that includes a thermal camera attachment as well.
- Enhanced Autonomy Package (EAP) – Boston Dynamic's LIDAR (Light Detection and Ranging) package, which allows SPOT® to navigate in environments without many physical features. The LIDAR is used during SPOT's Auto-walk sequence, which is where it follows a preprogrammed route based on the data points it creates during its initial controlled walk. Without the LIDAR, SPOT® can get "lost" in "feature deserts". The LIDAR extends SPOT's visibility for spatial environments from approximately 4m to 100m. The LIDAR unit can also be combined with a GPS unit to export the 3D point clouds for digital twin creation.
- SPOT® Core – Boston Dynamic's additional computing unit which works with the LIDAR unit, as well as any 3rd party operating systems or software.

FIGURE 3

ANS SPOT® features

2.4 FUTURE DEVELOPMENT

Boston Dynamics' ethos is to provide an open-source platform to allow development of 3rd party payloads compatible with SPOT®. This greatly enhances the potential for the SPOT® platform. With expertise in engineering system building, ANS will seek to develop and test new payload combinations for nuclear operators.

In addition, Boston Dynamics continue to develop new peripherals for customers who do not wish to do their own development. SPOT®, with its 30lb (14kg) payload capacity, can also be used to transport a light capacity robotic arm, remote radiation survey detector, hazardous gas measuring instrument, and thermal viewing systems. These "add-on" systems can be integrated into the SPOT® on-board process system or an additional standalone processor can be added allowing the robot to be used as a transportation package only.

Additional sensor packages for SPOT® are being evaluated by Boston Dynamics. These include the addition of:

- A highly accurate LIDAR system to gather data to be used in generating an accurate digital twin of facilities.
- A software package to allow live streaming of all SPOT® data and views.

3. Nuclear Sector Use Cases

Worker safety, in the nuclear sector, more than most other industries, is first and foremost, and therefore SPOT® will in many instances allow the limitation of hazard exposure to field personnel. The use of SPOT® to perform monitoring, surveys, and investigations will greatly reduce the time humans will spend in the areas where hazards exist. Hazard mitigation, where the hazard cannot be eliminated, focuses on limiting exposure to people. SPOT® enables this by allowing work to be performed remotely where possible. This will not only reduce personnel exposure to hazards but will allow work to be carried out more efficiently since a robot does not require breaks or personal protective equipment to complete its tasks. The potential for these types of robots is limited only by the user's ingenuity and the mechanical limitations of the robot (e.g., battery life, payload capacity).

Several initial use cases for this robotic technology have been identified in the nuclear sector:

- Performing tasks in hazardous environments such as those containing low level radiation, uncharacterized radioactive sources, chemical hazards or buildings and structures with unknown structural integrity (buildings that have collapsed (e.g. Hanford tunnel) or buildings/structures being demolished during Decontamination and Decommissioning)
- Performing routine and non-routine repetitive tasks such as performing "rounds"; observing equipment conditions and instrument readings hence freeing up personnel for more high functioning tasks.
- Mounting special analyzers to SPOT® to sense/characterize hazard areas, which could include chemical analyzers/assay units or three-dimensional radioactive material assay units.
- Potential emergency response within facilities prior to worker entry, such as determining the extent of potential radioactive contamination spread or airborne chemical releases.
- Performing simple tasks (with robotic arm feature) in hazardous areas.
- Perform simple tasks/inspections in areas with unknown, poor topography (rubble piles, etc.)
- Alternative inspection tool to airborne drones, where security limitations exist.
- Performing 3D laser scans to support development of digital twins for existing facilities.

ANS expect to demonstrate a range of these use cases at the Hanford site in 2021. Generally, nuclear sector operators can be supported in the adoption of mobile autonomous robots to address these use cases through a range of commercial approaches. This can include integration of robots into service delivery processes, or through procurement of customized solutions to meet bespoke requirements. Further opportunities will emerge for development of standard solutions to be mounted and integrated with the standard SPOT® platform.

SPOT® is being used in and around the Atkins Engineering Laboratory (AEL) located in Richland, Washington State, USA. The AEL is an ANS operated, Washington State University owned facility operated for the testing and development of technology and other nuclear customer needs. The land around AEL is similar in topography and vegetation to the nearby Hanford site where is expected to the be proving ground for the initial use cases SPOT®.

FIGURE 4

Atkins Engineering Laboratory

Previously testing was carried out at AEL to resolve critical issues with sludge waste mixing for the U.S. Department of Energy Hanford Waste Treatment and Immobilization Plant (WTP). Testing was performed at small scale, half scale, and the actual full-sized tank to be installed into the facility. Additional information on the half scale testing can be found at youtube.com/watch?v=bqC3JNxJQC0. Currently, the high and low bays of AEL are being modified to serve as the assembly facility for the WTP replacement vitrification melters.

4. Conclusion

SNC-Lavalin's nuclear business is pioneering the use of autonomous robots in the sector with Boston Dynamic's SPOT® robot. Using SPOT® and other digital technology, SNC-Lavalin will continue to be at the forefront of the world-wide digital transformation helping the nuclear sector efficiently manage liabilities and meet global sustainability targets.

Nuclear operators can reduce exposure of workers to risks. Will also increase efficiency of surveys and data collection as repetitive work can be performed with fewer by SPOT® freeing up workers for more complex tasks. SPOT® is focused on improving worker safety. In turn, significant short- and long-term cost benefits are expected through the application of this technology. The success of the robot will be measured by enhancement of worker safety metrics or improved efficiencies.

Acknowledgements

Videos highlighting the capabilities of SPOT® produced by Boston Dynamics can be found with the following links:

- Introduction to SPOT®: youtube.com/watch?v=wlkCQXHEgjA
- SPOT® Obstacle avoidance: youtube.com/watch?v=Ve9kWX_KXus
- SPOT® Learning to dance: youtube.com/watch?v=fn3KWM1kuAw

References

Boston Dynamics (2020) "Spot information for use, V1.0 Original Instructions". Boston Dynamics. July 2020.

Saleyard Bridge – An Improved Approach to Pre-casting Steel-Concrete Composite Bridge Decks

Robert N Wheatley, BEng CEng FICE,

Technical Director
Engineering, Design & Project Management,
Epsom, UK

Joe Niblett, MEng CEng, MICE,

Principal Engineer
Engineering, Design & Project Management,
Cardiff, UK

Chris Hendy, FREng, MA (Cantab), CEng, FICE, Eur Ing,

Technical Director, Atkins Fellow,
Head of Bridge Engineering,
Engineering, Design & Project Management,
Epsom, UK

Abstract

Saleyard Bridge carries the A465 Heads of the Valleys Road over the River Clydach near Gilwern, Monmouthshire. It comprises a 67m single span steel-concrete composite multi-girder superstructure made integral with the abutments. A full depth pre-cast deck was chosen to tackle site constraints and improve constructability. The alternative pre-cast panel connection detail developed used straight laps to overcome the problems that can arise from using typical U-bar loop type connections between pre-cast deck panels. The successful use of the pre-cast panels proved that a deck design with straight laps was a practical alternative. The ability to increase the multi-beam centres and avoid cantilever edge formwork created a more economical solution with savings estimated at £500,000. The paper examines the detailed design and construction planning needed to realise the savings and speed up construction, as well as improving site safety. The lessons learnt are also applicable to the wider use of pre-cast panels as an alternative to insitu concreting.

KEYWORDS

Pre-cast concrete; Steel-concrete composite; Bridge; River crossing

1. Introduction

Pre-cast deck solutions are a way of speeding up construction of bridge decks with cost and safety benefits. However, discussion exists over the method of achieving continuity between adjacent slabs and some technical authorities are concerned over the serviceability performance of overlapping loop joints that have been used in earlier designs.

On the A465 Heads of the Valleys Section 2 scheme in Wales, a pre-cast deck solution resulted in saving over £500,000 on the £5 million Saleyard Bridge. The stitch detail for this pre-cast deck solution provided fully compliant straight laps negating the serviceability and practicality concerns about the loop stitch details. At the time, the detail also avoided any need for a Departure from Standards although the anchorage of reinforcement using U-bar loops will be covered by a future revision of Eurocode 1992 1-1.

2. Previous Pre-cast Deck Limitations

Within the industry there is increasing desire to see more use of pre-casting, but pre-cast bridge decks have not become the norm, even after practical guidelines were produced in 2004 with The SCI Technical Report P316 "Pre-cast concrete decks for composite highway bridges" (Yanzido, Iles. 2004). This report proposes a stich using overlapping U bars to create the continuity in the deck reinforcement. (see Figure1)

FIGURE 1

Extract from P316
Figure 5.5 – Proposed transverse joint detail

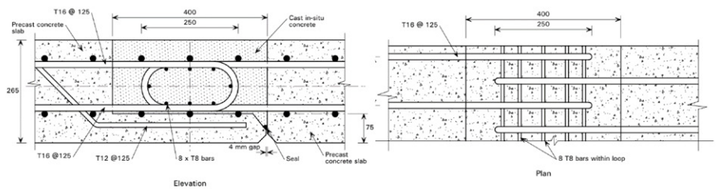

The main reasons behind a lack of uptake appears to focus on the difficulty of creating effective joints between panels using overlapping U-bar loop type details. Drawbacks include:

- The bar bend radius limits the size of the reinforcement that can be used, exacerbated by increased cover and fixing tolerance requirements.
- Fixing lacers inside the overlapping U-bars can be time consuming.
- Integral bridge load effects result in greater longitudinal reinforcement requirements in the deck panels at the abutments.
- Concern that overlapping U-bars might have poor fatigue performance if unsupported. Panel joints are therefore typically supported by main or ancillary steelwork.
- The overseeing organisation may require Departures from Standard to demonstrate performance or to adopt draft Eurocode rules before publication.
- Temporary falsework support may still be required to edge cantilevers.
- Concerns that clashes will occur and would be hard to rectify on-site.
- Concern over sealing of the pre-cast panels when stitching the units.

There are significant benefits to be realised if the above drawbacks can be overcome. These include:

- Saving girder steel weight and craneage required to lift in girders
- Reduced construction time once the steelwork is completed
- Improved quality through pre-casting
- No need for temporary cantilever formwork
- Construction traffic can be accommodated on the bridge at an earlier stage
- Improved safety for construction workers
- More efficient deck design as the full depth of the slab can be used
- Reduced cost through standardisation
- Avoidance of waste

FIGURE 2

Typical pre-cast deck details with overlapping U-bars or additional splice loop bars and threaded lacers.

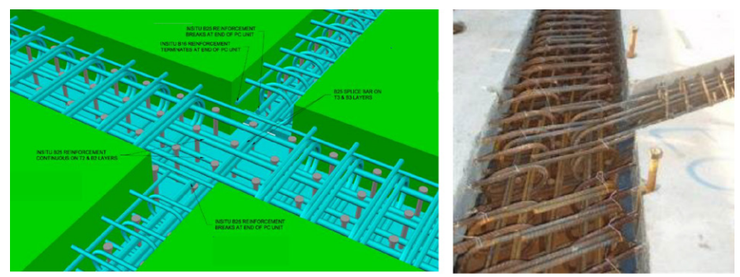

3. The Need for a Pre-cast Deck at Saleyard Bridge

The A465 Heads of The Valleys road crosses the River Clydach at Saleyard, Monmouthshire. The design chosen during preliminary design development for the A465 HOV Section 2 project with the ECI contractor Costain, was a 67m single span steel concrete composite bridge.

The desire to use a pre-cast deck originated from concerns over the cost of craneage to erect the steel beams. Ladder beams were too heavy for the standard 4 beam arrangement needed for a D2 carriageway plus slip road. Standard braced pairs of beams, limited to 3.8m centres, to suit permanent formwork, increased the overall steel tonnage and there was no practicable space for temporary trestling to allow splicing of the beams.

By pre-casting the bridge deck, we were able to increase the multi-girder spacing to 6.1m. This enabled the more efficient use of six braced pairs of girders to form deck. The braced pairs were lighter than the ladder deck beam enabling a smaller crane to be used for the steelwork erection and thereby saving cost.

It was quickly realised that using pre-cast deck units would also have important secondary benefits. The site is in the Brecon Beacons National Park and part of the Usk Bat Special Area of Conservation (SAC).

FIGURE 3

Overall bridge deck layout and proximity of the treeline.

Through the protocol developed with Natural Resources Wales (NRW) at the Public Local Inquiry, NRW experts were monitoring the construction very closely to ensure that a good bat habitat was always maintained. The bats regularly followed the treeline along the river and keeping as many trees as possible helped reduce the construction impact of the scheme (see Figure 3). Eliminating the need for temporary cantilever formwork meant that the contractor did not need to clear the trees immediately adjacent to the bridge in order to remove the falsework and a better habitat could be maintained.

Safety was also improved by providing self-stable deck cantilever edge units. The construction gangs found that it was much easier and safer to work on the pre-cast panels than using traditional permanent formwork methods. The speed of erection also was found to be a significant improvement on traditional cast in place designs.

4. An Improved Approach to the Joint Design

4.1 PLANNING

The integral nature of this 67m span bridge meant large diameter deck reinforcement was required near the abutments to carry the soil-structure interaction load effects. The traditional loop stitch detail was not considered practicable as the large diameter bars could not be bent into a loop that would fit within the deck thickness. Having to support all the construction joints was also a drawback as additional erection operations over the river would be required to install the connecting steelwork between the braced girder pairs.

Instead, a fully compliant straight lap stitch detail was revisited to see if it could solve many of the drawbacks of overlapping U-bar loops. The longer stitch length was not an issue to the contractor Costain, providing a practicable detail could be devised. The benefits were evaluated as being be significant for this project and have good potential for other schemes in the future.

All pre-cast construction must address the way to connect the components and manage the risk of planning, communicating, and executing the fit up of the parts. The process of ensuring a good fit is transferred from skilled site operatives to earlier in the design and construction process where the fit up is done electronically in the CAD model. The benefits to programme and cost are clear if done successfully, but if there are errors the cost of rectifying the work is high. Both the design and construction teams were fully committed to finding a practicable solution and address the associated extra design and supervision costs. The additional design cost was £30,000 for the 85 panels on Saleyard Bridge along with additional site supervision, but the savings were evaluated in excess of £500,000.

Currently, permanent formwork solutions push the lower mat of reinforcement higher into the deck cross section and reduce the reinforcements effectiveness in resisting sagging and punching shear. Adopting straight lap stitch connections allowed the pre-cast deck thicknesses to be maintained at 250mm with larger reinforcement bars and the full deck depth being available for the design. We could now design larger panels and increase the spacing of the composite girders.

The size of the pre-cast units is a key limitation. For readily available transportation, a maximum width dimension of 4.0m over the protruding reinforcement is the likely limit. There will also be craneage and handling limitations to consider. The largest panels used for Saleyard Bridge were 4.13m x 7.70m and weighed 20 tonnes. They were fabricated at a site pre-casting yard which did not require transportation on the public highway and allowed Costain to ensure a high level of site supervision. The enhanced level of supervision was required to permit agreed reduction of the construction tolerances. This is covered later in the paper.

The panel sizes that could be made available by on-site pre-casting, then generated valuable savings in steelwork, with the girder centres increased to 6.1m compared to the traditional 3.8m maximum centres.

A detailed casting plan was developed to minimise the number of mould types. The layout was colour coded into eight basic types and three different connection details (Figure 4). Variations were needed for cantilever units with pockets for shear studs, skew connections at the abutments and different splice lengths.

FIGURE 4

Pre-cast panel layout planning and mould types

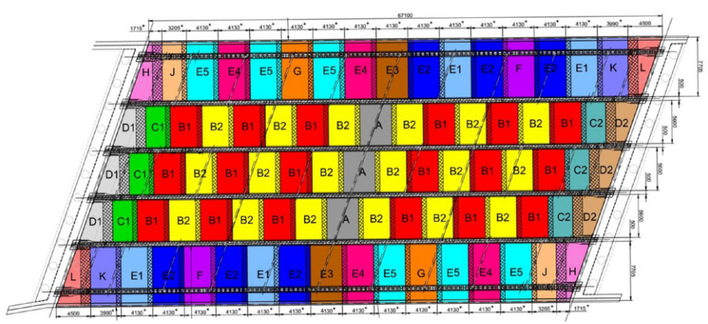

4.2 DESIGN OF THE STITCH CONNECTION

Three types of stitch connections were required.

- Shear stud pocket connections for cantilever panels (Figure 5)
- Supported connections resting on the longitudinal steel girders (Figure 6)
- Unsupported connections (Figure 7)

4.2.1 CANTILEVER PANELS

In general, panels were designed to span between longitudinal girders, but the edge units needed to be continuous over the outer girder and form the 2m deck cantilever. Over the outer girder, the panels were designed to have pockets that fitted over groups of isolated shear studs. The shear stud pocket connections were primarily required to carry the longitudinal shear between the concrete flange and the girder. The bottom mat had to avoid clashing with the shear studs but also had to be positioned below the shear stud heads for composite action. BS EN 1994-1 cl 6.6.5.5 (4) allows shear connectors to be placed in groups if conditions are met covering non-uniform longitudinal shear flow and the greater possibility of slip and separation between the concrete slab and the steel. For the Saleyard Bridge, the shear stud design also had to resist the prying forces acting on the central shear studs from the superimposed dead load and live load.

FIGURE 5

Shear stud pocket connection

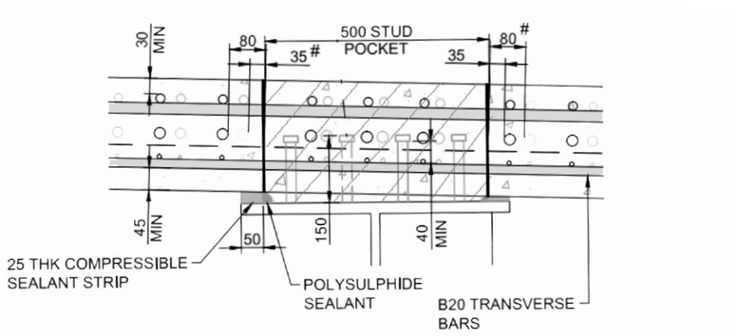

4.2.2 SUPPORTED CONNECTIONS

The connections supported on the longitudinal girders had the most restricted laps, limited by the width of the girder top flange and the construction tolerances needed to seat the pre-cast panels. The joints were formed using straight laps that are compliant to EC2 using reductions for higher strength

concrete (C50/60) and the actual stresses in the bars. Complying with this ensures that there is no need for Departures from Standards or fatigue concerns. A minimum width top flange of 650mm was used on Saleyard River Crossing, but a slightly wider flange would have made the design easier, even if the flange was less efficient. Saleyard Bridge was not subject to seismic effects but, if a design had to carry significant impact forces or where a bridge is located in a seismic zone, the laps would have to be designed for full bar stress to ensure ductility (BS EN 1992-1-1 cl.8.1(1)). The bottom reinforcement mat was orientated to put the transverse spanning bars in the lowest layer. The transverse top reinforcement was in the second layer with the intention that the longitudinal bars could be used as confining reinforcement and reduce the lap length. This was not achieved when it was realised that the cross fall of the deck was sufficiently different to the flange of the horizontal girders to cause the bars to be shifted out of vertical alignment (see Figure 6). The longitudinal bars were moved into a third layer locally over the beam to maintain cover. An improvement discovered during installation was that it would have been easier to install the unsupported connections if the T1 and T2 layers were switched as fewer threaded lacers would have been required.

FIGURE 6

Supported connections resting on the longitudinal steel girders

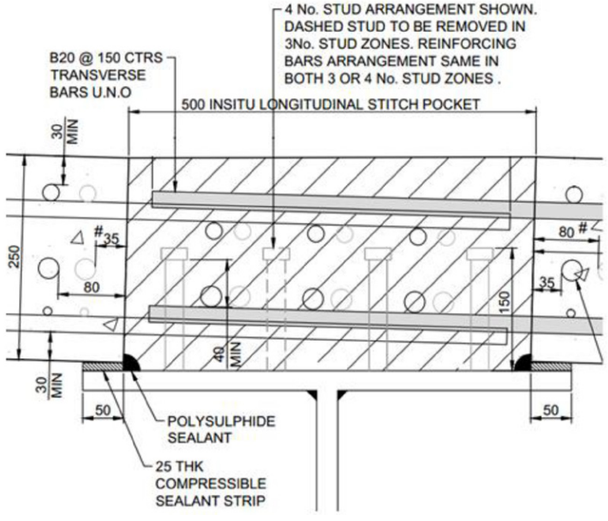

4.2.3 UNSUPPORTED CONNECTIONS

The unsupported connection used a lower nib in the pre-cast panel to avoid the need for all the joints to be supported on secondary steelwork. The length of the nib was designed to suit the lap length needed at the location. For the B32 bars required to carry the integral abutment hogging moment a 1.3m long nib was used. Having a lower nib section controlled the construction sequence so that the panel with the nib had to be placed before the lapping panel. However, with a straight lap, the bars are less likely to clash and can be more easily adjusted than U-bar loops. The T2 lacers are added after the slabs are placed (Figure 7).

FIGURE 7

Unsupported connection

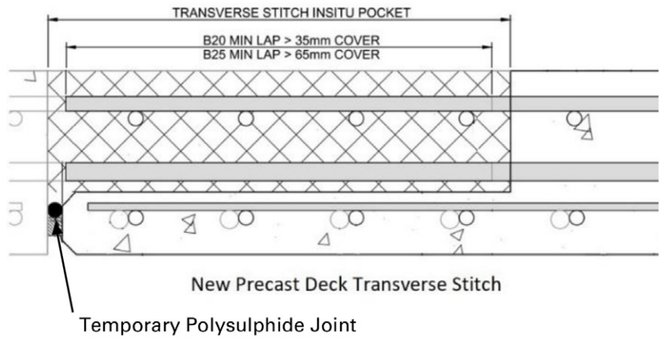

With a single layer of reinforcement in the lower nib the panels were viewed as being susceptible to damage during handling or panel placement, so the longer nibs were supplemented with cast-in 76 x 38 steel channel sections at 2m centres. This proved a robust solution and all the panels were placed without any issues.

5. Design for Construction

Much of the programme benefit of pre-casting is a realisation of the time that would otherwise been taken by carpenters and steel fixers resolving site issues of fit-up. The construction tolerances that would be accommodated by the skilled operatives on-site are transferred to the design planning and drafting stage with complex pre-cast components. In order to turn the theoretical design into a practical solution for pre-casting a greater level of precision in reinforcement bar setting out was required and closer coordination needed between the contracting and design team.

5.1 TOLERANCES

To get the alignment between components correct, the design must consider all the tolerances that occur during the whole fabrication process, including all dimensional and positional tolerances.

Unit size tolerances to Specification of Highway Works clause MCHW 1728.3s can be up to ±30mm whilst pre-cast code BS EN 15050:2007 A1 tightens the dimensional tolerance to the greater of 5mm or L/500. On-site the size tolerance for Saleyard was kept under ±5mm by using a high intensity supervision and checking processes, but ±10 mm would be more practical for future designs.

Bar length tolerances are ± 25mm for straight bar using BS8666. The Saleyard bridge bars were original supplied up to 200mm short, which delayed construction whilst the bars were reordered. In retrospect, it would have been easier to have bars supplied too long and then cut to length by the site team during panel assembly, so that the lap was assured, rather than risk the delay over bars being supplied incorrectly. For pre-cast decks, it is recommended to discuss with the contractor the option to disregarding the length tolerance in the design and to transfer this risk to a site operation of having to shorten some bars at the pre-cast yard. Reinforcing bar position achieved the jointly agreed tolerance of ±5mm.

Controlling the steel girder setting out with light transverse sections between girder pairs or accurately surveying the erected position of the beams are also mitigations worth considering. A panel positional tolerance of ±25mm is a reasonable assumption, although Saleyard Bridge achieved ±10mm, as the position was controlled by the clearance to the shear studs. One area that could have been improved on Saleyard Bridge was to use an additional 50mm box out around the top bars to allow longer top bar laps (Figure 8)

FIGURE 8

Additional top mat lap length using a box out.

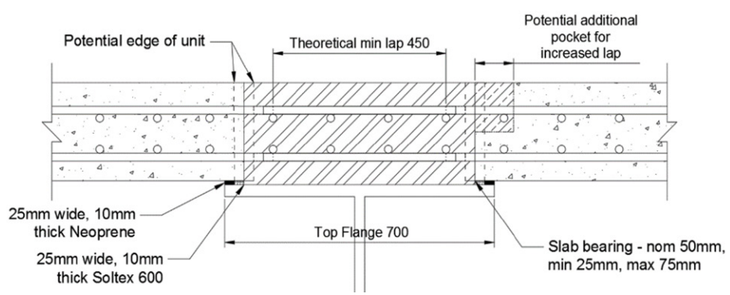

5.2 LEVELLING AND ALIGNMENT

If it is intended to use a visible pre-cast parapet plinth or if spanning over more than two beams, levelling screw details should be included but this increases cost and complexity. At Saleyard Bridge, it was concluded that these details were not needed, and a levelling accuracy of 10mm was achieved. The tight tolerances between bars and shear studs meant that creep of units along the bridge did not occur because incorrect placing of units was prevented by the stud arrangement.

5.3 SEATING AND SEALING

The weight of the pre-cast panels is much higher than permanent formwork. The seating strips under the edges of the pre-cast unit need to be soft enough to absorb imperfections in the concrete soffit, but strong enough to not crush under the weight of the panels. The detail used combined a 25mm wide Shore 60 strip (Neoprene) with a 25mm wide expanding sealing strip (Soltex 600).

Sealing of the unsupported butt joints was tricky and could be improved. The limited space available between stitch reinforcing bars made placing the polysulphide sealing time consuming. A compressible waterstop cast into the end of the nib or matching panel face could save time in future. A test of watertightness is recommended to check for leaks.

5.4 COVER

Minimising cover allows thinner bridge decks as effective depth is maximised to give greater capacity. However, cover also affects lap lengths with greater cover reducing the lap length required. As cover was carefully controlled on site, the cover tolerance was agreed to be set at ±5mm. The site team bettered this an achieved an accuracy of 2-3mm at critical bar positions.

5.5 LIFTING EYES

The panel lifting arrangement needs to be agreed with the Contractor usually to allow the unit to be lifted as soon as possible after the concrete has gained early strength. The lifting eye detail used at Saleyard required a concrete strength of 40 N/mm^2 which ended up delaying the fabrication of the panels during the winter. Lifting eyes that can work with a concrete strength of 20N/mm^2 or less would permit faster fabrication.

Leaving exposed lifting eye steelwork is unlikely to be acceptable to many bridge owners. Stainless steel lifting eyes are permissible but expensive, otherwise cover has to be restored. Burning out lifting eyes risks damaging the surrounding concrete so a two-part detachable lifting detail is preferred.

5.6 STEELWORK DETAILS

Care is needed in sizing the steelwork top flange splice plates to keep edge of splice plate at least 75mm from the edge of the flange. This allows the pre-cast deck units to be seated around the splice plate. Where pockets are used on cantilever panels the pocket positions were adjusted to match the splice plate locations. The girder lifting lugs were ground down to 2mm above the flange and also had the match pocket locations.

5.7 FIXING SHEAR STUDS

A 10mm tolerance was agreed for shear stud position and fully detailed on the drawings to control this, backed up with verification prior to erection. With studs in the right place, confidence is gained early in landing the pre-cast units that they will continue to fit when positioning from the abutments to middle. At Saleyard Bridge, 4 studs per row were required near the abutments and only 3 towards midspan. As we wished to avoid clashes with the deck reinforcement one row of studs were omitted, creating an asymmetrical detail rather than making the three studs equidistant (Figure 6).

Several discussions took place throughout the Saleyard Bridge pre-cast deck design as to whether it would be better to install the shear studs onto the beams after the pre-cast deck units were in place. Experience on-site, where a limited number of shear studs were welded to the top flange after the deck panels were installed, highlighted the significant problems associated with this strategy. Space between reinforcement is severely restricted and unlikely to be large enough to fit a shear stud gun. Manual welding was hindered by lack of space and was very slow to complete. Testing of these shear studs after installation was additionally hampered by the protruding reinforcement in the stitch zones or pockets. The conclusion was that studs should only be attached after the deck is in place as a last resort.

5.8 INTEGRAL ABUTMENTS

The use of straight laps allows larger reinforcement to be used at integral bridge abutments, but this also required more consideration of the reinforcement detailing. The contractor needs to confirm the construction sequence that is to be used. A straightforward sequence would be to construct the abutment up to deck soffit level prior to installation of the pre-cast panels. Units would be installed from either end towards the middle to create a safe access from the abutment. Casting the abutment to deck soffit level assists in restraining the ends of the girders thereby reducing buckling effects on the steelwork and allows foot access onto the installed pre-cast decks. To minimise the risk of the reinforcement clashing, the bottom mat of the abutment reinforcement where the deck units lap onto it, should be kept low. The transverse mat can be positioned above the longitudinal bars as shown in Figure 9.

FIGURE 9

Integral abutment detailing to avoid clashes

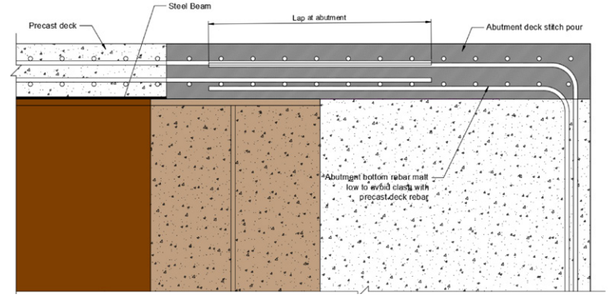

6. Site Performance

Installation of the units onto the beams started slowly while the team got used to the process, but rapidly increased to a max of 10 units per day for one crane and a three-person installation gang. This equated to 226m^2 of deck installed in a day. The graph shows the daily number of units installed, noting that lower figures were associated with switching the crane position between abutments and installation of the final units of the deck (Figure 10).

FIGURE 10

Daily placement rate for pre-cast deck panels.
C = crane reposition.
C/P = crane reposition and stitch pour.

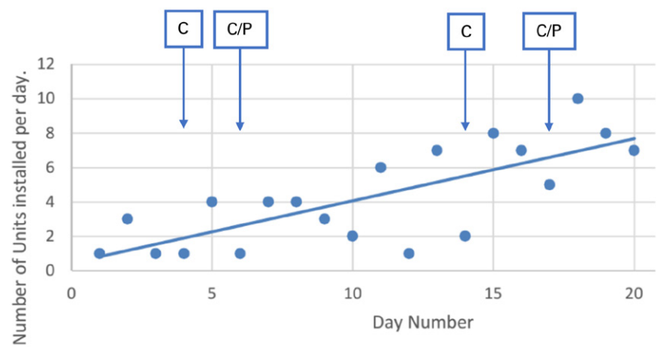

Stitch pours were required at two points during the erection programme to prevent girder buckling. Insitu rebar for the stitches was placed during unit placement. The polysulphide sealing of the stitch pocket edges took several days. The stitch pouring itself took one day and the strength gained allowed the next unit to be placed three days later.

7. Conclusion

The use of full-depth pre-cast deck panels proved that a deck design with straight laps was a practicable alternative to U-bars type connection details. The ability to increase the multi-beam centres and avoid cantilever edge formwork created a more economical solution. The detailed design and construction planning demonstrated ways of speeding up construction as well as improving site safety.

Acknowledgments

The authors would like to thank Costain, Welsh Government, and Jacobs for permission to produce this paper and all the support with developing approving and checking the design; particularly Toby Bedford who worked tirelessly with us to plan and oversee the very successful site execution of the design.

References

- BSI (2004), BS EN 1992-1-1:2004 Design of concrete structures. General rules and rules for buildings
- BSI (2004), BS EN 1994-1-1:2004 Design of composite steel and concrete structures. General rules and rules for buildings
- BSI (2007), BS EN 15050:2007+A1:2012. Pre-cast concrete products. Bridge elements.
- BSI (2005), BS 8666:2005 Scheduling, dimensioning, bending and cutting of steel reinforcement for concrete. Specification
- The Stationery Office (2019), Manual of Contract Documents for Highway Works, 2019. Specification of Highway Works 2019.
- Yanzido E., Iles D C. (2004), Pre-cast concrete decks for composite highway bridges SCI Technical Report P316, London, UK

EXAMPLE CALCULATION FOR A 450MM LAP TO BS EN 1992-1-1

NOTATIONS AND CLAUSE REFERENCES

Example calculations for the lap length are in accordance with BS EN 1992-1-1 and are referenced as 2-1-1/*clause number* or 2-1-1/*(equation number)*. All notation is used stated in BS EN 1992-1-1.

EXAMPLE

A 450mm lap arrangement is shown in Figure 11 below with a 25mm bar length tolerance included. The design considers main reinforcement of B20 bars at 150mm centres in the T2 layer and B20 bars transverse reinforcement also at 150mm centres in the T1 layer with 60mm of actual cover above the transverse bars and the concrete surface. Reinforcement is taken as stressed to 90% of capacity ($\sigma sd = 435N/mm^2$) so $\sigma sd = 392N/mm^2$ and the structure is not in impact or seismic zone.

The stitch concrete strength is C60/75 which is the upper limit set out in 2-1-1/8.4.2 (2) beyond which verification of increased average bond strength would be required.

FIGURE 11

Example Longitudinal Stitch Arrangement

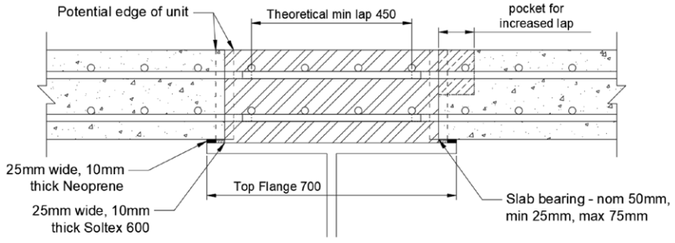

LAP LENGTH

The following equation is given in 2-1-1/8.7.3(1) for the design lap length, l_0:

$$l_0 = \alpha_1.\alpha_2.\alpha_3.\alpha_5.\alpha_6.l_{b,rqd} = 1.0x(0.7)x1.5x428$$
$$= 450mm \quad \geq l0,min=300mm \qquad 2\text{-}1\text{-}1/(8.10)$$

where

$$l_{0,min} = \max[0.3.\ \alpha_6.l_{b,rqd};15.\Phi;200mm]$$
$$= \max[203;300;200]= 300mm \qquad 2\text{-}1\text{-}1/(8.11)$$

Basic Anchorage Length

The basic anchorage length of a bar, $l_{b,rq}$, is taken from 2-1-1/8.4.3(2):

$$l_{b,rqd} = (\Phi/4).(\sigma_{sd} / f_{bd})$$
$$= (20 / 4) \times (392 / 4.57) = 428mm \qquad 2\text{-}1\text{-}1/(8.3)$$

where

$f_{bd} = 2.25.\eta_1.\eta_2.f_{ctd} = 2.25 \times 1.0 \times 1.0 \times 2.03$
$= 4.57\ N/mm^2$ 2-1-1/(8.2)
$\eta_1 = 1.0$ for good bond as stitches < 250mm deep 2-1-1/8.4.2(2)
$\eta_2 = 1.0$ for $\Phi \leq 32mm$ 2-1-1/8.4.2(2)
$f_{ctd} = \alpha_{ct}.f_{ctk,0.05} / \gamma C = 1.0 \times 3.05 / 1.5$
$= 2.03\ N/mm^2$ 2-1-1/(3.16)
$f_{ctk,0.05} = 0.7 \times f_{ctm} = 0.7 \times 4.35 = 3.05\ MP$ 2-1-1/ Table 3.1
$f_{ctm} = 2.12 \times \ln(1+(f_{cm}/10) = 2.12 \times \ln(1+(68/10))$
$= 4.35$ MPa For > C50/60 2-1-1/ Table 3.1
$f_{cm} = f_{ck} + 8 = 60 + 8 = 68$ MPa 2-1-1/ Table 3.1

LAP LENGTH FACTORS

Factors $\alpha_1,\alpha_2,\alpha_3$ and α_5 are taken from 2-1-1/Table 8.2

Shape of Bars

$\alpha_1 = 1.0$ (Tension straight bar)

Concrete Cover (see Fig.12)

FIGURE 12

Extract of BS EN 1992-1

Figure 8.3: Values of c_d for beams and slabs

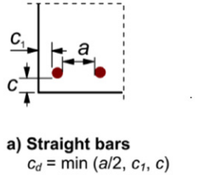

a) Straight bars
c_d = min ($a/2$, c_1, c)

$\alpha_2 = 1 - 0.15(c_d - \Phi) / \Phi = 1 - 0.15(60 - 20)/ 20 = 0.70$ $(0.7 \leq \alpha_2 \leq 1.0)$
Fig 8.1a c_d = min (a/2, c_1, c) = min (65, n/a, 60) = 60mm
Note Thomas Telford guidance cl.8.4.4 indicates c_{nom} can be used

Confinement by transverse reinforcement not welded to main reinforcement

$\alpha_3 = 1$ Ignore confining transverse reinforcement
Note: Thomas Telford guidance section 8.7.4 states it is reasonable to adopt $\alpha_3 = 1$ and ignore the benefit from transverse reinforcement to avoid the requirement of 2-1-1/8.7.4.1(3) to have the transverse reinforcement made up of links or U bars anchored into the body of the section.

Confinement by transverse pressure

$\alpha_5 = 1.0$ No transverse pressure

Combined $\alpha_2\alpha_3\alpha_5$

2-1-1/8.4.4(1) requires that the product of $\alpha_2.\alpha_3.\alpha_5$ is not less than 0.7. With α_3 and α_5 being taken as unity, and α_2 limited to being not less than 0.7 itself, this will be complied with.

$\alpha_2.\alpha_3.\alpha_5 \geq 0.7 = 0.7 \times 1.0 \times 1.0 = 0.7$ so use 0.7

Percentage of reinforcement lapped

$\alpha_6 = 1.5$ for 100% laps without staggering 2-1-1/Table 8.3

Note: 2-1-1/8.7.2(4) allows 100% laps if all of 2-1-1/8.7.2(3) is complied with and bars are all in one layer. A discrepancy in that 2-1-1/8.7.2(3) requires following 2-1-1/Figure 8.7 which shows a staggered 50% lap arrangement, as highlighted in the Thomas Telford Guide Figure 8.7-3 for arrangement (a) where an α_6 = 1.4 could be adopted. Obviously complying with a 50% staggered lap arrangement to allow a 100% non-staggered lap arrangement is contradictory and hence it is considered that so long as the other aspects of 2-1-1/8.7.2(3) are complied with, 2-1-1/8.7.2(4) will allow 100% non-staggered laps.

For nib stiches shown below in Figure 13, both the top and bottom mat of longitudinal reinforcement is in tension as acting as part of a composite beam. This could be interpreted as falling foul of the second part of 2-1-1/8.7.2(4) that says, *"where the bars are in several layers, the percentage should be reduced to 50%"*. However, as explained in the Thomas Telford guide section 8.7.2, the intention of this requirement was due to the importance of layer separation. Hence, it is considered that so long as the layer separation is greater than the 2Φ or 20mm requirement of 2-1-1/8.7.2(3), 100% laps without staggering are still considered valid.

FIGURE 13

Pre-cast Deck Transverse Stitch Example

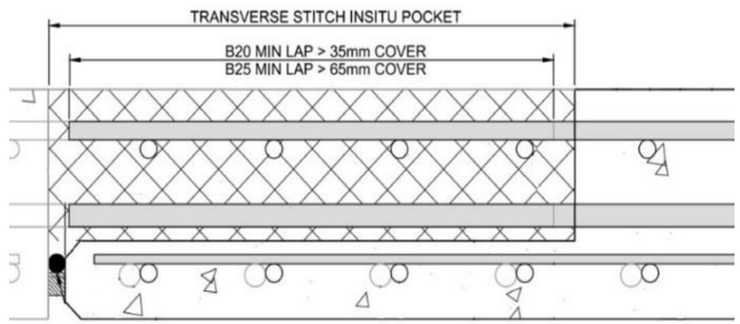

Tom Argyle, MEng CEng MICE

Principal Engineer
Engineering, Design and Project Management
Epsom, UK

Rachel Mitchell, MEng CEng MICE

Senior Group Engineer
Engineering, Design and Project Management
Epsom, UK

Construction of the Jack Williams Gateway Bridge - A Skewed Arch for the A465 Heads of the Valleys Scheme

Abstract

As part of the A465 Heads of the Valleys road improvement scheme a new 118m span steel arch bridge was constructed across the River Clydach gorge. The bridge provides a feature structure at the 'gateway' to the Brecon Beacons National Park, with the A465 mainline crossing into the park at this point.

The bridge construction took place between 2016-2018. This paper focuses on the construction methodology and how challenges that arose during the construction of the bridge were resolved between the designer, main contractor and steelwork fabricator. The items are considered in construction order, foundations, installation of deck steelwork, deck concreting, arch erection, and hanger tensioning.

FIGURE 1

The Jack Williams Gateway Bridge crossing the A465 and Clydach Gorge

1. Introduction

The Gateway Bridge carries a new two-lane single carriageway road over the split level A465, junction sliproads, River Clydach, Clydach Gorge designated geological Site of Special Scientific Interest and a national cycle route. The design was carried out by Atkins for the design and build contractor Costain with architectural input from Knights Architects. The steelwork fabricator was Victor Buyck Steel Construction. The bridge design was completed in early 2016.

The 14.5m wide steel-concrete composite deck consists of two 1.5m deep I girders 10.5m apart with full depth cross girders at 7.5m centres aligning with the cables. These cross girders alternate with secondary 0.6m deep girders. The steel deck is compositely connected to a 0.25m thick reinforced concrete deck slab. The deck, which spans 118m between abutments, has a 2.5% fall from the south to the north, the deck sits on pot bearings which provide longitudinal restraint at the low point at the north end. There is a Type 6 expansion joint at the free end.

The single span thrust arch rises 50m above the valley floor and 25m above the deck and spans over the deck at a skew of 15°.

The arch's longitudinally stiffened rectangular section varies from 3x3m at the base tapering to 3x1.5m at the crown. The deck is supported by 22 fully locked coil cables along its length. At the deck level these cables are attached to outriggers at 7.5m centres to allow sufficient clearance to the structure free zone around the carriageway. At the arch the cables are connected to external lug plates with internal stiffening inside the arch.

The deck and arch are fabricated from S355 weathering steel. The arch is painted externally for aesthetic reasons.

2. Construction Sequence

The construction method was developed at the outset of the design around the constraints imposed by the structure's location and the structural form, in close conjunction with Costain the contractor and with input from Victor Buyck. The construction sequence is outlined in Figure 2.

The reinforced concrete abutments and arch foundations were constructed first. Three sets of temporary trestles to support the deck were then erected. The deck was lifted in four sections as this was the maximum weight of lift that could be practically achieved from the crane platforms on either side of the gorge and the available cranes in the UK.

FIGURE 2

Outline construction sequence for Jack Williams Gateway Bridge

1 Deck steelwork is erected in four sections on temporary trestles to form a 4-span structure.

2 Precast reinforced concrete deck panels for the deck cantilevers are installed.

3 The main deck slab cast in-situ to provide restraint against the cables skewed loading

4 Three temporary trestles to support the arch are erected on the deck.

5 The arch is lifted into place in 4 sections using cranes located behind abutments.

6 The arch base is fixed against rotations and the arch temporary trestles are removed.

7 The cables are installed to correct length

8 The deck trestles are removed transferring the deck load to the cables.

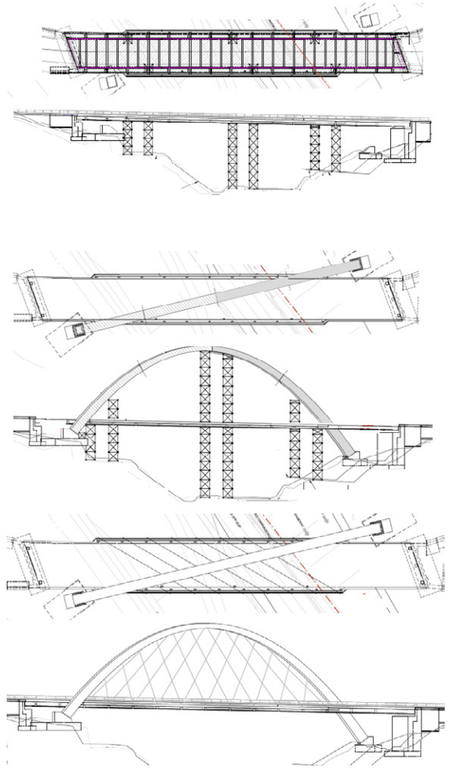

The deck sections are connected with bolted site splices on the main I girders. There is a C-shaped beam connecting and strengthening the hanger connection outriggers, this element is connected with a welded connection, and obscures the bolted connections to maintain the aesthetics of the bridge.

FIGURE 3

Deck during installation showing C-beam (welded) and I-girder (bolted)

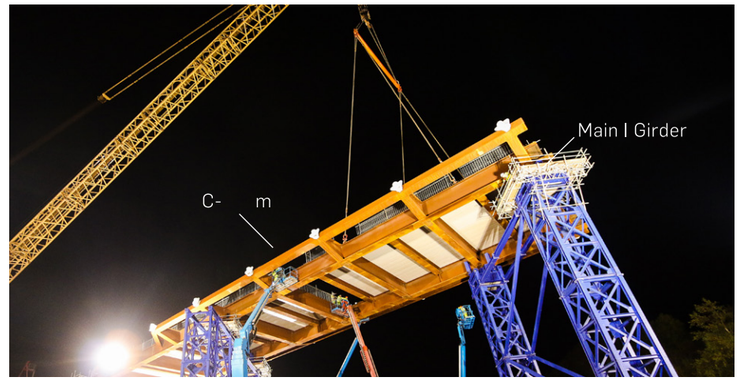

The deck concrete was cast before installing the arch and hangers because the asymmetric inclination of the hangers causes a twisting effect in the deck. The east side is pulled north, and the west side is pulled south. Without the deck slab the ladder deck arrangement of girders would need additional diagonal bracing to prevent slewing. The elimination of the need of temporary restraint at this stage was balanced against the logistical challenge of having the steelwork sub-contractor on site for two separate operations, deck lift and arch lift, with the concrete contractor carrying out their work in between.

Once the deck concrete had been cast the upper trestles were installed. The trestle footings on the bridge deck were held down with bolts connected to the steel beams and passing through the concrete deck. The arch was lifted into place in four sections, the arch sections were connected with bolted splices for speed of erection and then permanently welded once the full arch was installed. Once the arch was installed and fully fixed at the base the arch trestles were removed.

The hangers connecting the deck and arch were then installed. The deck was raised slightly on jacks at the trestle tops. The hangers were installed and nominally tensioned to remove catenary draping. The jacks supporting the deck were then released to effectively lower the deck onto the hangers. The deck trestles could then be removed and the surfacing and fittings installed on the bridge deck.

Alternatives considered and eliminated included: launching the deck rather than lifting it in sections. This was not feasible due to the lack of a suitable flat location at either side of the bridge to assemble and launch the deck from. Using more trestles and reducing the size of the lifts was not possible due to the constraints of locations for the trestles in the Clydach Gorge.

3. Foundations

The arch bases and abutment are founded on rectangular spread footings. Piles were not required as the structure is founded on rock, this was one of the factors leading to the selection of a thrust arch form. The pad foundations for the arch base are aligned with the valley slope, with the arch support wedge skewed. The exposed vertical concrete faces are clad in local stone. The north abutment wingwall are reinforced earth construction, at the south abutment they are T-shaped reinforced concrete walls. The local area is geologically complex with some voids identified in the siltstone/mudstone.

Boreholes were taken at the anticipated foundation locations, but there was a high level of local variation at the site. This was anticipated during the design and a programme of drilling and grouting was specified under the proposed foundations to fill any voids.

During construction the level of the strong siltstone/mudstone was found to be lower than expected at the exact foundation levels. The weak material was excavated and mass concrete used to fill back to the base of the spread footings. Geotextile was used to build up the slopes around the foundations to minimise the exposed concrete.

FIGURE 4

North abutment and arch footing during construction. Exposed vertical faces have been clad in local stone.

4. Lower Trestles

The location of the trestles was controlled by the need to avoid the A465 and River Clydach/Clydach Gorge SSSI and to make use of the existing level ground at the cycle path. Due to these constraints the trestle sets were skewed relative to the deck. Each trestle was locally positioned to align with the intersection between main and cross girders of the deck. The trestles are founded on reinforced concrete pad foundations designed by Costain. The midspan trestles were adjacent to the A465, to protect the trestles against vehicle impact 2m high reinforced concrete plinths were constructed for the towers on the pad foundations.

The trestles were built from reusable modular units provided and designed by Victor Buyck, with bespoke steelwork at the top to fit with the permanent structure. The sets of trestle towers at each location were connected with diagonal bracing.

FIGURE 5

Installation of the final section of arch showing the deck on lower trestles and arch supported by the upper trestles.

The bridge deck was supported by the trestles for several months whilst concreting, arch trestle erection, arch installation, arch trestle removal and hanger installation were progressed. During design it was assumed that the deck would have an articulation agreed with the steelwork fabricator of fixed at one abutment with longitudinal sliding on the trestles and other abutment and transverse fixity on one side. An initial proposal from the fabricator was to provide this by having the deck on shims with a layer of PTFE to allow sliding. Concerns about this proposal were that the PTFE was likely to become dirty on site and the resulting increased friction could overload the trestles when the deck expanded and contracted due to thermal actions. It was also a concern that the arrangement did not provide an adequate rotational release, as assumed by the permanent works design, as the shims were fairly large (400mm x 400mm) to spread the load on the permanent steel girders adequately. This issue was identified close to the time that the deck was due to be installed at the completion of the temporary works design details. There was no scope to delay the deck lift as the crane would only be on site for a limited time. The issue was resolved hours before the lift was due to start by using elastomeric bearings that were sourced from a previous project at very short notice. The experience highlighted the need for all parties to ensure that all critical temporary works details are agreed in good time.

5. Splice Connections on Steelwork

The location of the permanent bolted splices on the deck main beams was fixed by the designer and steelwork fabricator early in the detailed design stage to allow calculation of the stress build up and precamber. During erection of the deck these connections were made with a reduced number of bolts to allow shear connection, but not a full moment connection. The remaining bolts were installed to give the full moment connection after the crane had been removed. This was modelled in the design stage by including the temporary connections as pinned. During detailed design the agreed sequence was that the two northern sections were to be lifted in place first, and then the crane moved to the south side and the southern two sections installed. It was assumed in design that the full moment connection between the north sections would be installed before the final deck section was installed. As the actual lifts approached it was clear that to minimise the amount of time the high capacity crane was on site it would be preferable to make the full moment connections after all four deck sections were in place. This late change potentially affected the design assumptions and final built in stresses in the deck steelwork. To resolve this the bolt arrangement for the temporary “shear only” connection was reviewed. With only the steelwork in place the moments at the splice location are significantly lower than in the permanent condition. It was demonstrated that the temporary spliced connections actually provided enough strength to act as a full moment connection for the steelwork, as had been assumed to be present in the design. This allowed the altered sequence to be used, ensuring the north and south lifts could take place on consecutive weekends.

6. Precast Deck Units

Precast units were used for the parapet upstand and cantilevered section of the deck slab. Precast units were used for the full deck of another bridge on the scheme and the details developed by Atkins for that bridge were used for this structure too. Precast units were preferred by Costain for speed of installation and eliminating the need for cantilever formwork and subsequently minimising work at height on the edge of the deck.

The precast units were 7.5m long and 1.75m wide, sized to fit on the main steelwork below. They were supported on three sides at installation by the main longitudinal beam and the outriggers provided for the hangers. At the ends of the bridge outriggers were provided where there were no hangers to support the precast units. Concerns have been raised about the

fatigue life of connections between precast units where overlapping hoops are used and so a design was proposed that enabled full length straight laps to be provided at the connection between units and into the cast in-situ deck sections. The nibs used to allow this were too thin for full cover to be provided to their reinforcement and so stainless steel reinforcement was specified in these. The detail of connection between the precast units is shown in Figure 6.

FIGURE 6

Detail showing the connection between precast units used for the deck cantilevers.

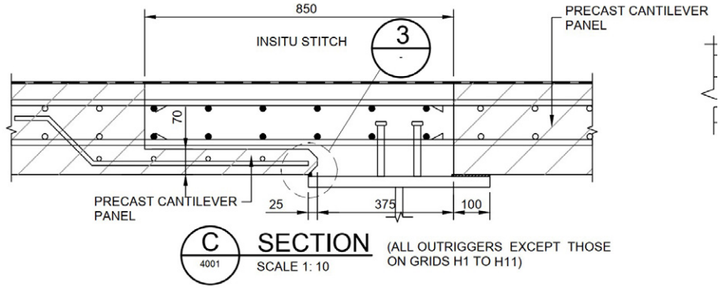

The units were installed by crane in sections, initially from the abutment and then from the section of deck that had last been cast. During construction there was a 1.6m high solid hording installed on these units, and therefore they had to be checked for overturning under wind actions and the corner units at the deck end needed to be held down mechanically until the in-situ deck concrete was cast. The units were standardised as far as possible, but due to several constraints (the deck flaring slightly at one end, cut outs to avoid clashes with the steelwork splice plates, lighting column plinths) there were 18 variations out of a total 32 units. Using precast units, it was important that the shear studs on the steelwork were positioned accurately and that the bars cast into the units were positioned correctly so that the units fitted on site. Both these aspects were highlighted to the respective fabricators (VB and Costain respectively) and then checked before installation of the units began. The installation of the units went well on site and saved time on the construction programme compared to having the whole deck cast insitu.

7. Upper Trestles

The trestles used to support the arch were positioned directly above the trestles supporting the deck. The central tower had two trestles resting on the deck and due to the skewed arrangement of the arch the two side towers had one leg on the deck and another founded on reinforced concrete pad foundations.

The upper trestles were not directly connected to the lower trestles. As the concrete deck was already cast at the point when the arch trestles were installed, connecting the trestles would have required holes to have been left in the deck and then filled in later. Instead, the upper trestles sat on steel plates on grout bearing onto the concretes slab, with a further connection to the top flange of the deck steelwork with bolts that passed through the concrete deck to provide holding down. These stainless steel bolts were located to coincide with the designed permanent shear stud locations. When the arch trestles were removed the bolts were cut back 30mm and left in the concrete slab, with the recesses filled with grout, to act as shear studs in the permanent condition. These bolted connections had to align with the main deck steelwork, but as the trestle legs were skewed to fit with the ground level site constraints, steel spreader beams below the legs were required to transfer the loads from the trestle legs to the bolted connections.

The detailing of how the arch trestles connected to the deck was developed collaboratively between the permanent works designer and steelwork fabricator. Initial fabricator proposals were simpler, using anchorages cast into the deck slab, not directly connected to the steel beams below. However, this was not possible in the final design as the deck slab did not have sufficient shear capacity for the trestle loads at the trestle leg locations. Moreover, with the deck slab reinforcement and shear studs, there was not space for simpler anchorages for holding down the trestle legs within the slab.

8. Arch Installation

The arch was installed in four sections using a crane on the north side for the first two and then on the south side for the third and fourth section. The fabricator designed temporary bolted connections between the arch sections used prior to full welding of the connection.

At the arch base there is a steel base plate grouted onto the concrete foundation with anchorage bolts cast into the concrete plinth. The initial design proposal was to have these bolts grouted into place once the arch was installed, but the fabricator and contractor proposed casting the bolts into the plinth and using oversized holes in the arch base to allow for dimensional tolerances on installation. In the permanent condition the arch is always in compression and shear connection is provided by friction between the steel base plate and grout. In the temporary case, before the base was grouted up, a temporary restraint system was required to restrain the arch base against lateral movement.

The steep slope below arch bases complicated the design of this restraint system as it was not possible to provide simple trestle supports in front to the foundations. The final arrangement consisted of a steelwork frame fixed to the arch base and sides of the arch wedge support. The design of this restraint system was the steelwork fabricators responsibility and occurred after the foundations had been designed and constructed, therefore a drill and fix solution was used for the temporary works anchorages. There would have been potential to have had a simpler solution if the design of this aspect of temporary works and the permanent works had occurred at the same time as the reinforced concrete bases could have made allowance for the temporary works support and fixity.

FIGURE 7

Arch base temporary restraint (blue steelwork) and permanent connection detail.

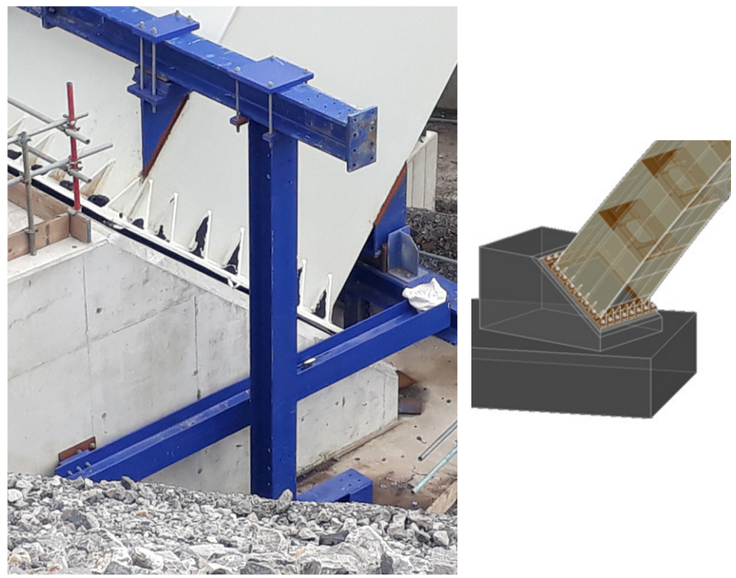

9. Hanger Installation

Once deck and arch had been installed the trestles supporting the arch were removed, with the arch designed to be stable freestanding. The hangers connecting the arch and deck were then installed. The hangers are connected to the arch with a pin passing through a lug aligned with the plane of the vertical plane of the hanger. At the connection to the deck a spherical socket type connection was used.

The hangers were installed with adequate tension to remove catenary sagging effects, but not tensioned to take the weight of the deck. Hydraulic jacks were used to lift the deck off the bearings at the tops of the trestles and once the hangers had all been installed the jacks were lowered at each trestle so that the deck's weight was transferred onto the hangers. At this stage the maximum downwards deflection of the deck was approximately 100mm, which had been allowed for in the deck precamber.

During the early stage of detailed design, it was assumed that the hanger forces required would be specified as part of the design and following the installation of the hangers they would be tensioned to the specified strains using jacks at the deck -hanger connection. The steelwork fabricator proposed the alternative method (ultimately used) of installing the hangers with minimal tension and then lowering the deck onto them, without setting the tension of each hanger with jacks, as achieving a fixed tension in each hanger can be a lengthy site operation. From their previous experience, when each individual hanger is tensioned those surrounding it lose tension and several rounds of tensioning for each hanger can be required to achieve target tensions.

During the design analysis the hanger forces used were based on a model of the bridge with the deck, arch and hangers all activated in one stage. Consideration was given to optimising the hanger forces to minimise the bending moments in the deck, but the advantage in terms of potential steel tonnage savings were not great when compared to design programme and cost, as the deck effects from the design model without modification were already fairly optimal.

The hanger forces generated by the adopted installation sequence differ to those in the design model used. To achieve the hanger forces used in the analysis model on site the design specified a hanger installation length for each hanger that differed slightly from the actual length between the hanger connection. Hangers that were installed slightly longer would pick up less load than others when the deck was lowered from the jacks.

To ensure that this approach had worked on site and the hanger forces were as expected, a number of checks were made on site:

- The deck levels and arch profile were surveyed before and after lowering the jacks.
- The force in hangers was measured by Vibratest method by VSL.
- Lift of tests were conducted on a few selected hangers.

The surveyed profiles before and after lowering of the deck were compared to those predicted in the design so that any significant discrepancies could be identified. The hanger forces in all hangers were measured using the Vibratest method which measures the natural frequency of the hangers and calculates the force in the hanger from this. The results of these Vibratests were then cross checked using lift off tests, carried out by jacking the deck level anchorage, on a sample of the hangers. The location of the lift off tests were selected to be representative but also selected based on ease of access on site. After some false starts on the lift off test methodology the Vibratest tensions ultimately agreed with a high level of accuracy with the lift off tensions.

The results of these site measurements were reviewed by the design team to establish if the hanger forces were acceptable or if a re-tensioning operation was required. The total force in all hangers, and on each side of the deck matched the design values closely (within 2%) and the final deck profile based on surveyed levels of the precast edge beam was also within the required tolerances. The deflection during the deck lowering operation was as anticipated during design.

However, it was found that some of the individual hanger forces did not match the design values closely. Where hanger forces differed from the expected design values the maximum force possible during service, based on the measured permanent effect plus the design live loading were compared to the resistance of the hanger and its connections. The hangers with higher tensions all had sufficient spare capacity. The impact of the variation in hanger forces on the deck and arch were also reviewed. An analysis model of the arch on its own with the measured hanger forces applied as loads was used to check the load effects in the arch against those assumed in the design. To check the effect on the deck the analysis model of the whole bridge, deck and arch was modified to include an additional load case of the difference in force between the tensions assumed in design and measured on site. The impact of the different hanger forces on the total moments, shears and axial forces in the deck was assessed and it was found that the deck had adequate spare resistance in any areas where the effects were increased. Figure 8 illustrates the difference in permanent bending moment in one beam due to the higher force in one hanger. The hogging moment at the hanger location is increased, and the moment away from that hanger is decreased slightly. Based on this analysis it was agreed that no re-tensioning of the hangers was required.

The difference in hanger tensions for individual hangers compared to the design values is most likely due to the difficultly in installing the hangers to the exact specified lengths prior to lowering the deck. The design analysis showed that a difference of just a few millimetres in the hanger length had a significant impact on the force picked up by the hanger. For this type of structure, it may be more practical to design for the hanger forces arising from the construction sequence when all hangers are installed at the exact length between the anchorages. Any increase in the required steel tonnage is likely to be outweighed by the simplification of the construction process. Although in that case, the design would be reliant on the adherence to initial assumptions on temporary support locations.

FIGURE 8

Bending moment in main I-girder from dead load as predicted in the design and as given with the measured hanger forces on site.

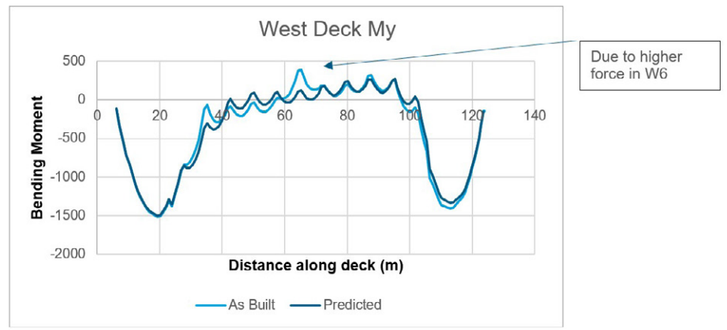

10. Conclusion

The collaborative approach adopted between Atkins, Costain, Victor Buyck and independent checkers during the construction of this landmark bridge allowed challenges to be resolved rapidly so that construction could proceed without delay.

This paper focuses on areas where there were challenges to be overcome and delves less into the aspects that proceeded without issue on site. Overall, the construction of the bridge was a technical success and all members of the team are proud of their involvement.

Acknowledgements

This paper is published with the permission of the Welsh Government and Costain. The temporary works design described in this paper was carried out by Victor Buyck.

Variable Loads for Foundation Design - Experience from the A14 Project

Paul Antoni Nowak

Technical Director
Engineering, Design and Project Management
Epsom, UK

Brijes Patel

FTI Consulting
London, UK

Jessica Sandberg

Senior Group Engineer
Engineering, Design and Project Management
Epsom, UK

Abstract

The A14 Cambridge to Huntingdon Improvement scheme required the construction of 28no new structures on piled foundations. The substructure and superstructure design was the result of close cooperation between bridge and geotechnical designers. This paper describes the approach for deriving variable loads for foundation design through consideration of average operating conditions typically appropriate to foundation limit states rather than reliability-based maximum envelope conditions appropriate for bridge structures.

KEYWORDS

Structures; Foundations; Loads

NOTATION

γ	is a partial safety factor
γ_G	is the partial factor for a permanent action to BS EN 1997-1
γ_Q	is the partial factor for a variable action to BS EN 1997-1
γ_s	is the partial factor for a shaft resistance of a pile to BS EN 1997-1
γ_b	is the partial factor for a base resistance of a pile to BS EN 1997-1
SV	Special Vehicle to Highways England CD 350
SOV	Special Order Vehicle to Highways England CD 350

1. Introduction

The route corridor of the A14 Cambridge to Huntingdon improvement scheme is underlain by predominantly cohesive strata comprising Glacial Till and over-consolidated clays of Jurassic age. Due to the prevailing ground conditions, the 28no new structures required by the scheme were designed on piled foundations. Additionally, a majority of the structures were designed with an integral deck in order to minimise maintenance of their design life.

The substructure and superstructure design involved close cooperation between bridge designers and geotechnical designers, and it became evident through the design process that the loading developed by the structural team for the superstructure may be considered overly onerous when applied to the design of the foundations.

This paper describes an approach for deriving variable loads using current design practice and codes through consideration of average operating conditions typically appropriate to foundation design rather than those derived for the design of the structural elements.

The approach has been accepted by Highways England and is now included on their Technical Knowledge site. Eurocode terminology has generally been used in the paper but can be interchangeable with dead and live loads where traditional analysis with final factors of safety are discussed.

2. Design Approach to Live Loading

2.1 STRUCTURAL DERIVATION OF LOADS

The derivation of Live Loads for use in design of superstructure have been such as to prevent Ultimate Limit State failure of the structure defined as that which would result in loss of service. By its nature this approach considers "factored" live load effects in combination even though the likelihood of occurrence is extremely small.

Historically, for highway structures designed in the UK these variable actions would have been derived using BS5400, Part 2 (BSI, 1978 & 2006) as modified by BD 37/01 (HA, 2001). These loads may have been presented as a combination of Permanent and Variable loads or split into the two components that were typically "unfactored" when they were presented to the geotechnical engineer for design of the structure foundations.

The development of Eurocodes, particularly BS EN 1991, requires that the variable loads for structure and sub-structure design are determined for each component of the variable load.

With respect to the A14 project: Traffic loading was derived from BS EN 1991-1-2 (BSI, 2003) but considering SV and SOV vehicles to the UK National Annex (BSI, 2008) together with a dynamic impact factor.

Wind loading was derived from BS EN 1991-1-4 (BS, 2005) with UK contour plots of maximum wind speed as set out in the UK National Annex (BSI, 2008) but with higher γ values than the default values given in BS EN 1990 (BSI, 2002) to modify the 50 year return period on the chart to the 120 year design life.

Temperature loading for integral bridges was derived from BS EN 1991-1-5 (BSI, 2003) with UK contour plots taken from the UK National Annex (BSI, 2008) but with higher γ values then the default values given in BS EN 1990 to modify the 50-year return period for the 120 year design life.

2.2 GEOTECHNICAL USE OF LIVE LOADS

Historically, soil mechanics and foundation design textbooks did not specifically derive live load as a load component and treated both dead and live load as a single component applied to the foundation. CP2004 (BSI, 1972) and BS 8004 (BSI, 1986) refer to dead and live loads but do not provide specific guidance as to how live loads, apart from wind load, are to be determined or incorporated into foundation design.

Prior to the adoption of BS EN 1997-1 (BSI, 2004), and in parts of the world where it has not been adopted these loads were incorporated into the foundation design with the approach of calculating allowable foundation capacity to a nominal "lump factor" Factor of Safety. If live load is considered in the "lump factor" method the transient nature of the live load component can be accounted for by adoption of a reduced design Factor of Safety with the foundation designed with a higher Factor of Safety for dead load only, or dead and live load considered with a reduced Factor of Safety.

With the introduction of BS EN 1997-1, all of the "Actions" set out in the BS EN 1991 suite of standards have to be considered in geotechnical design.

The UK National Annex to BS EN 1997-1 (BSI, 2006) defines two Combinations to be considered for the adopted Design Approach 1 and applies partial factors to the input parameters with respect to actions. This approach is detailed in design guidance texts such as Bond and Harris (2008) and Barnes (2010), namely:

Combination 1 (soil parameters unfactored)

Permanent Unfavourable (γ_G) = 1.35,

Variable Unfavourable (γ_Q) = 1.35

Combination 2 (soil parameters factored)
Permanent Unfavourable (γ_G) = 1.0,
Variable Unfavourable (γ_Q) = 1.3

Both Combination 1 and Combination 2 should be considered but normally loads from Combination 2 will control foundation design. This approach is stated in BS8004:2015 (BSI, 2015) cl 6.7.2.1.2. For Combination 2, with respect to pile design, partial factors are applied to the shaft friction (γ_s) and base resistance (γ_b).

It should be noted that the partial factors for actions detailed above were derived from those applied to building structures as partial factors to be applied to bridges had not been developed in the National Annex to BS EN 1990 (BSI, 2009) when BS EN 1997-1 was completed and published in 2004. Definitive guidance is, however, provided in Table A.NA.3 of the UK National Annex to BS EN 1997 (BSI, 2006) which refers the designer specifically to Tables NA.A1.2(B) and (C) for buildings and Tables NA.A2.4(B) and (C) for bridges.

Current design guidance refers to compliance with BS EN 1990 but there is no clear definition of the live load combination to be considered. Recommendations in PD6694-1 (BSI, 2011), section 4.3 refers to the application of actions but provide no specific guidance on how these should be combined. Similarly, BS8004:2015, clause 6.7.2.1.3, refers to the combination of actions as a principle but contains no specific guidance on their combination. Tomlinson and Woodward (2015) refers to a combination of actions and implies that they should be combined.

3. Proposed Approach for Geotechnical Design

In considering the approach for foundation design on the A14 project it was considered necessary to understand the background of the combinations in the Eurocodes to understand how they could be pragmatically applied to the pile design by taking account of reasonable load combinations to prevent failure of the foundations.

As detailed in Section 2.1, bridge engineers develop the worst credible combination of variable actions in the design of the structure and sub-structure in order to allow sufficient design redundancy and prevent loss of service over the design life of the structure.

This is shown graphically in Figure 1 and represents a situation that may possibly occur once in the design life of the structure.

FIGURE 1

Load Combination considered by Structural Designer

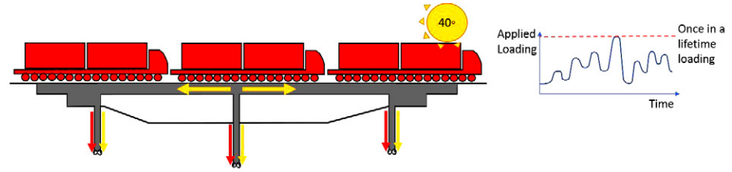

If these loads are directly adopted by the geotechnical engineer, further partial factors will be applied to BS EN 1997-1 either to the actions or foundation design depending on whether Design Approach 1 Load Combination 1 or Load Combination 2 are considered. The application of these additional partial factors essentially creates loading that will apply over the design life of the structure.

In order to consider a more realistic application of actions to geotechnical design, a mechanism was explored whereby an average combination of actions was applied to foundation design with partial factors mirroring close to the peak values considered by the bridge designer. Additionally, settlement of the foundation was considered in relation to a number of combinations of actions.

The case considered is shown graphically in Figure 2 below.

FIGURE 2

Proposed Load for Foundation Design

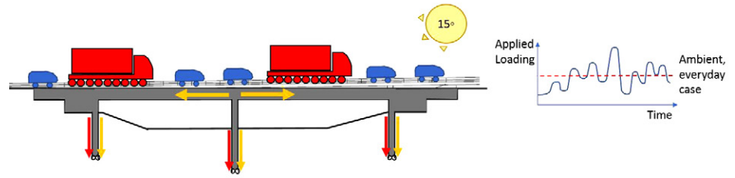

In order to reflect the design load case illustrated in Figure 2, the load combinations in section 6.4 and 6.5 of BS EN 1990 were examined.

It was considered that application of the partial factors from the Ultimate Limit State (ULS) approach in Section 6.4 would introduce additional conservatism into the analysis of foundations. This approach would further increase the input loads to the foundation design which, as described in Sections 2 and 3, were considered appropriate for design of the structure but conservative for the design of the foundation.

The application of a Serviceability Limit State (SLS) approach from Section 6.5 was considered more appropriate as the variable design values generated from the bridge designers could be reduced when considered for foundation design. Use of this approach would bring the variable loads considered in the foundation design from that shown in Figure 1 closer to that shown in Figure 2.

When considering the SLS approach, three possible load combinations could be used to derive variable loads for foundation design, namely;

- Characteristic Combination (Equations 6.14a & 6.14b)
- Frequent Combination (Equations 6.15a & 6.15b)
- Quasi – Permanent Combination (Equations 6.16a & 6.16b)

The choice of the most appropriate combination was determined based on the description of the situation modelled in BS EN 1990.

The Characteristic Combination represents the most onerous SLS condition with a probability of exceedance of 5% over the design life of the structure. BS EN 1990 cl 4.1.3 states that this case "is normally used for irreversible limit states" with respect to the design of the structure.

BS EN 1990 cl 1.5.3.17 states that the Frequent Combination is used when the value of an action will be exceeded/have a fixed probability of exceedance over short periods of time within the reference period. BS EN 1990 Section 4.1.3 defines the Frequent Combination value as used for verifications of reversible serviceability states and is considered the "typical" condition of the structure where the design load could be exceeded, but this would occur infrequently.

The Quasi-Permanent Combination is the least onerous of the three SLS cases. BS EN 1990 cl 1.5.3.18 states that the Quasi-Permanent value is determined "so that the period for which it will be exceeded is a large fraction of the reference period."

Based on the descriptions of the SLS combinations given above, it was decided that the use of the Frequent combination was most appropriate to reflect the conditions illustrated in Figure 2 with respect to variable load. The use of the Characteristic Combination did not afford a significant reduction on the loads provided by the bridge engineer and that the Quasi-Permanent Combination effectively ignored the impact of variable load on the design of foundations

It is worth noting that, if the Frequent Combination is considered then the traffic load requires use of Load Group gr1a but gr5 and gr6, relating to SV and SOV vehicles, need not be considered with the ψ factors being assigned a value of zero in Table NA.A2.1 This is considered realistic for the distribution of traffic over a highway structure during its design life where the likely occurrence of these vehicle types is infrequent, although they would have to be considered with respect to the performance of the superstructure to prevent ULS failure under exceptional loading

4. Example from the A14 Project

The piled foundations for the structures on the A14 project took the form of either a single or double row of piles beneath each structural support. Piled foundations were of 900mm, 1050mm or 1800mm diameter, the larger usually as a single row of piles for abutment foundations.

The loads for foundation design were provided by the bridge engineers from their structural analysis of the bridge deck. They were provided either as:

- Individual permanent and variable load combinations at node points for a single row of piles, or;
- Overall load combinations per support for abutments or piers on multi row pile groups.

It was considered by the geotechnical and structural design teams on the A14 project that a variable load calculated from the Frequent Combination, which was approximately 50% of the permanent load, was the most reasonable for foundation design of a highway structure where traffic loads are transient over a daily cycle.

The piled foundations on the A14 project were designed to BS EN 1997-1 for both Design Case 1, Combinations 1 and 2 as described above using the Frequent Combination variable load in order to ascertain the required design pile length. It was found that Design Case 1, Combination 2 gave the longer design pile length.

For the single row piled foundations, pile design length considered the worst-case load for an individual pile in the pile group.

For the multi row pile groups, the piled foundation was analysed using the REPUTE Boundary Element program with the variable loads for the overall pile group modelled as the Frequent Combination.

In addition to the pile design to BS EN 1997-1, the settlement of the piled foundations under applied load were considered after the approach of Fleming (1992) to calculate the theoretical settlement versus the applied load.

This approach was applied to the most and least loaded piles in a single row foundation to ascertain the potential differential settlement under load across the pile group.

For the multi row pile groups, the most heavily loaded pile from the group analysis was analysed to determine the likely maximum settlement under load to compare with that generated from the REPUTE analysis.

To illustrate the effect of the approach outlined above, an example is taken for an integral bridge abutment taking a local road over the main A14 route corridor that was deigned on a single row of 1050 mm diameter bored cast in situ piles.

The following Characteristic design loads for the most heavily loaded structural node were provided from the structural analysis by the bridge engineering team:

Permanent Load from Structure:	1380 kN
Variable Load (Traffic gr1a)	500 kN
Variable Load (Traffic gr5)	850 kN
Variable Load (Thermal)	300 kN
Variable Load (Wind)	100 kN

Table 1 below summarises the factored variable loads derived for each of the load combinations from the Characteristic structural loads provide by the bridge engineers.

TABLE 1:

Derivation of Variable Load Cases for Design

Load Case	Traffic (kN)	Thermal (kN)	Wind (kN)	Total (kN)
Unfactored	850	300	100	1150
BSEN 1990 ULS	978	234	73	1285
Characteristic	575	234	73	812
Frequent	431	234	0	665
Quasi-Permanent	0	195	0	195

It should be noted in Table 1 that, under BS5400 and BS EN 1991, thermal and wind loads would not be combined. The smallest value has not been considered in the load comparison.

The results presented show that the unfactored (BS5400) and ULS variable loads are close to the design dead load value of 1380 kN per pile. If the unfactored variable load is multiplied by Q = 1.3, as suggested by Bond and Harris, a value of 1495 kN results, which is higher than the permanent load. The results for the example described above are illustrated in Figure 3 below.

FIGURE 3

Comparison of predicted pile settlement under design loading

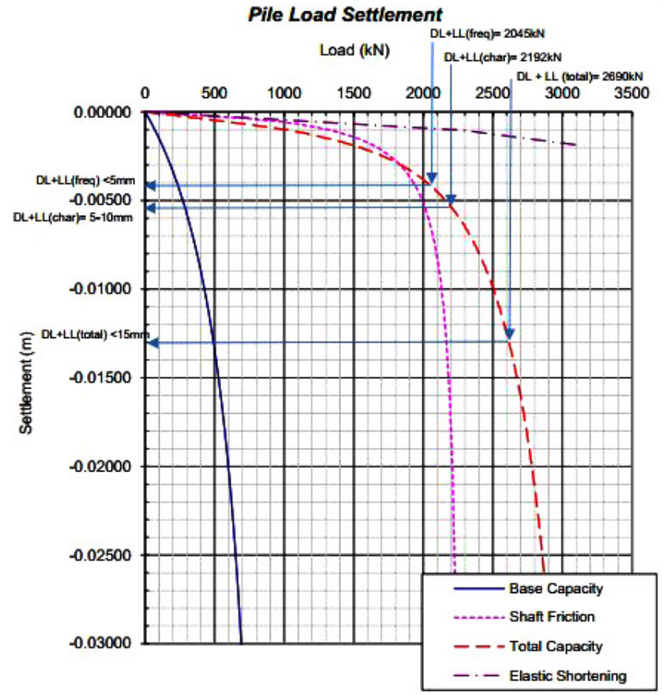

It can be seen that for the Permanent load and Frequent Combination variable load a settlement of some 4mm was predicted. This value was within the maximum differential settlement value of 25mm between adjacent supports supplied by the bridge engineers. As this was the first time the approach using the Frequent Combination had been employed it was decided that the Characteristic Combination should also be checked with regard to settlement to determine that it did not result in settlement on the steeper part of the load settlement curve where a small increment in increased load produced a settlement that approached the maximum defined by the bridge engineer. In the example case, it can be seen that a settlement of some 6mm is predicted and is still acceptable as it is on the lower gradient of the curve.

The adoption of the Frequent Combination for the determination of the variable load component on the A14 project resulted in a reduction of some 4.0 metres in design pile length compared with the approach where BS EN 1990 ULS Load, in Table 1, was considered. This resulted in a cost saving of some £4 million on the project construction cost. The method was checked by examination of the settlement vs applied load from 8no preliminary test piles carried out prior to the commencement of foundation construction. These showed very similar behaviour to the theoretical behaviour calculated after Fleming and illustrated in Figure 3.

5. Other Considerations

It is recognised that the approach from the A14 project relates to piled foundations predominantly working in skin friction. If predominantly end bearing piled foundations are considered, it is unlikely that the design length of the pile can be reduced. Optimisation of the foundation design can, however, be affected by considering the reduction in the number of piles required within the group if the Frequent Combination variable load is considered.

Additionally, the same approach can be applied to ground bearing foundations and was utilised for the design of footbridge foundations on the A465 Heads of the Valleys contract 2.

The acceptance of the Frequent Combination for the design of structure foundations led to the consideration of how it could be applied to other aspects of geotechnical design. Nowak (2012) and Nowak and Gilbert (2015) note that the variable traffic load utilised for the design of earthworks, particularly embankments, is taken that derived formerly from BS5400 and latterly from BS EN 1991 as applied to the bridge structure with which it is in direct contact. A typical highway load of 20 kN/m^2 is normally considered as a Uniformly Distributed Load (UDL) by geotechnical engineers which results in a design value of 26 kN/m^2 if a $\gamma_Q = 1.3$ is applied as is commonly the case. If a Frequent Combination approach is adopted the design value reduces to 17.25 kN/m^2.

6. Conclusions

The design of piled foundations for the new structures on the A14 Cambridge to Huntingdon Improvement project identified that the variable loads derived by bridge engineers through BS EN 1990 and BS EN 1991 represented an extreme load case that may not be realised over the design life of the structure as a degree of redundancy is inherent in the method to prevent loss of service of the structure.

Discussions between the bridge and geotechnical engineers on the design team developed a method of deriving variable load, through BS EN 1990 SLS Combinations, to represent operating conditions of the structure that could be used in conjunction with BS EN 1997-1 for the design of piled foundations. As variable load is a design input the design method did not require any amendment to the design of foundations to BS EN 1997-1.

As the application of variable loads to earthworks design has, historically, been derived from the application of variable load in bridge engineering the proposed method was also adopted and accepted in the design of earthworks on the A14 project.

Acknowledgements

The authors would like to acknowledge Highways England for their permission to publish this paper. Originally published as: Nowak PA; Patel B; Sandberg J. Variable Loads for Foundation Design – Experience from the A14 Project. In: Higgins KG; Ainsworth Y; Toll DG; Osman AS, eds. Piling 2020: Proceedings of the Piling 2020 Conference, 2021 Mar 23-26; Durham, UK. London, UK: ICE Publishing; 2021. p.79-84.

References

- Barnes G. (2010) Soil Mechanics: Principles and practice, Third Edition, Palgrave MacMillan, UK
- Bond A. and Harris A. (2008) Decoding Eurocode 7, Taylor and Francis, Abingdon, UK
- BSI (1972) CP2004, Code of Practice for Foundations, BSI, London, UK
- BSI (1978) BS5400: Part 2, Steel, concrete and composite bridges, Part 2, Specification for loads, BSI, London, UK
- BSI (1986) BS8004, Code of Practice for Foundations (Formerly CP2004), BSI, London, UK
- BSI (2002) BS EN 1990:2002 +A1 2005, Eurocode - Basis of structural design, BSI, London, UK
- BSI (2003) BS EN 1991-1-5:2003, Eurocode 1 Actions on structures - Part 1-5: General actions - Thermal actions, BSI, London, UK
- BSI (2003) BS EN 1991-2:2003, Eurocode 1 Actions on structures - Part 2: Traffic loads on bridges, BSI, London, UK
- BSI (2004) BS EN 1997-1:2004, Eurocode 7 Geotechnical design general rules, BSI, London, UK
- BSI (2005) BS EN 1991-1-4:2005 +A1:2010, Eurocode 1 Actions on structures - Part 1-4: General actions - WInd actions, BSI, London, UK
- BSI (2006) BS5400-2:2006, Steel, concrete and composite bridges, Part 2, Specification for loads, BSI, London, UK
- BSI (2006) NA to BS EN 1997-1:2004 +A1 UK National Annex for Eurocode 7 - geotechnical design, general rules, BSI, London, UK
- BSI (2007) NA to BS EN 1991-1-4:2005 +A1:2010, UK National Annex to Eurocode 1 Actions on structures - Part 1-4: General actions - Wind actions, BSI, London, UK
- BSI (2007) NA to BS EN 1991-1-5:2003, UK National Annex to Eurocode 1 Actions on structures - Part 1-5: General actions - Thermal actions, BSI, London, UK
- BSI (2007) NA to BS EN 1991-2:2003, National Annex to Eurocode 1 Actions on structures - Part 2: Traffic loads on bridges, BSI, London, UK
- BSI (2009) NA to BS EN 1990:2002 +A1 2005, UK National Annex for Eurocode - Basis of structural design, BSI, London, UK
- BSI (2011) PD6694-1, Recommendations for the design of structures subject to traffic loading to BS EN 1997-1:2004, BSI, London, UK
- BSI (2015) BS8004:2015. Code of practice for foundations. BSI, London, UK
- Fleming W.G.K. (1992) A new method for single pile settlement prediction and analysis. Geotechnique, 42, No.3, 411-425
- Highways Agency (2001) Design Manual for Roads and Bridges, Vol.1, Section 3, Part 14, BD 37, Loads for Highway Bridges, HMSO, London, UK
- Highways England (2020) Design Manual for Roads and Bridges, Highway Structures & Bridges Design, CD350, The design of highway structures, HMSO, London, UK
- Nowak P.A. (2012) Design of new earthworks. In ICE Manual of Geotechnical Engineering, Volume 2, Geotechnical design, construction and verification, Chapter 70, Institution of Civil Engineers, London, UK
- Nowak P.A. and Gilbert P. (2015) Earthworks: A guide, Second Edition, ICE Publishing, London, UK
- Tomlinson M. and Woodward J. (2015) Pile Design & Construction Practice, Sixth Edition, CRC Press, UK

Ground Risk and Rail Asset Management in East Anglia

Simon Holt BSc, MSc, Eur Geol, CGeol, CSci, FGS, CEng, MIMMM

Principal Engineering Geologist, Engineering, Design and Project Management, Atkins Limited, London, UK

Isaac Griffiths BSc, MSc, CEng, MICE

Senior Geotechnical Engineer, Engineering, Design and Project Management, Atkins Limited, London, UK

Ian Payne BSc, MSc, CEng, MICE, CIHT

Senior Asset Engineer (Geotechnical), Anglia, Network Rail, London, UK

Lee Clifton EngTech, MICE

Contracts Manager, Volker Fitzpatrick Limited, Hoddesdon, UK

David Wadesmith BSc, MSc, CGeol, FGS

Head of Ground Engineering, East West Railway Company, Milton Keynes, UK

Abstract

The Network Rail Anglia region has 1091km of earthworks, many of which are steep-sided embankments constructed of locally won fill materials in Victorian times. In order to extend the serviceable lifespan and to ensure the safety of the public with the ever-increasing demand on railway infrastructure, understanding the geological and geotechnical risks is of critical importance. Approaches to control risks and optimise mitigation works were adopted on the Control Period 5 framework with collaborative partners Network Rail, Volker Fitzpatrick and Atkins. Owing to budget constraints, harder engineering fixes applied early in the framework, such as sheet-piled walls, could no longer be readily adopted. Embankment renewal projects took on a more staged approach using shorter-design-life solutions with sustainable benefits. Detailed interrogation, phased investigation and zonation of sites allowed the targeting of higher-risk areas and intervening at a greater number of sites within the region, meeting Network Rail asset policy objectives. Slope movement monitoring combined with more detailed approaches was integral in assessing the instability causation, effective mitigation design and assessing performance during and following construction. A continued monitoring of lower-risk untreated areas and a future works strategy plan allowed greater control and proactive management of the asset.

KEYWORDS

Geotechnical engineering; Railway tracks/slopes – stabilisation

1. Introduction

Embankments dominate the Anglia route earthworks portfolio and typically comprise non-engineered over-steep slopes constructed in Victorian times using local materials – commonly superficial glacial deposits in the north and London Clay Formation in the south of the region. Many of the earthworks are underlain by problematic soils with poor drainage, and signs of instability have been identified through visual inspection, investigation and monitoring. The aim of the paper is to illustrate the investigation and influence of ground risks on railway earthworks and show examples of various mitigation techniques and what influences their selection.

Network Rail manages asset risks and prioritises intervention at sites based on passenger safety and disruption in line with the Network Rail earthworks asset policy (Network Rail, 2016). The geographical coverage of the Anglia region is shown in Figure 1 and includes busy commuter lines into London and freight and tourist routes to the coast, including the port of Felixstowe. Many site defects are addressed through ongoing maintenance interventions, but occasionally the problem lies within or beneath the embankment. Interrogation of the site through desk study, geomorphological mapping, site investigations, instrumentation monitoring, earthworks examinations, linear asset decision support (LADS) track recording data and aerial lidar surveys is required to evaluate the appropriate intervention.

The Anglia Route Collaboration (ARC) established for Control Period 5 (CP5) running between 2014 and 2019 comprised Network Rail, Volker Fitzpatrick Limited (VFL) and Atkins as framework partners. Although the sites were prioritised and the work bank was estimated early on, budget constraints meant that more innovative approaches were required through close interaction between client–designer–contractor as the Control Period evolved.

This paper will present lessons learned from efforts to understand and manage the root cause of stability risks at particular sites. Site investigation for rail schemes can include analysis of data from multiple sources, together with targeted ground investigation (GI) and subsequent monitoring where appropriate to enable sufficient interpretation. A careful balance is required to design optimised solutions to control risks, maintain a safe railway and minimise future maintenance. Unplanned emergency works cannot always be avoided; however, more proactive strategies may be able to reduce their impact.

Digital tools are becoming a major part of railway asset management and the case studies are intended to highlight the importance of automated monitoring and explore other ways whereby sites can be managed more efficiently in the future, alleviating the need and inherent risk of working close to the railway.

2. Geological Factors Influencing Earthworks Stability

East Anglia's low-lying landscape has been moulded by glaciations and is underlain by relatively young geological deposits presenting engineering risks and challenges for railway infrastructure. The extent of superficial deposits across the region is shown in Figure 1, with the main rail routes and sites presented in this paper. Superficial deposits include glacial tills from ice sheets and soft organic sediments from swamps and marshes, including the peat Fens. To the south of the region in Essex, superficial deposits are generally absent, and the London Clay Formation is the dominant bedrock, commonly weathered, with low strength and susceptible to seasonal moisture variation. The region exhibits a large proportion of the UK's high-plasticity soils with "significant" shrink–swell potential according to the British Geological Survey. Some of the rail routes cross estuaries and are susceptible to flooding, with scour potential of the earthworks.

FIGURE 1

Site location plan.
For details of regional geology See https://www.bgs.ac.uk/geological-data/map-viewers/
Contains public sector information licensed under the Open Government License v3.0.

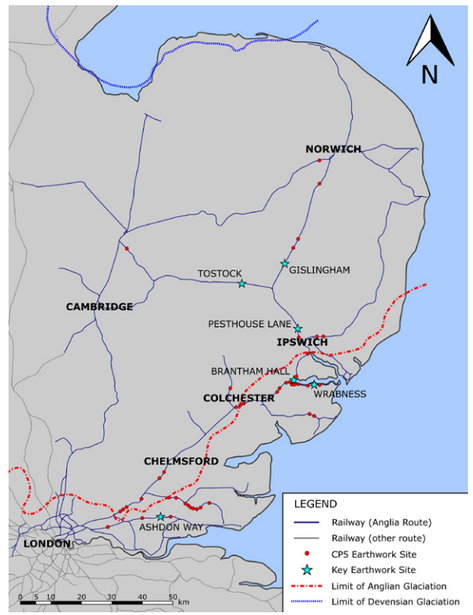

The majority of the embankments in the southern part of Anglia have a clay core that was constructed from nearby cut material without any consideration of its engineering properties (Ridley et al., 2004). Birch and Evans (2018) reported many clay core embankments suffer loss of cross-fall drainage over time, with water infiltration into the embankment causing soft spots, inducing instability. The loss of formation was balanced by the use of readily available boiler ash and, as a result, many embankments today have an outer layer of weak ash material. Typically, embankment shoulders made of ash give rise to track problems and these will be explored further.

3. Approach to Investigating Sites

The first phase in understanding the problems at a particular site is to do a thorough desk study, including a site walkover. Much in the same way as a proposed development site, a railway earthwork has a history of events that needs to be reviewed to provide clues to the potential risks. It is important to ensure all the available Network Rail earthworks examination records, maintenance events and historic GI and remediation records are consulted, and early engagement with the Route Asset Manager and maintenance engineers is vital. In parallel, ecological and environmental considerations at sites are important and can dictate when intrusive and remediation works can take place, potentially influencing site prioritisation and what precautions are required. Desk study and GI activities are now discussed using some key CP5 sites, including the demonstration of early targeted slope monitoring.

3.1 TOSTOCK

Tostock is a 350m long, approximately 7m high railway embankment located 5 miles to the east of Bury St Edmunds, Suffolk. It is on the Cambridge Coldham Lane junction and Haughley junction line. It was selected for intervention due to reports of persistent track defects, an elevated track maintenance liability and the risk of service disruption on a key passenger route due to excessive movements. A temporary speed restriction (TSR) was in place on one line.

A detailed desk study identified geotechnical risks, including nearby peat and head deposits within the site extent. The proximity of a local watercourse (main river) and chalk bedrock also indicated the potential influence of groundwater. Subsequent geomorphological mapping of both sides of the embankment recorded various evidence of deformation of

FIGURE 2

Screenshot showing an extract of Network Rail LADS data with correlation between GPR anomaly, track faults and maintenance. Worst-affected area (boxed) showing repeated track twist faults.

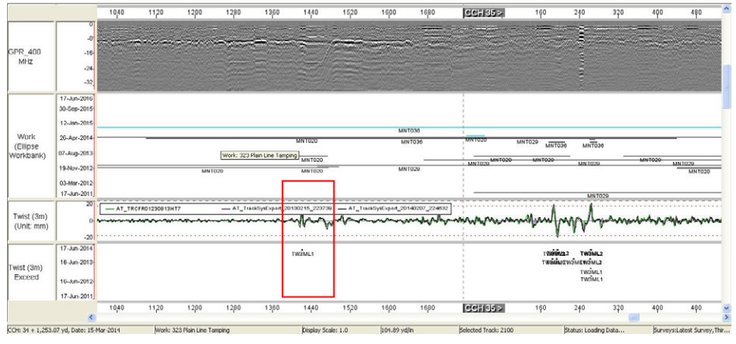

railway infrastructure, slope movement including bulges, breaks of slope and backscarps, along with evidence of high groundwater, poor drainage and hydrophilic vegetation. These features were then targeted during a phased GI to further develop the ground model.

The Network Rail LADS data (Figure 2) were reviewed and a correlation was observed between disturbance in ground penetrating radar (GPR) survey, the presence of recurrent track twist faults and frequent track maintenance interventions. The LADS data were of importance when identifying areas for further investigation.

The GI included installation of biaxial inclinometers, and five biaxial micro-electro-mechanical sensor (MEMS) automated inclinometers in the areas of greatest concern, which were identified from the geomorphological mapping findings and review of LADS data. The instrumentation was remotely monitored to obtain real-time data, with trigger levels set for use by the asset manager. Automated monitoring offers a major benefit over manual monitoring due to the instant and constant availability of data, meaning that the asset manager is better informed on the current condition of the asset. The instruments recorded progressive displacements, which were interpreted as both deep-seated and medium-seated slope movement on both sides of the embankment, with a larger failure influencing track displacement towards the north side.

A thickened layer of ballast in the centre of the earthwork was interpreted as evidence of historic embankment settlement and spreading, which may have allowed ponding of perched water and softening of cohesive materials, leading to slope movement. This feature correlated with the GPR reflector disturbance and the deepest recorded slope movement.

The MEMS slope inclinometers in the most problematic section recorded accelerated movement during August and September, but then stabilised during the winter months; this is interesting as Briggs et al. (2017) have reported that five times as many rail delay incidents due to geotechnical causes occur in winter months compared to summer months. The reasons for these observations are unclear and such trends have been observed elsewhere in the region and are being further explored.

3.2 WRABNESS

The Wrabness site is an 880m long, up to 12m high embankment on the Manningtree to Harwich line which has a long history of track problems associated with embankment instability. The embankment is on sidelong ground with the adjacent catchments sloping downwards towards the south side and generally away from the north side towards Copperas Bay. Like many embankments on this line, poor drainage has been one of the main causes of instability.

GI data was available from as far back as 1966, undertaken by the soil mechanics division of the British Railways eastern region. It was apparent that there had been historical intervention, including sheet pile walls and rubble berms, and problems with the drainage from the south to the north towards the estuary. Given the dense woodland vegetation, lidar data (Figure 3(a)) were used to supplement the geomorphological map shown as the background on Figure 3(b). The geomorphological mapping was a crucial part of the early studies and this was linked in to the topographical survey and railway mileages to provide accurate referencing to known problems with slope movements, track and maintenance issues, including LADS data which in turn allowed a fully targeted GI.

The desk study also provided a summary of the historical slope monitoring data and a new monitoring regime was established together with further recommended GI in areas of concern from the mapping and track/maintenance data. GI was undertaken to supplement existing information and to replace damaged instruments. A slope-climbing rig such as the P60 rig from Geotechnical Engineering Limited in Figure 4 could access the steep crest and provide sufficient capacity for deeper boreholes. Automated real-time slope monitoring was set up in the worst-affected area that was subject to a TSR due to excessive track movements following a very wet winter period in 2014. Having long periods of historical monitoring and across the seasons early in CP5 allowed trends to be identified. It is imperative to ensure sufficient monitoring is available before designing mitigation solutions at any site.

FIGURE 3

(a) Lidar data at Wrabness provides good visibility of the slope contours through dense woodland; (b) existing and proposed exploratory hole layout overlaid with the geomorphological mapping, historical interventions and track issues.

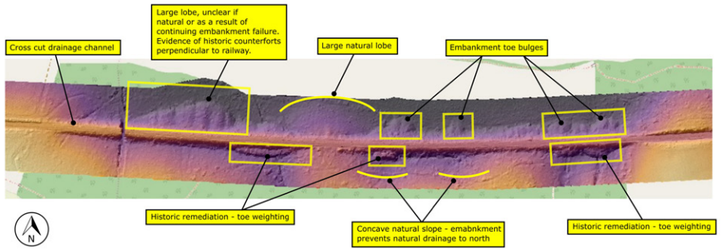

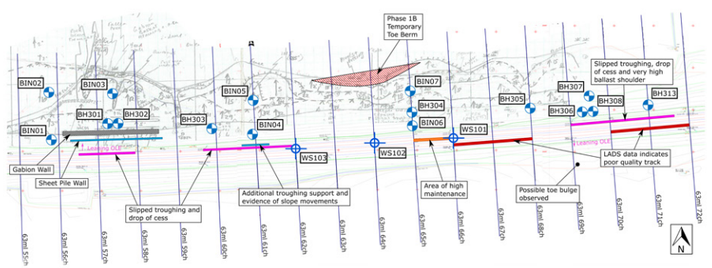

FIGURE 4

Supplementary GI used a slope-climbing rig, enabling access near the crest for inclinometer and piezometer installations.

The Wrabness ground model in Figure 5 shows the embankment interface with the underlying natural ground included an organic soft clay layer and head deposits/weathered Harwich Formation of the Thames Group. Slope failure at the site was deep seated with a failure plane identified through GI and inclinometer monitoring at a depth of approximately 6m below ground level. Previous sheet pile and gabion walls at the site had not fully fixed the issues and this may be attributed to not intercepting the deeper slip surface identified through continued monitoring.

Wrabness was presented as a more detailed case study managing slope instability through phased investigation, monitoring and planned intervention by Payne et al., (2017), at the 2017 railway engineering conference. The phased mitigation and risk management to determine the extent of intervention is discussed later.

3.3 HAROLD WOOD

Cohesive rail embankments commonly fail in three different ways: through seasonal shrink–swell, pore water pressure increases and progressive embankment failure (Briggs et al.,2017). These failure mechanisms can act independently, but they are often interlinked and can act in sequence. The Harold Wood embankment located approximately 5km southwest of Brentwood is a typical example of a site experiencing high shrink–swell issues with an interlinked progressive failure and pore pressure increase issues. Harold Wood is typical of many Anglia embankments in the south of the region – a poorly compacted heterogeneous reworked London Clay embankment with local high-permeability lenses overlain by loose ash fill and high-permeability ballast. The high-permeability ballast covering allows water infiltration during wet winter periods, causing swelling of the embankment clay core. Desiccation during the summer period then leads to some degree of shrinkage of the soil before rehydration in the following winter leading to swelling and ground heave (BRE, 1996). At Harold Wood, embankment progressive deterioration is evident from this annual shrink–swell cycle in the form of progressive downslope movement recorded during inclinometer monitoring (Figure 6). This progressive downslope deterioration amounts to approximately 20mm of movement per year, which is not recovered. The magnitude of desiccation and shrink–swell movement is sufficient to cause track alignment issues, leading to increased maintenance (Figure 6). There is also concern that the progressive shrink–swell cycles can lead to softening of the clay embankment, which can instigate larger-scale global slope failures. Payne et al. (2018) review progressive failure trends at another London Clay embankment (Ashdon Way in Figure 1) in south Essex and show how such failure mechanisms can become active and result in the need for an immediate intervention.

FIGURE 5

Development of the ground model through phased GI and proposed mitigation works. A full-colour version of this figure can be found on the ICE Virtual Library (www.icevirtuallibrary.com)

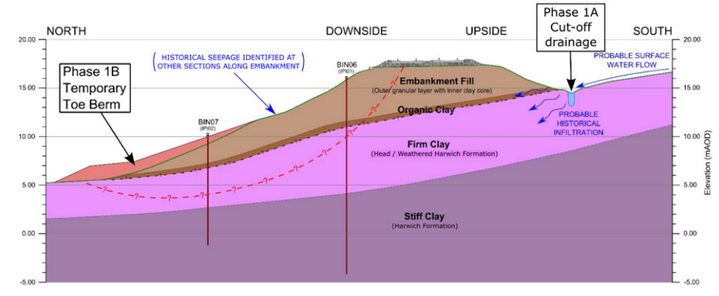

4. Hard Full-Fix Planned Renewal Solutions

At the start of the CP5 framework, Tostock was a priority site given an imposed TSR. A good bank of monitoring and thorough understanding of the problems meant it could proceed to detailed design and construction relatively quickly. A sheet-piled toe wall with granular reprofiling of the embankment was agreed with Network Rail. The design solution was selected to restrain both the significant deeper-seated movement (by increased sheet pile resistance) and more medium-seated movement (by toe weighting/slope regrade). The extents of the remedial works were instructed by Network Rail following a review of the risks associated with three option extents and a review of costed options against the available budget. The shortest extent of the three was selected for implementation with ongoing monitoring of the adjacent earthworks to manage the risk of further movements. The transition zones at the outer edges of the works were formed by earthworks reprofiling rather than by gradually reducing the sheet pile retained heights (and embedment). This transition treatment facilitated future extension of the same ‘full-fix’ solution, if justified by review of ongoing monitoring data, without the requirement to extract shorter transition piles or to re-drive and weld extension pieces.

The railway remained operational (with line speed restrictions) during construction with the risk of slope movement managed by daily topographic survey of all rails at 3m centres and clear trigger thresholds and actions set. The key construction activities included:

- pre-augering for piling through stiff glacial till
- driving sheet piles up to 12m embedment
- temporary excavation for embankment reprofiling

FIGURE 6

Inclinometer downslope displacement at Harold Wood embankment. Seasonal shrink-swell behaviour is observed, along with progressive downslope deterioration between each shrink-well cycle. Progressive deterioration is most evident in inclinometers located close to the embankment crest.

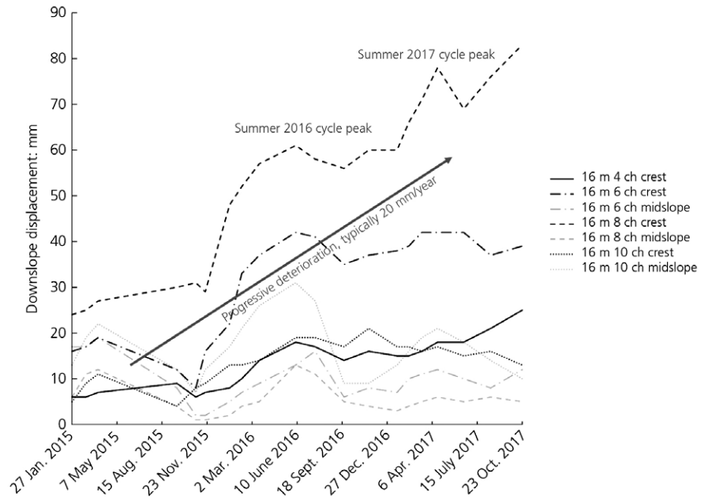

The vertical track movements recorded during construction were most pronounced during the pile pitching and driving phase. This observation may be related to a requirement to pre-auger the pile locations to drive through a layer of stiff glacial till. The resulting ground relaxation can be related to the deflections recorded at track level. Movements had stabilised by the end of the site works and have been reported as stable since.

Movement of the track was evident at Tostock following installation of the sheet piles with 40 mm of vertical movement occurring in a 10-week period following installation of the sheet piles, after which movements ceased. Soil deflections are required to induce the resisting forces in cantilever sheet-piled walls with the observed movements compatible with wall deflections predicted using Wallap software.

It is documented that the mitigation has resolved the issues observed within the extent of the remedial works. The inclinometer monitoring plot for BH10B (Figure 7) within the remediated area illustrates the mobilisation of passive resistance. The second to fourth readings represent the first six months post construction, where approximately half of the deflection was recorded. The last four readings represent an 18-month period with a marked reduction in the rate of deflection indicating mobilisation of a greater proportion of the available passive resistance. The completed sheet pile retaining wall remediation work can be seen in Figure 8.

FIGURE 7

BH10B down side mid-slope inclinometer monitoring plot. Direction A is downslope and direction B is along slope.

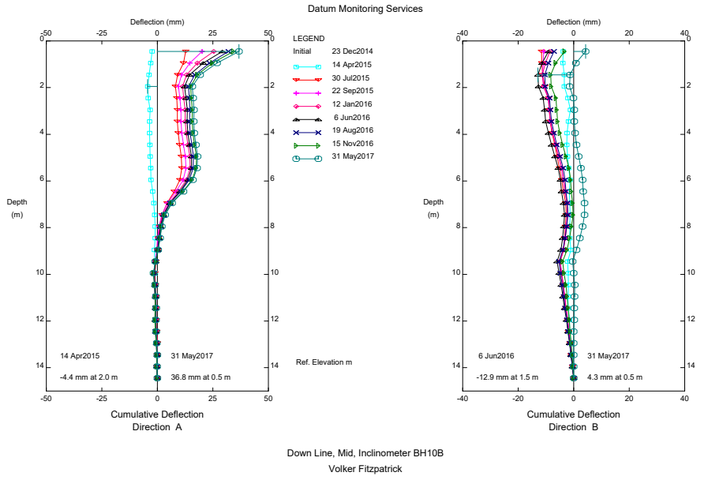

FIGURE 8

Completed sheet pile retaining wall, slope regrade and toe drainage at Tostock embankment.

5. Risk-Managed Renewal Solutions

Remediation of sites like Tostock provided a "full fix" with a 120-year design life, but capital expenditure to achieve such results was high, meaning that mitigation could only be implemented at a minimal number of sites across the Anglia region. As the Control Period progressed, the ARC framework was subject to unforeseen external budget constraints, meaning that the mitigation approach had to be reviewed. Owing to these issues, a new, more innovative risk-based approach was adopted to further target and focus mitigation to reduce capital expenditure at each site and release funding to allow intervention at more sites across the region meeting Network Rail policy objectives (Network Rail, 2016). This approach is considered to be an adaption of the observational method to earthworks asset management.

5.1 RISK-MANAGED PHASED INTERVENTION – WRABNESS

The risk-managed approach to earthworks renewals involved dividing each site into low-, medium- and high-risk areas based on a set of failure criteria and targeting initial mitigation only at higher-risk areas and some medium-risk areas. In the remaining areas, additional instrumentation would be installed to allow ongoing monitoring of the assets with trigger levels set to instigate further investigation or additional mitigation. Figure 9 shows an example of the risk zonation at the Wrabness embankment derived from the various interrogation techniques discussed earlier.

Within the higher-risk areas (red and amber), a high number of slope issues were identified during the mapping (bulges and berms) along with line side and track issues, such as exposed sleeper ends, misaligned cable troughing and leaning gantries. The red and amber areas were differentiated by interrogation of the LADS and slope monitoring data. At the worst-affected area at 65ml 65ch track twist faults were recorded on the LADS data along with high numbers of maintenance activities. Slope movement was also high with up to 28mm of displacement recorded in a 2-month period during the winter of 2014. In comparison, the green risk areas showed limited visual signs of instability, no track defects and slow or negligible rates of slope movement.

A phased approach was adopted to the mitigation measures to further drive value engineering of the solution at the site and take account of the many ecological and environmental constraints, including dormice and the site being adjacent to a site of special scientific interest (SSSI), ancient woodland, a Royal Society for the Protection of Birds nature reserve and an estuarine special protection area (SPA).

FIGURE 9

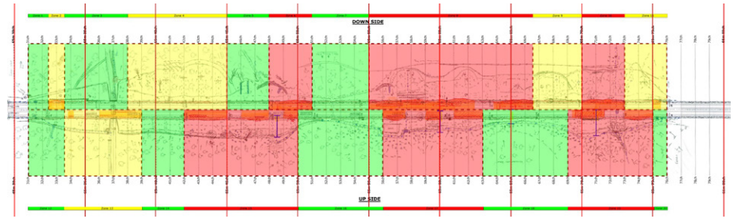

Risk categorisation map for the Wrabness embankment. The critical area for mitigation is highlighted red with less critical areas highlighted amber and green. The complete phase 1 drainage works are shown on the up side. A full-colour version of this figure can be found on the ICE Virtual Library (www.icevirtuallibrary.com)

One of the main instability drivers was poor drainage given that the steep embankment on sidelong ground was underlain by predominantly impermeable deposits of the Thames Group. Initial drainage works (phase 1A) followed by localised short-term toe weighting (phase 1B) shown on Figure 5 were implemented, which slowed the rate of slope movements to manage the immediate problem and to remove the TSR. As the embankment is located on sidelong ground, the drainage works were installed on the south side to intercept water draining from the surrounding area towards the embankment. The localised toe weighting was implemented in the worst-affected area at 65ml 65ch on the north side. Permanent mitigation measures comprising slope regrading and installation of soil nails have also been designed ready to mitigate fully all red and amber risk areas when the planned phase 2 works commence in Control Period 6 (CP6). The phased intervention in CP5 and continued slope monitoring have enabled Network Rail to remove the TSR and prolong the life of the asset before further engineering mitigation is required.

5.2 SOIL NAILING AND CESS RETENTION – ASHDON WAY AND GISLINGHAM

The Gislingham embankment, located approximately 12km north of Stowmarket, and the Ashdon Way embankment, located immediately east of Basildon station, are two sites where the risk-managed approach was successfully applied and option selection was used to develop appropriate mitigation measures. The embankments at both sites are similar: up to 10m high and composed of cohesive fill with deep-seated progressive failure surfaces identified approximately 3m below ground level. After identifying the highest risk areas, an option selection exercise was undertaken to ensure that the most appropriate mitigation option was selected. Optioneering included sheet pile with regrade, gabion wall with regrade, toe berm with regrade and soil nails with cess retention. VFL undertook an exercise to evaluate the cost and constructability of each of these design options. The soil nail with cess retention option was selected. In addition to satisfying the design

FIGURE 10

Analysis of soil nail remediation at the Gislingham embankment site. A full-colour version of this figure can be found on the ICE Virtual Library (www.icevirtuallibrary.com).

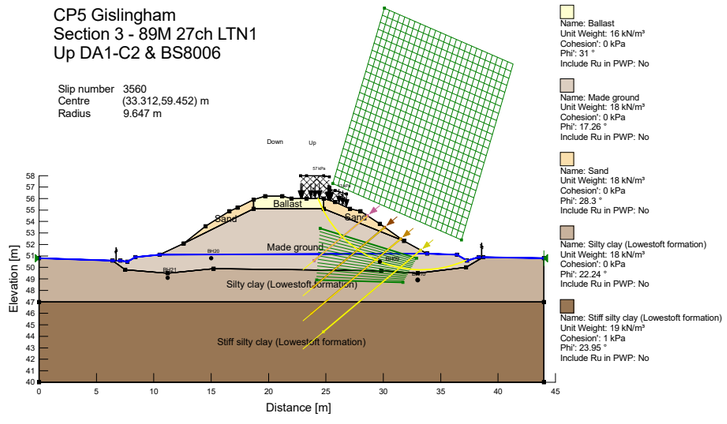

in stabilising the embankments, the solution provided environmental, social and economic advantages, making it the most sustainable. Both projects were undertaken in parallel with design teams in Atkins and shared value engineering and construction workshops, which brought efficiencies to the framework. A cross-section extract from the Gislingham soil nail analysis and the completed site works are shown in Figures 10 and 11, respectively.

FIGURE 11

Completed soil nail and Grundomat cess retention at the Gislingham embankment site.

The Ashdon Way embankment stabilisation was a good example of how understanding the behaviour of the progressive and active slope failure mechanisms can help optimise asset management (Payne et al., 2018). Ashdon Way was also shortlisted for the 2016 Emap Ground Engineering Awards Sustainability Award.

The use of a combined soil nail and cess retention remediation approach was selected due to the different benefits of each approach. The soil nails were designed in accordance with Eurocode 7 (BSI, 2007, 2010) and Network Rail geotechnical design NR/L3/CIV/071 (Network Rail, 2011) to prevent further global stability failures at the site and support the imposed rail load at the embankment crest (Figure 10). The soil nails were the main intervention at each site to prevent future large-scale embankment failures. However, the installation of soil nails may not immediately stop slope movement as strain must develop along the shaft of the soil nail before it takes full effect. It can also be difficult to install soil nails next to the track, therefore the ballast shoulder can be left unsupported, which can lead to track issues and faults. The Grundomat cess retention system was specified in addition to the soil nails to address these issues. The cess retention was installed close to the track to provide support to the ballast shoulder and prevent loss of ballast down the steep embankment slope (Figure 11). The cess retention system also had an immediate impact on reducing slope movement at both sites. Automated inclinometer monitoring data at the Ashdon Way site showed slope movement at the embankment crest to reduce to almost zero on the same day as cess retention installation (Payne et al., 2018). The automated monitoring system also allowed earthwork movement to be reviewed throughout the construction period, giving confidence that the site activities were not having an adverse impact on the earthwork assets.

Following the risk-managed approach to earthwork mitigation results in residual risk remaining at “unremediated” sections of earthwork. This residual risk is managed through the development of a “future works strategy” document (Atkins Limited, 2015). This document acts as a manual for the future maintenance and management of the earthwork asset. A future works strategy was developed to manage residual risk at the Ashdon Way and Gislingham sites. The document provides details of monitoring requirements using inclinometer data, LADS data and observational track monitoring. Red and amber trigger levels were proposed which would instigate further investigation of potential issues at the site. The manual also includes outline emergency works that could be implemented if slope issues were experienced. Since completion of this project, Network Rail

(2017) have published formal guidance on earthworks monitoring in the 'Earthworks monitoring strategy selection and implementation' technical standard. This standard covers many of the concepts included within the future works strategy document.

6. Emergency Works

Network Rail earthwork asset management in Anglia is normally proactive, with intervention undertaken prior to full failure of an earthwork. However, there are some occasions when earthworks fail before an intervention can be made. This problem is exacerbated in winter months during periods of high rainfall, which causes increases in pore water pressures in earthwork slopes.

Brantham Hall cutting slope north of the Stour estuary at Manningtree failed shortly before planned remedial works were to be undertaken early in 2014. The instability was triggered by the perched water table at the interface between the London Clay Formation and the overlying sands and gravels. The intense rainfall in December 2013 caused increases in pore water pressure in the slope further reducing the stability of the slope which caused the initial instability. The slip back scar was evident prior to construction, as were additional tension cracks during the slope remediation works with the sand and gravel/London Clay Formation interface clearly visible above the toe of the slope during remediation (Figure 12).

FIGURE 12

Exposed sand and gravels overlying London Clay Formation – perched water/intense rainfall triggered landslide.

The dip of the interface between the London Clay Formation and the overlying sand and gravel has resulted in a patchwork of treatments over time along just the western side of the cutting, including localised rock regrades, gabion walls, drystone walls, sheet-piled walls and counterfort drains to manage the instability risk, with a rock regrade used to repair the 2014 failure.

7. Refurbishment of Earthworks

Subsidence beneath railway tracks caused by events such as washouts, softening, burrowing, mining collapse or ground loss during under-track crossing construction have the potential to derail trains, either as a result of track geometry faults such as longitudinal dips in the track or as a loss of edge support causing track twist. Lesser impacts such as TSRs and rough rides also adversely affect train services.

The principal burrowing-related problems are created by rabbits and badgers, and the closer the burrows are to the track and associated track ballast then the greater the risk of subsidence becomes. The subsidence risks are greatest for embankments where loss of support at the crest of the embankment can derail a train or where spoil can block toe drains, potentially reducing the stability of a larger area of the slope. Figure 13 shows the effects of extensive rabbit burrowing through the sandy embankment fill, which has resulted in a drop of the ballast shoulder, slipping of cable troughing route and lean on the line-side cabinet at Pesthouse Lane.

Extensive burrowing at the toe of cutting slopes may also require treatment. Spoil from burrowing can lead to contamination of the ballast and blockage of drainage, which can cause soft spots beneath the track. The resulting voids from burrowing at the toe of a slope also reduce its stability.

FIGURE 13

Rabbit burrow problems at Pesthouse Lane.

Rabbit burrowing is generally reasonably shallow and tends to affect the near-surface layers of the earthworks slopes, including the shoulder of the embankments closer to the track. Rabbits and badgers both tend to favour sandy soils that are more easily burrowed into and rabbits also favour the upper layers of ash fill that was used historically as past maintenance historically to top up the early life levels of many embankments throughout Anglia. Large numbers of rabbits are often present and this can result in a rapid deterioration of the near surface layers that progressively undermine cable troughing routes, overhead line electrification mast foundation, track ballast shoulder areas and other track assets, and often lead to shallow slumping and creep-type movements if not remediated. Surface settlement and other loosened areas produced by such burrowing in the cess area in particular also pose significant trip hazards to staff walking adjacent to running trains.

Badger burrows beneath the tracks may be less frequently encountered, but they do generally present a greater subsidence risk due to their larger size. Deep unsupported tunnels that are continually enlarged by badger clearing activities are vulnerable to collapse under dynamic loadings and associated vibrations of passing trains. Stress relief associated with tunnels also induces surface settlement troughs, which can exacerbate the dynamic loading effects of the trains and also produce low points that encourage ponding and flows of water towards such low points from the track ballast. It is not, however, possible to readily predict when such unsupported tunnel collapses will occur, with other external influences such as prolonged or heavy rainfall also increasing the risk of collapse.

The remediation work typically comprises exclusion of the vermin and infilling of the burrows followed by netting the slopes along the earthworks slopes to deter new excavations. Troughing restraint and/or cess support structures may also be required for particularly disturbed embankment shoulder areas, as illustrated in Figure 14. Early intervention where burrow entrances are close to the track or cess areas will manage the burrowing subsidence safety risk. Badgers are, however, a protected species under European legislation and therefore are less readily dealt with than rabbits and may require the formation of artificial setts with the associated cost, time and seasonal working implications.

FIGURE 14

Refurbishment at Pesthouse Lane including cess retention to realign the troughing route and reinstate a compliant cess and rabbit netting to resist future burrowing.

8. Future Railway Asset Management

The development of new technology and the improvement of data collection and management are having a big impact on railway earthwork asset management. Network Rail's development of the existing LADS system and other systems such as Geo-RINM is putting large amounts of their asset management data into a format that can be easily interrogated, which allows improved asset management processes, such as the risk-based approach discussed in this paper, to be adopted. Atkins has been developing a number of digital tools that can be integrated with these asset management systems. The Atkins Assist tool is a digital proforma which can be loaded onto rugged site tablets to allow earthwork inspection data to be collected electronically and directly uploaded into asset management databases. The tool has been successfully deployed on highways earthwork inspections for the South Wales trunk road agent and a similar tool is currently being developed to aid in risk-based inspections of railway earthworks.

The cost of automated instrument monitoring is continually reducing, such that it is possible to deploy it at a greater number of sites. The technology for automated monitoring is also continually improving, with high-quality cameras available to provide high-resolution images and video of sites, improvement to the amount of information that data loggers record and transmit, and more user-friendly internet-based interfaces available for viewing collected data. The main area for development for inclinometer slope monitoring equipment is in the initial installation of the inclinometers. Installation requires large drilling rigs and it can be difficult

for plant to access constrained railway earthwork sites. Innovation in the installation method or type of inclinometer would allow a greater number of instruments to be installed across the network. Early in CP6 the Anglia route has adopted a targeted asset management (TAM) approach and a case study is presented by Payne et al. (2019). The implementation of this strategy should reduce capital expenditure across the contract, allowing mitigation to be undertaken at a greater number of sites to reduce risk and disruption to the travelling public.

9. Conclusions

The Anglia region has been heavily influenced by past glaciation giving rise to young geological deposits which present engineering risks to railway infrastructure. Soft superficial organic sediments from swamps and marshes on the peat Fens and weathered upper layers of the London Clay Formation with high shrink–swell potential pose particular risks to the rail infrastructure in the region.

The risk-based asset management approach was successfully demonstrated on a number of schemes through initial drainage intervention, temporary toe berms, soil nails and cess retention. Key lessons learned are being applied in CP6 adopting the TAM approach. Many sites had complex constraints such as boundary restrictions and adjacent areas of ecological interest, which influenced the mitigation selection. Desk study and phased site investigation was critical to ensure a robust ground model was developed for each site.

At the higher-risk sites, automated inclinometer instrumentation was utilised to provide real-time earthwork monitoring information, both before, during and post construction to provide further risk assurance. Finally, a "future work strategy plan" was developed to provide guidance on future management of the earthwork asset, including setting trigger levels for slope movements and outlining emergency work plans so that works can be proactive rather than reactive, with the latter resulting in greater expenditure.

Moving forward into CP6 there are plans to make more use of emerging digital technology to assist in mitigation of earthwork failures and to assist in risk management and zoning of an individual site.

Acknowledgements

The authors would particularly like to acknowledge Jonathan Garelick and Rachael Fearnhead (Network Rail), John Quinlan and Bob Brickwood (Volker Fitzpatrick) and Richard Dowling and Stuart Fielder (Atkins). The input of a wide range of staff from contractors, instrumentation specialists (Socotec and Datum Monitoring) and Network Rail is also acknowledged.

This paper was originally published as: Payne I, Clifton L, Holt S, Griffiths I and Wadesmith D. Ground risk and rail asset management in East Anglia. Proceedings of the Institution of Civil Engineers – Transport, https://doi.org/10.1680/jtran.19.00047

References

- Atkins Limited (2015) CP5 Anglia Critical Earthworks Risk Management Sites Package 1 – Ashdon Way Embankment Future Works Strategy Plan. Atkins Limited, Croydon, UK, Doc Ref: 142456-ATK-REP-EGE-000002 Rev2.0.
- Birch G and Evans E (2018) Railway earthworks with particular emphasis on the behavior of clay embankments in the south east. Ground Engineering, 15 January.
- BRE (Building Research Establishment) (1996) Digest 412, Desiccation in Clay Soils. BRE, Watford, UK.
- Briggs KM, Loveridge FA and Glendinning S (2017) Failures in transport infrastructure embankments. Engineering Geology 219: 107–117, https//doi.org/10.1016/j.enggeo.2016.07.016.
- BSI (2007) NA to BS EN 1997-1: 2004 National Annex to Eurocode 7: Geotechnical design – Part 1: general rules. BSI, London, UK.
- BSI (2010) BS EN 1997-1: 2004. Eurocode 7: Geotechnical design – Part 1: general rules. BSI, London, UK.
- Network Rail (2011) NR/L3/CIV/074. Geotechnical design issue 4. Network Rail, London, UK.
- Network Rail (2016) CP5 Earthworks Asset Policy. Network Rail, London, UK, Issue 6, 27 April 2016.
- Network Rail (2017) NR/L2/CIV/086/Mod06. Module 6 Earthworks monitoring strategy selection and implementation issue 1. Network Rail, London, UK.

- Payne I, Holt SJ and Griffiths I (2017) Wrabness railway embankment managing slope instability through phased investigation, monitoring and planned intervention. 14th International Railway Engineering Conference, Edinburgh, UK.
- Payne I, Holt SJ and Griffiths IW (2018) Railway embankment stabilisation: economical asset management. Proceedings of the Institution of Civil Engineers – Geotechnical Engineering 171(4): 332–344, https://doi.org/10.1680/ jgeen.17.00101.
- Payne I, Holt SJ and Griffiths IW (2019) Targeted asset management approach to mitigating railway earthwork instability – Chitts Hill Embankment, Colchester, Essex. Permanent Way Institution Journal 137(Part 4): 26–37.
- Ridley A, McGinnity B and Vaughan P (2004) Role of pore water pressures in embankment stability. Proceedings of the Institution of Civil Engineers – Geotechnical Engineering 157(4): 193–198, https://doi.org/10.1680/geng.2004.157.4.193.

Anastasios Batilas, MEng, M.Sc., Ph.D, Eur Ing, CEng MICE

Chartered Geotechnical Engineer
Infrastructure
Birmingham, UK

Babak Bahmani, CEng MICE

Principal Geotechnical Engineer
Infrastructure
Birmingham, UK

Doug Bannister

MSc Student
Université Savoie Mont Blanc
Aix-les-Bains, Auvergne-Rhône-Alpes, France

Dan Roberts

Technical Manager
GeoGrow Ltd
Brownhills, UK

Andrew Benson, CEng MICE

Practice Director
Infrastructure
Birmingham, UK

10: Geotechnical Engineering

Design Methodology for Bridge Abutment Pile Group Foundations - A Case Study

Abstract

A reliable assessment of immediate and long-term deflections is vital for a cost-effective pile group design supporting a bridge abutment. This paper reports on some key challenges involved in the design methodology developed for the assessment of 8 over bridges on a railway scheme in UK. The unconventional construction sequence involved placement and locking of the bridge deck prior to backfilling. This resulted in reduction of the allowable translational and rotational movements of the abutments' foundations to eliminate the risk of exceeding the bearings' movement tolerances. To test this scenario and based on engineering judgement, careful interpretation of the available field, laboratory and numerical analysis results was carried out, and the use of at-rest (K0) static earth pressure is considered to be suitable in pile design for the case where the foundations are required to be comparatively rigid to meet the above performance criteria. Also, as part of the design process, the output of linear and non-linear analysis from commonly used pile group analysis software packages: Repute and PIGLET were compared with finite element analysis using Plaxis 3D which are presented.

KEYWORDS

Pile design; Bridge abutment retaining wall; Numerical analysis; Lateral earth pressure distribution; Repute, PIGLET and Plaxis comparison.

1. Introduction

Movement of bridge abutments is significantly important when considering the overall serviceability and safety of the structure. A reliable assessment of the lateral earth pressure distribution and the immediate and long-term deflections is vital in order to create a cost-effective design which satisfies the design requirements.

Earth pressure distribution behind retaining wall systems is a soil-structure interaction problem and therefore should be determined interactively with the deflection of the wall. In the current design practice, the earth pressure distribution behind the wall is adopted according to the at-rest or active earth pressure theories. However, relatively 'non-yielding walls' such as bridge abutments on stiff piles usually undergo relatively small movement which can be insufficient to initiate the sliding wedge behind the wall and to relieve the pressure to its active or passive state (El-Emam, 2011).

In this study, each bridge comprised inverted 'non-yielding' T-shape abutments and wingwalls founded on two rows of circular concrete piles with an off-centre abutment stem creating a longer heel. The bridge deck is supported on elastomeric bearings on both sides. Anticipated deflections in the bearings were of concern due to (a) an unconventional construction sequence which involved placement and locking of the deck prior to backfilling substructure to streamline the scheme's construction sequence and (b) high estimated lateral loading induced by traffic and backfill material. As a result of the above construction sequence and the required structure rigidity, the anticipated movement of the structure was thought to be unlikely to be sufficient to mobilise the active state. In order to make an informed decision about the mobilisation of active (K_a) or at-rest (K_0) static earth pressure, analytical and numerical analysis was conducted and the results were interpreted against field and laboratory data as well as published literature.

It is important to note that this paper follows the design methodology developed for the design of the substructures of a major railway scheme in the UK. More specifically, the

- Details about the typical geometry of the bridge,
- Geotechnical investigation and the advanced in-situ and laboratory testing which are required to consider the soil non-linearity in routine design, and
- Unconventional construction stages are presented.

As part of the development of the design methodology it was observed that despite availability of many different pile group design software packages, little information could be found to compare the results of analyses carried out with alternative programs (Pirrello and Poulos, 2013). Therefore, a comparison is made between the results obtained from Repute and PIGLET which are often used in current pile design practice against PLAXIS 3D.

2. Description of Typical Structure

2.1. STRUCTURE GEOMETRY

For the purpose of this paper, a representative structure was selected. The proposed structure is a semi-integral bridge with a clear square span of 18.5m. The substructure comprised abutment walls and parallel wingwalls built from precast concrete units. The substructure is supported by individual pile caps which function individually (Figure 1). The abutment retained height from the top of the pile cap to the top of the road level is ~8.7m and the abutment length is ~14m long which is supported on a pile cap 1.5m thick by 6m wide.

FIGURE 1

Three-dimensional view of structure including sub structure and abutment pile cap arrangement.

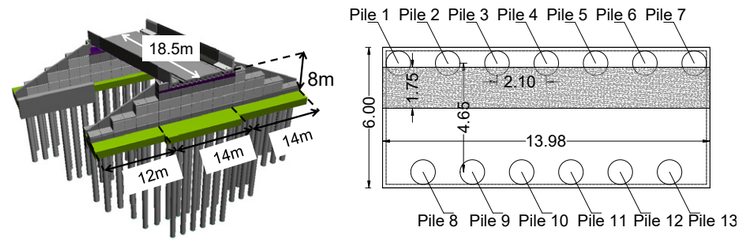

2.2. CONSTRUCTION SEQUENCE

The construction sequence of the bridge is as follows:

- Installation of piles and pile caps
- Construction of the abutments and wingwalls
- Installation of bearings followed by bridge deck locking
- Placing and compaction of the backfill

2.3. FOUNDATION DETAILS

The substructure is supported by a 1.5m thick pile cap connecting 1050mm diameter bored concrete piles with a total embedment length of 23m. The base of the pile cap is +88mAOD. As shown in Figure 1, the piles are arranged in a staggered formation with spacings of 2.1m and 4.65m in the x and y axis respectively.

3. Description of Geology and Subsurface Conditions

3.1. REGIONAL & LOCAL GEOLOGY AND SOIL FEATURES

The local ground conditions consist of minor thicknesses of cohesive glacial deposits (CGD) in the form of firm to stiff clay to a depth of 1.3mbgl. These deposits overlie the Oxford Clay Formation (Peterborough member) which encompasses a 4m weathered zone characterised as firm to locally stiff clay (OXC-PET (W)) overlying unweathered Oxford Clay (OXC-PET (UW)) characterised as stiff to very stiff clay (tending to extremely weak Mudstone) as shown in Figure 2.

FIGURE 2

Shear wave velocity (Vs) vs. elevation profile.

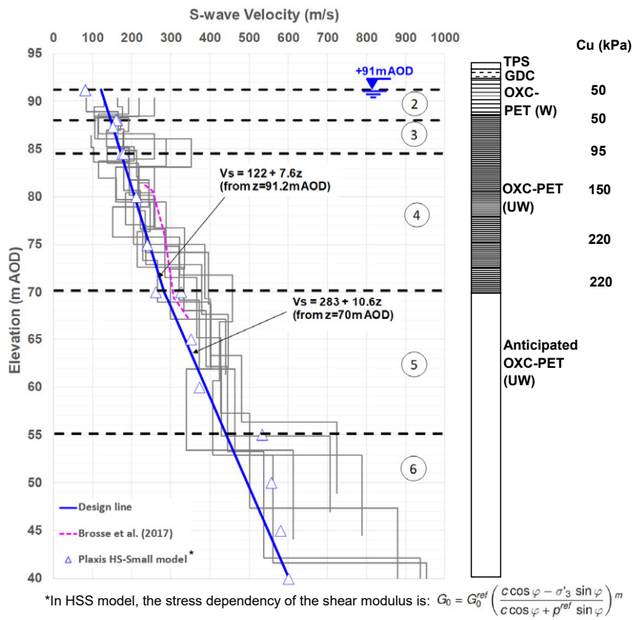

3.2. GEOTECHNICAL INVESTIGATION

The subsurface investigation of the examined area consists of a combination of a) borings with sampling and SPT measurements to a depth of 20m, b) hand shear vane tests in trial pits and c) in-situ evaluation of low-strain shear wave velocity, V_s, at 3 locations within 100m by Surface Wave Methods: Multi-channel Analysis of Surface Waves (MASW) and Refraction Microtremor (ReMi). Self-boring pressuremeter testing (SBPM) was made available at a site ~15km away conducted in Mid and Lower OXC Formation with similar ground conditions. Figure 2 shows the V_s-depth profile which agreed well with results obtained from literature (Brosse et al., 2017). Laboratory testing consisted predominantly of measurement of limited number of advanced K_0-consolidated undrained triaxial with local strain gauges (CK_0U) as well as oedometer testing. Similar lab and field testing from the wider site were also available and used in conjunction with the site-specific data.

3.3. PILE LOAD TEST RESULTS

Although pile load tests are very useful in developing an efficient design, no preliminary pile testing was conducted in the examined area. However, the results of two pile load tests undertaken on 0.9m diameter test piles 25m in length were available from other locations in the UK with similar ground conditions (Vardanega et al., 2019). The pile group analyses conducted as part of the design (see Section 8.2) included both linear and non-linear load-displacement behaviour of the pile groups. To make an informed decision about the parameters to be used in the pile group analysis software (see section 8.2) and on the basis of engineering judgement, the load-settlement behaviour of a single pile was modelled in Repute, Plaxis 3D and PIGLET against the aforementioned pile load test data as shown in Figure 3.

FIGURE 3

Vertical load-settlement behaviour compared to the pile load test results

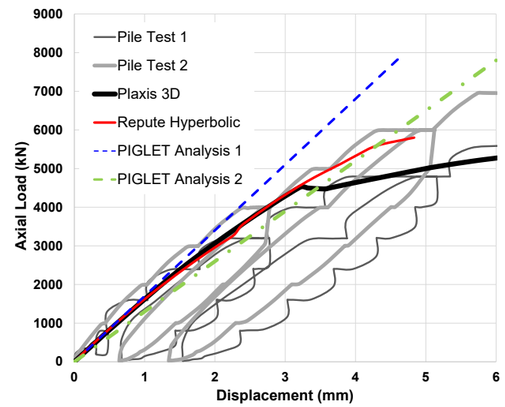

4. Design Methodology

4.1. BRIDGE LOAD COMBINATION

The forces and moments acting on the structure have been calculated and resolved about the centre of the pile cap (point B) as illustrated in Figure 4. The resultant forces and moments have been calculated from the following:

- Structural loading at the deck bearing level including the structures self-weight (F, M at point A);
- Traffic loading in accordance with PD6694-1:2011 section 7 (F line load, UDL);
- Active (P_{ah}) and passive (P_p) earth pressures;
- Permanent self-weight (SW); and
- Hydrostatic pressures (w).

The load combinations used in the pile group analyses are given in Table 1.

FIGURE 4

Load combination diagram.

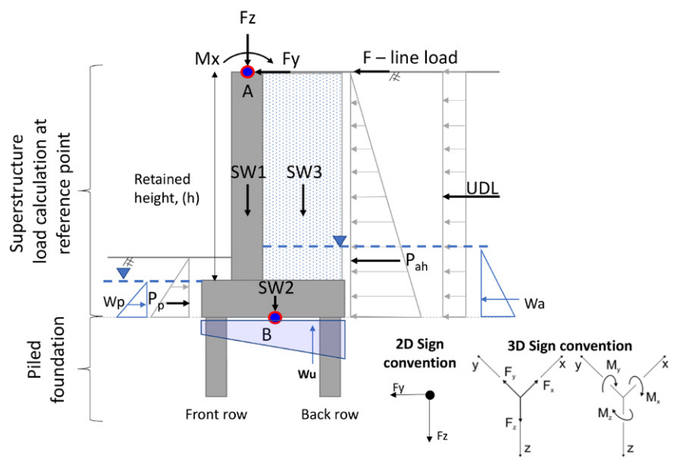

4.2. PILE GROUP ANALYSIS SOFTWARE

Methods employed by commercial software packages for the design of pile groups are predominantly the Boundary Element Analysis (BEM) and the Finite Element Method (FEM). In this study, PIGLET, Repute and Plaxis 3D are used as tools to employ the analysis methods. The basis and limitations of each software are described by Pirello and Poulos (2013).

TABLE 1:

Load combinations used in pile group analyses

Load case	Fx (kN)	Fy (kN)	Fz (kN)	Mx (kNm)	My (kNm)	Mz (kNm)
2D Analysis Structural Loading Input (at point A: bearing level)						
Permanent	6	16	282	0	-62	0
Variable	9	-7	68	0	-69	-34
3D Analysis Geotechnical and Structural Loading Input (at point B: bottom of pile cap)						
Permanent	83	5126	17565	-18470	-144	105
Variable	388	836	953	-6078	3466	631

Note: Fx is into the page

4.3. SOIL MODEL INPUT PARAMETERS

The very small strain (~10^{-4} %) shear modulus (G_0) parameter in this study is derived from surface wave measurements (Figure 2). Unlike the small strain stiffness, the knowledge of $\gamma_{0.7}$ first requires the measurement of G_0 (e.g. geophysical survey, bender element testing) followed by the measurement of shear modulus at small (~10^{-2} %) to large strain level (e.g. advanced triaxial with local gauges triaxial, resonant column and pressuremeter test). Next, the normalised stiffness degradation curve can be constructed and the $\gamma_{0.7}$ can be read from the curve (Figure 5). $\gamma_{0.7}$ is later utilised in the Hardening Soil Small (HSS) model in Plaxis. The reference threshold shear strain ($\gamma_{0.7}$) is regarded herewith as a soil parameter to define the stiffness degradation curve. Three empirical methods of calculation were used to determine the parameter $\gamma_{0.7}$ as shown in Figure 5: a) Vucetic and Dobry (1991), (b) Vardanega and Bolton (2013) and c) Darendeli (2001). In addition, pressuremeter test data and triaxial testing (CK_0U) were considered for derivation of $\gamma_{0.7}$. It is noted, however, that a smaller weighting was given to the pressuremeter tests as they are related to a different location with similar soil conditions and unknown soil stress history conditions. The characteristic at-rest earth pressure coefficient K_0 for the Oxford Clay was evaluated from triaxial testing and literature (Brosse et al., 2017) and ranged between 1.5 and 2.5.

FIGURE 5

Comparison of $G/G_0 - \gamma$ curve from undrained triaxial experiments and literature on Oxford Clay.

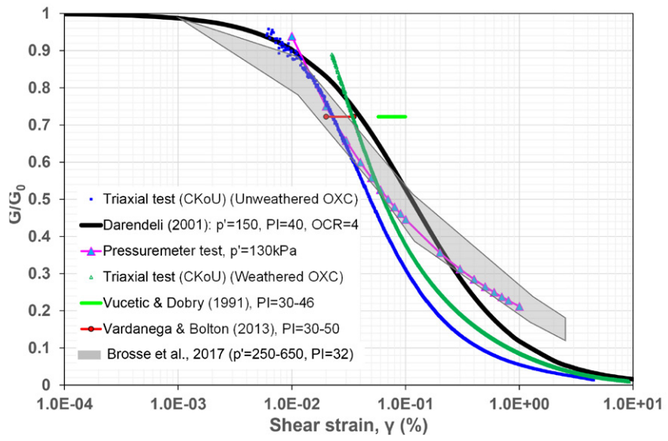

5. Analysis Results

5.1. K_a OR K_0 EARTH PRESSURE COEFFICIENT?

The mobilisation of active (K_a) or at-rest (K_0) static earth pressure behind the bridge abutment wall was one of the design challenges. To make an informed decision about the mobilisation of K_a or K_0 earth pressure distribution, 2D numerical analyses were conducted. A non-yielding inverted T-shape wall (founded on 23m piles) with a height of H=10.2m (retained height h=8.7m) and heel length b= 3.4m was considered. The compacted dense granular backfill (φ=38°) behind the wall was applied in 7 steps in layers of 1m, an interface was defined with a maximum wall friction angle of δ = 27.6°. The numerical simulations were carried out using Plaxis 2D (Figure 6). The Mohr Coulomb (MC) and Hardening Small Strain Stiffness (HSS) material model used for the backfill (layer 1) and soil layers 2-6, respectively.

FIGURE 6

Plaxis 2D finite element model.

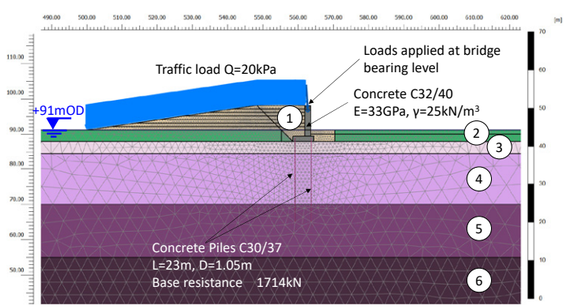

The soil lateral earth pressure distribution over the height of stem wall and the theoretical pressure distribution for active and at-rest state are shown in Figure 7. It should be noted that the K_0 and K_a coefficients are calculated using Equation 8 proposed by Federico and Elia (2009) and Coulomb theory, respectively. According to the numerical model results, the abutment wall was displaced translationally ~18.5mm and 23mm at bottom and top, respectively, to the active side and vertically 8.9mm at the toe and ~6.8mm at the back of the heel). Also, the wall rotated clockwise by an angle $\theta \approx 0.02°$.

It is noted that the effect of soil-wall friction ($\delta = 21° - 35°$) on lateral earth pressure distribution was found to be negligible. Eurocode 7 (Appendix C.3) suggests that for non-cohesive dense soil, at-rest (K_0) conditions should be assumed if horizontal movement (uh) normalised by the wall retained height (h) is less than a) 0.05% - 0.1% for translation mode and b) 0.1% - 0.2% for the top rotation mode. In practice, the designer can potentially assess the lateral wall deflection and rotation based on K_a lateral pressures acting on vertical virtual back plane and check against the movements to obtain an indication as to whether active or at-rest lateral earth pressure is mobilised based on the aforementioned criteria. However, other factors shall be considered whilst making this decision including the Category of the structure and this requires engineering judgment.

In this study, the ratio u_h/h is ranging from 0.19% – 0.23% for translation mode indicating that active earth pressure (K_a) is mobilised. On the other hand, the corresponding ratio due to wall rotation (assuming the wall is behaving as a rigid body) is 0.036% indicating that, according to both EC7 and Achmus (2017), at-rest (K_0) pressure is acting on the face of the abutment wall. This means that an interim state between K_a and K_0 occurs along the stem wall height in line with field measurements of lateral pressures on retaining walls (see Coyle and Bartoskewitz 1970). Based on the numerical results, the earth pressures acting behind the abutment wall increase from active (K_a) at the top, to at-rest (K_0) at the bottom. However, K_0 pressures are mobilised along the vertical virtual back plane. A plausible explanation is that because of the existence of the heel length, a triangular soil wedge (BCD) occurs (see Figure 8) between the stem and the heel of T type cantilever retaining walls with a short heel. Hence, the contact surface (or friction area) does not occur between the stem and the backfill (line BC in Figure 8). Correspondingly, due to the friction, less lateral earth pressure acts on the upper (line AB) compared to the bottom part of the inverted T-shape wall. This behaviour agrees with the results presented by Achmus (2017). Interestingly, as shown in Figure 7, the earth pressure is higher than at-rest pressures at the bottom part of the wall (+92mOD).

Below this level (i.e. the structure's point of rotation) the relative movement between the stem wall and the backfill material, due to the rotation and the bending deformation of the stem wall indicates that the passive state occurs. It would be of particular interest if this could be confirmed by in-situ measurement of the lateral pressure as the study presented from Coyle and Bartoskewitz 1970, although this would be practically difficult. The normalised lateral earth pressure distribution ($\sigma_h/\sigma_{v,max}$) vs. normalised depth z/H acting on the stem of the abutment wall above pile cap level is shown in Figure 8. It is seen that a scattered pressure distribution is obtained from the contact surfaces (line AB and DE). On the other hand, a smooth lateral earth pressure curve is observed from z/H = 0.45 - 0.85 where no strain fields occur (line BC). The normalised lateral earth pressure acting on the stem varies between 0.02 and 0.6. The above observations are in a good agreement with the results presented from Kamiloğlu et al (2019).

FIGURE 7

Lateral earth pressure distribution over the wall height.

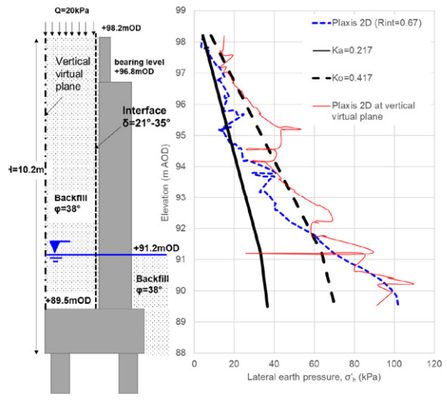

FIGURE 8

Normalised earth pressure distribution acting on the stem of the abutment wall

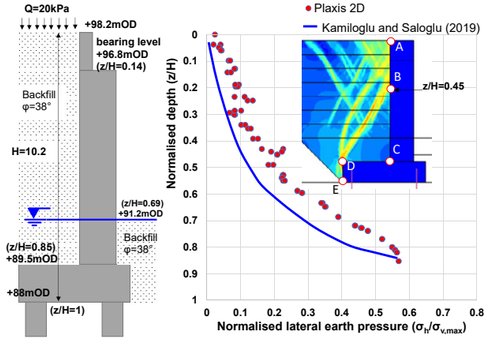

5.2. COMPARISON OF PIGLET, REPUTE AND PLAXIS 3D

The pile group shown in Figure 1 working under the general three-dimensional loading condition is assumed capped by a rigid pile cap in all three pile group analysis software (i.e. PIGLET, Repute and Plaxis 3D) used. The loads applied at the bottom of the pile cap level are presented in Table 1 and the design methodology is described in Section 4. In all three software, the undrained shaft and bearing resistance of the piles were limited to the single pile capacity (calculated using the methodology outlined in Tomlinson & Woodward, 2007) for the specific soil conditions i.e. 77.3kPa and 1980kPa, respectively. The soil models used in the analysis software are shown in Table 2. In Plaxis 3D uniform loads were applied to generate the resolved forces and moments at the centre of the pile cap.

The degree of anisotropy for Oxford clays ranges from 2-3 (Brosse et al., 2017). However, Plaxis 3D can only model isotropic soil behaviour. Therefore, the anisotropy R=1 used in PIGLET and Repute as well as at rest coefficient K_0=1 in Plaxis 3D was assumed throughout in all soil layers for each analysis.

It is noted that under lateral loading, the high strains which occur in the soil close to the pile give rise to lower secant modulus. Therefore, for cohesive soils the PIGLET manual recommends a lateral stiffness value which is equal to the half of the vertical stiffness value i.e. anisotropy R=0.5. However, this value is not valid for the soil conditions encountered in this study where anisotropy value is ranging between 2 to 3 according to Brosse et al. (2017). This recommendation is not considered in this study to a) avoid manipulating PIGLET analysis results and b) make direct comparisons with Plaxis 3D results where anisotropy cannot be taken into account.

TABLE 2:

Soil models used in analysis software

Analysis Software	Soil model
Repute	Hyperbolic
Plaxis 3D	Hardening Small Strain Stiffness (HSS)
PIGLET	Linear increase (see Analysis 1 & 2)

In PIGLET analyses, the soil is modelled as a linear elastic material with a stiffness which varies linearly with depth. The influence of pile group size (O'Brien 2012) on the selection of the appropriate 'elastic' modulus is shown in Figure 9. Two analysis cases were examined in PIGLET:

- Analysis 1: A selection of large strain stiffness (strain amplitude of 0.5%) at the pile head and intermediate strain (amplitude of 0.01%) stiffness at the pile toe level with a linear variation between these levels. The average G/G_0-γ curve at the centre of the soil layers encountered along the pile length is used in Analysis 1 (Figure 9).
- Analysis 2: Elastic shear modulus (G) was taken as $300c_u$ (PIGLET manual).

Although the selected soil stiffness profile is different across all three software and the structural forces might be affected, the stiffness value is considered credible for design purposes.

It should be noted that Repute's hyperbolic model factors were compared against the vertical load test results as shown in Figure 3. In the same figure, the vertical load vs. settlement curve for a single pile for "Analysis 1" and "Analysis 2" are shown. The comparison shows a good agreement between the computed and the load-settlement behaviour derived from the pile test.

Figure 10 shows the comparison of the maximum (long term) pile cap settlement and lateral deflection. It is noted that the loading and consolidation stage were considered separately in Plaxis 3D as shown in Figure 10. The axial force (N), resultant shear force (Q) and bending moment (M) of corner pile No 7 are compared in Figure 11. The results indicate a general agreement between the three software. For the condition examined herein, the settlement predicted by the linear elastic analyses (i.e. PIGLET) is strongly affected by the selection of 'elastic' moduli. On the other hand, the effect of 'elastic' moduli on lateral movement is less pronounced. In comparison with non-linear analyses (i.e. Plaxis 3D and Repute), PIGLET results indicate: a) an over- or under-estimation of the settlement and under-prediction of the main lateral movement Sy (Figure 10a) and b) that under-predicts the horizontal movement independent of the selected shear modulus profile (Figure 10b). It should be noted that the lateral movement Sy predicted from Repute is higher compared to Plaxis 3D.

Figure 11 shows the structural pile reactions. The structural reactions of the corner pile No 7 calculated by Plaxis 3D are in very good agreement with the pertinent results obtained from Repute. On the other hand, PIGLET over-estimates both the axial and shear force and under-predicts the resultant moment. It is worth noting that the pile cap stiffness is known to particularly affect the axial load in the corner pile in PIGLET, however the fully flexible cap option in PIGLET is only applicable for purely vertical loading conditions. Therefore, fully flexible pile cap option is not applicable in this study not only because the loading is applied in all three dimensions but also the pile cap is designed and behaved in a fully rigid manner to distribute load uniformly as the maximum span to thickness ratio of the cap is less than 5 (Gambhir 2011).

Following this assessment, it was determined that using REPUTE (hyperbolic model) was the most appropriate approach for the given structures and ground conditions, due to its versatility and ease of use. However, it will be interesting to verify the above predictions with field measurements, but at this stage no data is available as the railway over bridges are under construction.

FIGURE 9

Influence of pile-group size on the selection of the appropriate 'elastic' modulus.

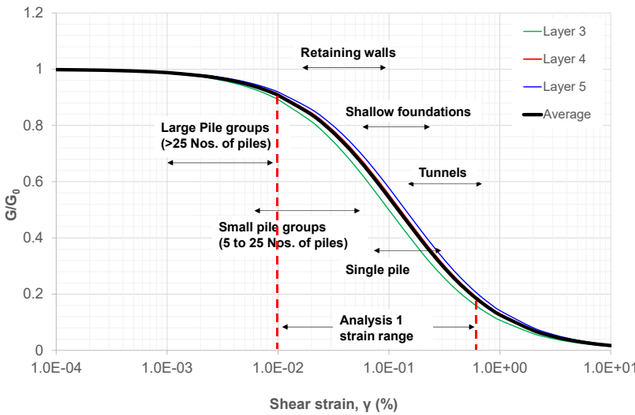

FIGURE 10

Pile cap movement (drained analysis) using Plaxis 3D, Repute and PIGLET

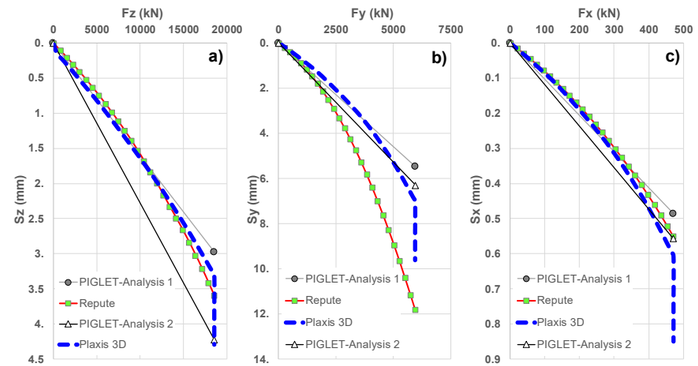

FIGURE 11

Structural forces (drained analysis) for the corner pile No.7 using Plaxis 3D, Repute and PIGLET.

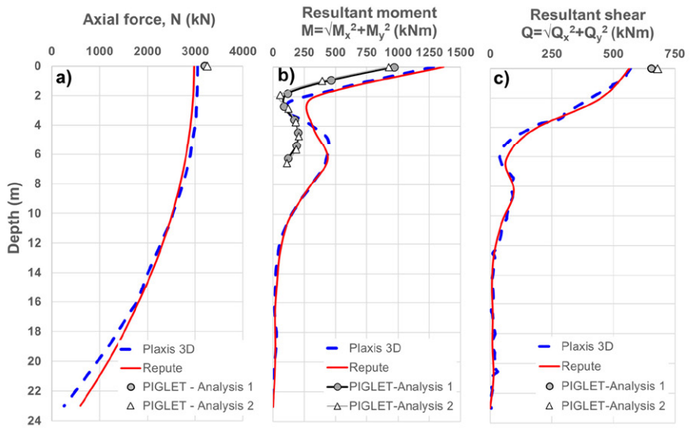

6. Conclusion

The current study presents the bridge abutment pile group design methodology and key design challenges. More specifically, the following design challenges were investigated: a) the earth pressure distribution behind the stem of the abutment wall, b) the selection of an appropriate pile group design software package and c) linear vs. non-linear analysis. Based on the results presented in this study regarding a non-yielding inverted T-shape cantilever retaining wall subjected to high lateral loading, the following conclusions can be drawn:

- The unconventional construction sequence (i.e. placement and locking of the deck prior to backfilling substructure) and the required structural rigidity to limit movements of the bridge bearings, indicate that the restrained movement of the structure is not sufficient to fully mobilise the active (K_a) earth pressures. The present study outlines a comprehensive methodology which can be followed in practice and can augment the database on lateral earth pressure distribution of cantilever retaining walls founded on piles.
- Based on 2D numerical results and engineering judgement regarding the variability of the input parameters, the earth pressures acting behind the abutment wall decreased from active (K_a) at the top, to at-rest (K_0) at a certain level (point of rotation of the structure). Below this level the passive state occurs. The determination of the point of rotation of this structure is complex and hence, the prediction of the transition from active to passive state along the stem of the wall is difficult without performing a numerical analysis. Notwithstanding the last remark, for practical use, K_0 pressures combined with a vertical virtual back plane (which is advantageous as it leads to simpler geometry) can lead to satisfactory results and a reliable design where limiting movement is required.
- The predicted movements and structural pile reactions using Repute and Plaxis 3D are in good agreement. In this study, PIGLET under-predicts the lateral movement and bending moments but over-predicts the axial and shear forces. Although the selected soil stiffness profile is different across all three software and the structural forces might be affected, the stiffness value is considered credible in engineering practice.
- The selection of a representative 'elastic' modulus profile is a key parameter to reliably perform a linear analysis and capture the pile group behaviour (i.e. PIGLET). In this study, linear analysis using PIGLET was not considered reliable for pile groups subjected to high lateral loads, even if the soil stiffness profile results in the same maximum pile group settlement among the software used. On the other hand, as is well known, non-linear analyses are capable of improved predictions, however good quality data on small to intermediate strain stiffness is required.

References

- Achmus M (2017). Earth pressure acting on L-shaped walls. https://www.igth.uni-hannover.de/winkelstuetzwaende.html?&L=1.
- Brosse A et al. (2017) The shear stiffness characteristics of four Eocene-to-Jurassic UK stiff clays. Géotechnique 67(3): 242–259.
- Coyle HM and Bartoskewitz RE (1970). Field Measurements of Lateral Earth Pressures and Movements on Retaining Walls, Texas Transportation Institute, Texas A&M University.
- El-Emam M (2011). Experimental and Numerical Study of At-Rest Lateral Earth Pressure of Overconsolidated Sand. Advances in Civil Engineering, Vol. 11, pp. 1-12.
- Federico A and Elia G (2009). At-rest earth pressure coefficient and Poisson's ratio in normally consolidated soils. Proceedings of the 17th International Conference on Soil Mechanics and Geotechnical Engineering, doi:10.3233/978-1-60750-031-5-7, pp. 7-10
- Gambhir, M.L., (2008). Design of Reinforced Concrete Structures.
- Kamiloğlu HA et al. (2019) Numerical analysis of active earth pressures on inverted T type and semi-gravity walls. 3rd International Conference on Advanced Engineering Technologies, ICADET, Sept. 19-21.
- O'Brien A (2012) Pile-group design. In ICE Manual of Geotechnical Engineering Volume II (Burland J et al. (eds.)). ICE Publishing, London, UK, pp. 823-850.
- Pirello S and Poulos H (2013). Comparison of four pile group analysis programs. International Symposium on Advances in Foundation Engineering, ISAFE, Dec. 5-6.
- Tomlinson, M. and Woodward, J., (2007). Pile design and Construction Practice, 5th Edition, pp. 566.
- Vardanega PJ et al. (2019). The DINGO Database: June 2019, v1.0. University of Bristol, Bristol, UK, https://doi.org/10.5523/bris.3r14qbdhv648b2p83gjqby2fl8.
- Vardanega PJ and Bolton MD (2013) Stiffness of clays and silts: normalizing shear modulus and shear strain Journal of Geotechnical and Geoenvironmental Engineering 139: 1575-1589.

SNC·LAVALIN

snclavalin.com

Contact Information
Akshaye Sikand
Manager, Knowledge Management
akshaye.sikand@snclavalin.com